The Dissertation Committee for Kaijun Lu Certifies that this is the approved version of the following Dissertation:

Biogeochemical Processes of Dissolved Organic Nitrogen in Aquatic Environments

Committee:

Zhanfei Liu, Supervisor

Wayne S. Gardner, Co-Supervisor

James W. McClelland

Amber K. Hardison

Ronald Benner

Biogeochemical Processes of Dissolved Organic Nitrogen in Aquatic Environments

by

Kaijun Lu

Dissertation

Presented to the Faculty of the Graduate School of

The University of Texas at Austin

in Partial Fulfillment

of the Requirements

for the Degree of

Doctor of Philosophy

The University of Texas at Austin

August 2018

Dedication

This work is dedicated to my mother, grandmother, and my family. Thank you for keeping me company all these years, and for supporting me to pursue my dreams. Without your encouragement and confidence in me, I could not make it this far. Words cannot express my gratitude. Thank you and love you wholeheartedly.

Acknowledgements

I would like to take this opportunity to thank my advisors and my mentors, Drs. Zhanfei Liu and Wayne Gardner. Both of them are far more than a Ph.D. advisor to me. What I learned from them all these years, besides numerous scientific skills, are their ways of developing thoughts in science, their enthusiasm on both science and life, and their attitude of "never give up". They have inspired me so much and I believe what I learned here at UTMSI has laid a solid foundation for my future academic career.

I also appreciate all the help I received from every member in Liu Lab and Gardner Lab (Shuting Liu, Jianhong Xue, Hernando Bacosa, Mark McCarthy, Xianbiao Lin, John O'Connor, Jason Jenkins, Kai Wu, Jiqing Liu, Zucheng Wang, Nick Reyna, Meredith Evans) during lab work and all kinds of field trips and cruises. I thank Drs. Leila Hamdan and Wei-Jun Cai for the cruise opportunities. I thank the crew members of R/V *Pelican* for their help with sampling. I thank Dr. Hans Paerl and staff members at Taihu Laboratory for Lake Ecosystem Research (TLLER) for providing lab space, sampling field trips and field accommodation at Lake Taihu. I thank Dr. Ryan Hladyniuk from UTMSI Core Facility Lab for helping assemble and maintain the IM QTOF LC/MS instrument, and Drs. Carol Haney Ball, Dawn Stickle, Caroline S. Chu, and Daniel Cuthbertson from Agilent Technologies for invaluable technical support. I am grateful for the bacterial DNA sequencing and community structure analysis by the Research and Testing Laboratory at Lubbock, Texas, and the invaluable advice for the bacterial community analysis from Dr. Bongkeun Song at VIMS. I also would like to thank Dr. Douglas Walker at Emory University for letting me use their instrument.

I am grateful for the comments and suggestions provided by my committee members (Drs. Zhanfei Liu, Wayne Gardner, James McClelland, Amber Hardison, and Ronald Benner). I thank the experimental help from REU undergraduate students (Alex W. Bianco and Andrea Reynolds). This dissertation work is funded by National Science Foundation (NSF Grants # 1240798 to WSG, and OCE1129659 to ZL), NOAA (NA15NOS4780185), and an Institutional Grant (NA14OAR4170102) to the Texas Sea Grant College Program from the National Sea Grant Office. I am grateful for the fellowship endowed by Lund-Page and Lund-Stuckey, Barton Regents, Batterton Family, and Graduate School Dissertation Writing fellowship. I appreciate the travel awards for attending scientific meetings provided by UTMSI. Special thanks to Dr. Bob Dickey (and Dr. Ed Buskey) for making the state-of-art IM QTOF LC/MS instrumentation available at UTMSI, and for leading us through Hurricane Harvey and dealing with the aftermath. Thanks to Dr. Dong-Ha Min and Heather Herrick for helping me out in my first year at Austin. Many thanks to Jamey Pelfrey, Patricia Webb, and Olivia Gonzalez for helping me with administrative stuffs. I thank my cohorts (Amanda Fitzgerald, Aubrey Converse, Jordann Young, Kathryn Ondricek, Sara Wilson, Stephanie Mohan, and Tracy Harvey) for being the best friends and supports. Last but not least I would like to express my gratitude to all UTMSI faculty, staff and students in creating the friendly and nice research and learning environments, also to everyone and every organization that help us survive through Hurricane Harvey.

Abstract

Biogeochemical Processes of Dissolved Organic Nitrogen in Aquatic Environments

Kaijun Lu, Ph.D.

The University of Texas at Austin, 2018

Supervisor: Zhanfei Liu

Co-Supervisor: Wayne S. Gardner

Dissolved organic nitrogen (DON) is a dominant form of nitrogen in aquatic environments. Knowing source, transformation and fate of DON is important to understand global carbon and nitrogen cycling. However, our knowledge of DON in aquatic environment is still limited partly due to inherent analytical challenges. In this dissertation, DON dynamics, including urea, peptide, and natural DON, are systematically studied through field sampling and laboratory-based incubation experiments using the state-of-art analytical techniques. The dynamics of urea, a labile DON molecule, and how its cycling relates to blooms of *Microcystis* in Lake Taihu, China were investigated. The metabolism rate of urea ranges from non-detectable to 1.37 μmol L^{-1} h^{-1} for regeneration, and from 0.04 μmol L^{-1} h^{-1} to 2.27 μmol L^{-1} h^{-1} for potential urea-N removal. *Microcystis* culture experiments demonstrated that Microcystis only has minor effect on urea dynamics, and bacterial community analysis further suggested that heterotrophic bacteria play a major role in urea metabolism, even though Microcystis is the dominant bloom organism. To investigate the long-term fate of labile DON, incubation experiments were conducted using

^{15}N-labeled tetra-peptide (Ala-Val-Phe-Ala) as substrate. The fate of ^{15}N was monitored throughout the incubation with a newly developed holistic analytical method. Over 40% of peptide N was transformed into uncharacterized DON within several months, in comparison with typically less than 10% for C from previous studies. Moving forward into the mystery of the black box of DON and dissolved organic matter (DOM), molecular structure of DOM was investigated using an Ion Mobility Quadrupole Time of Flight Liquid Chromatography Mass Spectrometer (IM Q-TOF LC/MS). Geometric conformation of DOM molecules was introduced into molecular-level analysis via the ion mobility (IM), and an actual measurement of isomers was achieved for the first time. We established a quantitative measurement of isomers in natural DOM from south Texas Rivers and coastal seawater. Our result showed that about 10% of natural DOM molecules had at least one but no more than four isomers. Overall, the new information on the dynamic, the long-term fate, and the molecular-level information of DON provided in the dissertation opens new dimensions of this field in the future.

Table of Contents

List of Tables

List of Figures

Chapter 1. Introduction

The basis of the operational definition of dissolved organic matter (DOM) was formed in the mid-20th century when glass fiber or silver fiber filters became available in oceanographic researches (Kalle 1966; Bronk 2002; Ridgwell and Arndt 2015). The organic materials passing through filters with a pore size of ~0.45-1.0 μm are considered arbitrarily as "dissolved matter", whereas the retained particles are termed "particulate matter". This definition persists to today, even though we now know that seawater actually contains a continuum of discrete units from the size of a water molecule to that of a whale without any discernible break (Sharp 1973; Bronk 2002).

DOM represents the largest exchangeable carbon reservoir on earth, with a total amount of C estimated over 660×10^{15} g (Carlson 2002; Dittmar 2015). Dissolved organic nitrogen (DON) is a subset of the DOM pool containing nitrogen (N) and is often the dominant N form in aquatic environments. About 58-77% of the bulk of the TDN pool is comprised of DON, except in the deep-ocean and the high nutrient low chlorophyll (HNLC) Southern Ocean (Berman and Bronk 2003; Sipler and Bronk 2015). Concentrations of DON have been measured systematically by the U.S. Global Ocean Carbon Repeat Hydrography program (http://ushydro.ucsd.edu/) since 2003. The mean global DON concentration in surface waters is 4.4 ± 0.5 μmol N L^{-1}, with a range of 2 to 7 μmol N L^{-1}, while deep ocean has a lower DON concentration with most values in the 2 to 5 μmol N L^{-1} range and a mean of 3.6 ± 2.2 μmol N L^{-1} (Letscher et al. 2013; Sipler and Bronk 2015). DON concentrations often increase along a decreasing salinity gradient, with

higher values in coastal, estuarine, and then river waters, with corresponding increases in the range of variability (Sipler and Bronk 2015).

The DON pool is especially important to microorganism, considering that one molecule of DON will provide them with needed N, carbon (C) and energy (Bronk 2002; Sipler and Bronk 2015). Despite its importance, the research effort into DON dynamics lags far behind that of dissolved organic carbon (DOC) (Bronk 2002; Sipler and Bronk 2015). This situation mainly results from the substantial analytical challenges inherent in DON research: for instance, the substantially lower concentration of DON compared with DOC, the multiple chemical analyses required for a single DON measurement, the difficulties in inorganic N removal, and the lack of easy-to-use radioactive isotope (like ^{14}C for C, Bronk 2002).

The marine DON pool is referred to as a "black box" due to our lack of insight. Most of the specific compounds are not identified but can change over small space and time scales (Bronk et al. 2007). So far, only limited information on the processes that control the smaller, relatively labile DON has been identified. In aid of simplification, this "black box" is operationally divided into three different subsets based on stability (Sipler and Bronk 2015) ranging from labile DON (i.e., urea, peptides, fresh proteins, dissolved free amino acids [DFAAs], etc.), to semi-labile DON (i.e., proteins, dissolved combined amino acids [DCAAs] and amino polysaccharides), and finally to refractory DON (mainly unidentified compounds). The definition of these three subsets is quite dynamic, and can be context or study specific. In this work, we define that DON with a turnover time less than a few days as "labile DON"; DON with a turnover time over a year as "refractory

DON"; and DON with a turnover time ranging from days to year as "semi-labile DON", following a previous DON study (Bronk et al. 2007; Sipler and Bronk 2015). DON can transfer from one subset to the other through abiotic or biotic processes (e.g., Amon and Benner 1996), and microbial organisms play an important role in the transformation processes (Brophy and Carlson 1989; Tranvik 1993; Heissenberger et al. 1996; Ogawa et al. 2001).

As a consequence, research efforts in DON can be placed under the umbrella of two extreme aspects, with one focusing on the sources, cycling, and sinks of labile DON in aquatic systems, whereas the other one aims at unfolding the black box of unidentified refractory DON. With DON being transferred among different pools, these different DON research directions are intertwined. Advances in analytical techniques within the last decade or so have greatly increased our knowledge of the chemical composition of the DON pool, especially its labile fraction, and is poised for rapid advances in the future (Sipler and Bronk 2015). Urea, one of the simplest labile molecules of DON, plays an important role in the N cycling on a global scale, and was studied as early as the 1970s (McCarthy 1970). In general, urea concentrations in open ocean systems are very low, with a mean of <1.0 μmol N L^{-1}, only accounting for a minor percentage of the overall DON pool in marine system, ranging from 4.4% in the Chukchi Sea (Baer et al. 2017) to 22.1% in the Sargasso Sea (Sipler and Bronk 2015). However, the impact of urea is much higher in coastal, estuarine, and freshwater systems, with concentrations as high as 25 μmol N L^{-1} (Lomas et al. 2002; Glibert et al. 2006; Kudela et al. 2008). Both phytoplankton and bacteria use urea (Solomon et al. 2010b), but phytoplankton are often the primary users

(Collier et al. 2009; Allen et al. 2011). Urea uptake is documented by many studies in many different regions, and can account for a wide range of the total N uptake from ca. 4% in Hong Kong estuarine waters (Xu et al. 2012), to over 80% in coastal South Atlantic Ocean (Varela et al. 2005).

Urea has drawn attention recently due to a huge increase in industrial urea production over the last 40 years (Glibert et al. 2006, 2014), along with rising harmful cyanobacteria bloom problems worldwide. However, only a few studies have focused on the relationship of urea cycling and cyanobacteria (e.g., Belisle 2014; Belisle et al. 2016; Yang et al. 2017), and the role of urea in cyanobacteria blooms remains unclear. Knowing how urea is cycled through cyanobacteria activity, and to what extent urea supports the growth of cyanobacteria is crucial in understanding how labile DON cycling affects the N cycle on a larger scale. Specifically, it will improve our perception of the formation, development, and prevention of harmful cyanobacterial blooms (CyanoHABs).

Proteins and peptides are another group of labile DON that play irreplaceable roles in global nitrogen cycling, as they account for 25-70% of phytoplankton and zooplankton biomass (Lewis 1973; Emerson and Hedges 2008; González López et al. 2010), and are important substrates for microbial populations. Proteins and peptides are released from marine biota via different processes such as extracellular release by phytoplankton, "sloppy feeding by grazers", and bacterial metabolism of organic matter (Carlson 2002). Even though proteins and peptides occur in low concentrations in natural environments (e.g., ranging only from 0.2 to 4 μmol L^{-1} in coastal ocean; Bronk 2002), they still support a major portion of bacterial growth via rapid turnover (Kirchman and Mitchell 2008). Small

peptides, for instance, are incorporated into bacteria biomass, metabolized to CO_2 and NH_4^+, or released as DOM in other forms. The utilization of peptides by bacteria in short time scales (hours to days) has been extensively studied recently (e.g., Liu et al. 2013, 2017; Liu and Liu 2015b; a, 2018).

Besides its rapid decomposition, as an important intermediate connecting protein degradation, nutrient regeneration, and DON preservation, peptides are an excellent substrate for longer controlled incubation experiments to study the formation of semi-labile or even refractory DON, and to interrogate possible mechanisms for the long-term stability of DON. The role of heterotrophic bacteria as well as autotrophic microbes in the uptake of DON is important (Bronk et al. 2007; Mulholland and Lomas 2008). Roughly 35 ± 13% of total DON in coastal oceans was bioavailable on time scales from 2.5 to 300 days, in contrast to 22 ± 12% for DOC (Sipler and Bronk 2015). However, studies of the production of DON through microbial activity are still scarce compared with C. Tracking the fate of a known N compound throughout an incubation can provide insights into the DON production. This approach also leads to the second aspect of DON research, the study of "black box" DON with intermediate stabilities.

One common approach to study uncharacterizable DON is through controlled incubation experiments, in which the metabolism of organisms combined with the compounds, which they create, degrade and/or modify, is studied (Kujawinski 2011). Many different substrates, including but not limited to glucose (e.g., Gruber et al. 2006; Lønborg et al. 2009), leucine (e.g., Heissenberger and Herndl 1994), glucose and leucine (e.g., Brophy and Carlson 1989), glucose and glutamate (e.g., Ogawa et al. 2001), and detrital

lignocellulose (e.g., Moran and Hodson 1989; Bergbauer and Newell 1992), have been used to investigate the formation of semi-labile and refractory DOM. Only small fractions of substrate, ranging from 1.4% when using leucine as the substrate (Brophy and Carlson 1989) to 7.3% when using glucose as the substrate (Lønborg et al. 2009), were transformed into unidentifiable DOM at the end of the incubation in terms of C. Depending on the length of incubation, these uncharacterizable DOM can be semi-labile or refractory according to our definition. However, these studies focused on the C part of the DOM, and the N information was often ignored possibly due to analytical challenges. The combination of N isotopic techniques and holistic analytical methods to measure ^{15}N concentration in different forms are needed to improve understanding of the short/long-term fate of N.

Another burgeoning approach to investigate unidentified DON is through isolation and characterization of natural DON. An explosion in unidentified DON characterization information has resulted from advanced analytical instrumentation such as high resolution Nuclear Magnetic Resonance (NMR), and Fourier Transformation Ion Cyclotron Resonance Mass Spectrometry (FT-ICR MS). However, our understanding of DON structural characteristics remains far from comprehensive. High sensitivity direct-measurement methods for DON are still lacking (Bronk 2002). DON concentrations are estimated as the difference between total dissolved nitrogen (TDN) and dissolved inorganic nitrogen (DIN) measurements, in which the relatively large analytical errors confound our ability to resolve small but significant changes in DON, particularly in environments with low DON concentrations. Moreover, with thousands of formulas resolved with ultrahigh

resolution MS, researchers still only possess limited knowledge of the isomeric information of DOM and DON molecules. Only limited information is available about the total number of compounds and their variability in natural DOM, which is crucial in exploring reasons behind the long-term stability of DOM and DON (Dittmar 2015). One recently reignited hypothesis about the long-term stability of DOM is that extreme dilution limits DOM utilization (Jannasch 1967; Arrieta et al. 2015). The dilution hypothesis argues that even though the total concentration of DOM is about 40 μmol C L^{-1}, the concentration of each individual compound is too low for microbes to use, because the total amount of compounds may be over the order of million (Hertkorn et al. 2007, 2008, 2013). However, even with ultra-high resolution mass spectrometry FT-ICR MS, the total amount of compounds detected hardly exceed ten thousand. As a consequence, the concentration of each compound is not low enough to support the dilution theory. Under this scenario, it has been argued that each individual compound detected in MS can have tens, if not hundreds, of isomers (Zark et al. 2017; Hawkes et al. 2018). Current estimates of the number of isomers in natural DOM solely relies on modelling (Hertkorn et al. 2007, 2008; Zark et al. 2017), assuming no constraints on the existence of isomers. Modelling returns a total number of isomers in natural DOM ranging from over a hundred thousand (Zark et al. 2017; Hawkes et al. 2018) to several million (Hertkorn et al. 2007; Dittmar and Stubbins 2014). However, modelling results cannot explain why natural DOM has a unimodal distribution with the maximum intensity reached at around 400 Da, if there truly is no constraint on isomers. An actual measurement of isomers in natural DOM is therefore critical.

Our overall understanding of the DON pool is still limited. It is still unclear what fraction of measured DON is cycled in aquatic systems, how unidentified semi-labile and refractory DON is formed, and why it persists through time. **Therefore, my Ph.D. research focused specifically on three topics to shed light on these complicated issues: (1) urea cycling in a hypereutrophic aquatic ecosystem; (2) how microbial organisms form unidentified semi-labile DON in the ocean; (3) new analytical approaches, leading to direct isomeric measurements and 3D shape of marine DOM including DON molecules.** In this dissertation with six chapters, cycling, formation and molecular-level characterization of DON are addressed. Specifically, this chapter provides general background information about DON cycling. Chapter 2 considers the metabolism of a typical labile DON, urea, in a hypereutrophic freshwater lake and how urea cycling is connected to harmful cyanobacterial blooms (CyanoHABs) in the lake. In Chapter 3, a holistic method is introduced for quantifying $^{15}NH_4^+$, $^{15}NO_x^-$ ($^{15}NO_3^-$ and $^{15}NO_2^-$), DO^{15}N, and particulate organic N (PO^{15}N). In Chapter 4, the long-term fate of peptide is quantified with the established analytical method. In Chapter 5, DON is characterized multi-dimensionally at the molecular-level achieved through a state-of-art technique: ion mobility quadrupole time of flight liquid chromatography mass spectrometry (IM Q-TOF LC/MS), and a quantitative measurement of isomer percentage in DOM is achieved. Finally, in Chapter 6, the previous chapters are summarized and broad implications and future work are discussed.

Chapter 2. Urea dynamics during Lake Taihu cyanobacterial blooms in China

This chapter is submitted for publication in *Harmful Algae.*

Authors: Kaijun Lu, Zhanfei Liu, Ruihua Dai and Wayne S. Gardner

The dissertator's contribution includes: designing the experiment, performing research, analyzing data, and writing the dissertation.

ABSTRACT

Lake Taihu, the third largest freshwater lake in China, suffers from harmful cyanobacteria blooms caused by the cyanobacteria *Microcystis* spp., which do not fix nitrogen (N). Reduced N (i.e., NH_4^+, urea and other labile organic N) is an important factor affecting the growth of *Microcystis* in lakes. The world use of urea as a fertilizer has escalated dramatically during the past decades. An understanding of how urea cycling relates to blooms of *Microcystis* is critical to predicting, controlling and alleviating the problem. In this study, we show that the metabolism rate of urea in Lake Taihu ranges from non-detectable to 1.37 μmol L^{-1} h^{-1} for regeneration, and from 0.042 μmol L^{-1} h^{-1} to 2.27 μmol L^{-1} h^{-1} for potential urea-N removal rates. A drastic light/dark difference in the fate of urea-N was also observed, with more apparent $^{15}NH_4^+$ generated and higher quantities of the removed urea-^{15}N remaining in $^{15}NH_4^+$ form in the dark than in the light. A *Microcystis* experiment confirmed the growth of *Microcystis* on urea but its minor effect on urea dynamics indicated that *Microcystis* was not the factor causing the observed difference in urea fate under different light conditions in Lake Taihu. Bacterial community

composition and predicted functional genes data further suggest that heterotrophic bacteria metabolize urea, even though *Microcystis* spp. is the dominant organism in the bloom.

INTRODUCTION

The global expansion of cyanobacterial harmful algal blooms (CyanoHABs), which threatens eutrophic freshwater ecosystems, is accelerating under the scenarios of climate change and global warming. In particular, the wide-spread occurrence of non-N_2 fixing, toxin-producing cyanobacteria *Microcystis* affects many large lake systems, and estuarine and coastal waters worldwide (Paerl et al. 2014). Lake Taihu is located in the Yangtze River delta in east China. Situated in a highly industrialized area, this lake serves the drinking water needs of 20 million or more local inhabitants (Xu et al. 2015) and is a key regional fisheries and tourism resource. Economic development since the 1980s has resulted in excessive loads of nutrients and pollutants discharged into the lake. Total nitrogen (TN) discharged to Lake Taihu exceeded 2.8×10^4 T in 2001 (Qin et al. 2007), and increased to 3.7×10^4 T in 2016 (Wang et al. 2017), with nearly 50% of the N originating from non-point agriculture sources (Qin et al. 2007). As a result, TN concentrations in Lake Taihu have increased over 2-fold from 0.90 mg L^{-1} in 1981 (Qin et al. 2007) to about 1.96 mg L^{-1} in 2016 (Taihu Basin Authority 2016). CyanoHABs now develop throughout the lake from early spring to late fall as a consequence of eutrophication (Chen et al. 2003b; a), and *Microcystis* generally compromise up to 50% or even more of the phytoplankton biomass during Lake Taihu blooms (Xu et al. 2015). In May 2007, the bloom caused a drinking water crisis in the city of Wuxi, raising concern for local and central governments about the CyanoHABs issue in Lake Taihu.

The success of *Microcystis* in Lake Taihu relates closely to its morphological, ecological, and physiological features. For instance, *Microcystis* can regulate its buoyancy

through its gas vesicles in response to a changing environment (Reynolds and Walsby 1975; Šejnohová and Maršálek 2012), providing this species the advantage of accessing both higher availability of nutrients at depth and greater illumination at surface (Oliver et al. 2012). Other special strategies such as internal self-shading through the formation of large colonies further help them adapt to high solar irradiation at surface (Sommaruga et al. 2009; Šejnohová and Maršálek 2012). The reactive oxidants caused by UV can be alleviated or counteracted by carotenoids synthesized by *Microcystis* (Jiang and Qiu 2005; Häder et al. 2007; Šejnohová and Maršálek 2012).

Phosphorus (P) is often considered as the nutrient limiting CyanoHABs in freshwater systems (Schindler 1977; Šejnohová and Maršálek 2012), since cyanobacteria can obtain carbon (C) and nitrogen (N) from the atmosphere through photosynthesis and nitrogen fixation (Schindler 1977; Sterner 2008). However, *Microcystis,* which often dominates toxic CyanoHABs, does not fix N_2 and can accumulate P in the form of polyphosphate granules (Saxton et al. 2012). It also has a high affinity for NH_4^+ (Takamura et al. 1987; McCarthy et al. 2009; Paerl et al. 2011; Gardner et al. 2017). These factors provide *Microcystis* a competitive advantage during nutrient (especially P) limiting conditions. As evidence, the resurgence of *Microcystis* blooms in Lake Erie after decades of P abatement, suggests that N along with P, is critical to the development, composition, and persistence of HABs (Paerl et al. 2011; Gardner et al. 2017).

Different groups of phytoplankton have different preferences for respective N forms (Glibert et al. 2016; Yang et al. 2017). Many cyanobacterial species use multiple N sources such as nitrogen gas (N_2), ammonium (NH_4^+), nitrite (NO_2^-), nitrate (NO_3^-), as well

as organic N urea (CH_4N_2O) (Solomon 2006; Sterner 2008; Solomon et al. 2010a; Oliver et al. 2012). *Microcystis* spp., in particular, can grow faster on urea than NH_4^+ and NO_3^- (Berman and Chava 1999; Solomon et al. 2010a; Belisle et al. 2016). The world has experienced a 100-fold increase in the usage of urea as a fertilizer and feed additive in the past several decades because of its high N content, relatively stable chemical property, and high economic benefits (Glibert et al. 2014). The linkage between anthropogenic urea and increased occurrences of CyanoHABs was recognized (Solomon et al. 2010a), as world consumption of urea escalated from about 1 million tons in 1960 to over 100 million tons in 2010 (Constant et al. 1992; Glibert et al. 2006). In the Yangtze River watershed alone, annual urea fertilizer use exceeded 2.0 million tons in 2005 (Glibert et al. 2014). However, direct measurements of urea cycling rates are rare for Lake Taihu blooms (Yang et al. 2017). Thus, determining the direct or indirect (via internal recycling) role of urea to cyanobacteria species, *Microcystis* in particular, is important to understanding the potential importance of urea-N in the initiation and maintenance of the blooms. A further understanding of the degree that CyanoHABs themselves contribute to urea (Steffen et al. 2012) and NH_4^+ dynamics (Hampel et al. 2018) are crucial to understanding critical interactions between internal N dynamics and their effects on *Microcystis*-dominated CyanoHABs.

The goal of this study is to understand how urea affects the development and success of *Microcystis* spp. dominated CyanoHAB, and what role *Microcystis* spp. plays in urea cycling in Lake Taihu. To achieve these goals, we conducted microcosm incubations to investigate urea metabolism and degradation in Lake Taihu and how it

interacts with *Microcystis*. Urea metabolic rates were calculated following an isotope dilution model (Blackburn 1979; Caperon et al. 1979; Hansell and Goering 1989). Bacterial community interactions with urea were analyzed further using 16S rRNA sequencing and bioinformatics tools.

MATERIALS AND METHODS

Study Area

Lake Taihu is located in the southeastern region of Yangtze River delta (30º55'40'' – 31º32'58''N; 119º52'32'' – 120º36'10''E; Figure 1). The lake is 2,340 km^2 in area, with a mean depth of ca. 2 m. This polymictic lake has a drainage area of over 36,000 km^2, containing over 100 input sources (Xu et al. 2015), with no more than 20% of them over 40 m in width (Wang et al. 2017). The annual freshwater input to the lake is approximately 8.8×10^9 m^3, and the water residence time is about 180 days (Xu et al. 2015). With a volume of over 4.4 billion m^3, Lake Taihu serves as the key drinking water source for about 20 million people from several nearby cities including Shanghai, Wuxi, and Suzhou (Qin et al. 2007, 2009; Paerl et al. 2014; Xu et al. 2015), and over 60 million people living in the Lake Taihu watershed heavily rely on the quality of Taihu water (Taihu Basin Authority 2016).

Experimental Design

Microcosm incubation experiments were performed to investigate urea cycling under different light conditions in Lake Taihu. Surface and bottom water was collected from four stations in the northern and central part of the lake in June 2014 (Figure 1; Station 1: 31º30'49''N, 120º11'26''E; Station 3: 31º28'35''N, 120º11'40''E; Station 7: 31º20'18''N, 120º10'49''E; Station 10: 31º18'52''N, 119º56'42''E). Water samples were brought to the laboratory within 6 hours, amended with ^{15}N labeled urea (^{15}N-urea) to a final concentration of 32 μmol L^{-1} (urea-^{15}N concentration 64 μmol L^{-1}), and incubated at ambient temperature. Ambient urea-N concentrations ranged from ca. 9.1 μmol L^{-1} to ca.

22.2 μmol L^{-1}, with the lowest ambient urea-N concentration observed at Station 7 and the highest at Station 1. ^{15}N-urea concentrations used in this study are comparable to previous studies (e.g., Belisle, 2014; Huang et al., 2014; Belisle et al., 2016; Yang et al., 2017). For surface water samples, incubations were conducted both under natural light and in the dark. Light samples experienced natural cycles of light and dark whereas dark incubation bottles were wrapped with aluminum foil. Bottom water samples were incubated only in the dark. Incubations were duplicated.

Stations 1 and 3 samples were incubated for 48 hours. Besides the 48-hour incubation, samples from Stations 7 and 10 were incubated further to two weeks to provide insights into the long-term fate of urea, and to estimate the bacterial consortium's potential ability to process urea over a long period of time (335 hours, roughly 14 days). At designated time points (0h, 2h, 17h, and 47h for short incubations; 0h, 2h, 18h, 47h, 120h, 215h, and 335h for long incubations), 1 mL subsamples were collected and preserved with formaldehyde for bacterial abundance analysis, and 60 mL subsamples were filtered through 0.2 μm nylon membrane filters. Filters and filtrates were preserved in -20 ºC for later bacterial community and chemical analyses, respectively.

A xenic *Microcystis* culture incubation was conducted in March 2015 to investigate the role of *Microcystis* activity and light conditions in Lake Taihu urea cycling. The *Microcystis* culture was obtained from Nanjing Institute of Geography and Limnology (NIGLAS). Surface water from Station 10 was collected during a sampling trip and filtered (0.2 μm pore size nylon filter) right after returning to the lab (within 3 to 4 hours) to remove ambient microbes. Six experimental conditions were implemented: (1) filtered lake water;

(2) filtered lake water + *Microcystis*; (3) filtered lake water + 10 μmol L^{-1} $^{15}NH_4^+$; (4) filtered lake water + 32 μmol L^{-1} ^{15}N-urea; (5) filtered lake water + *Microcystis* + 10 μmol L^{-1} $^{15}NH_4^+$; and (6) filtered lake water + *Microcystis* + 32 μmol L^{-1} ^{15}N-urea. Treatment groups were duplicated, and control groups were single measurements. Incubations were conducted under different light conditions, as in 2014 incubations. March 2015 microcosm incubations were conducted in an incubator to maintain an ambient temperature of 25 ºC. The *Microcystis* cell density used in incubations exceeded 1×10^9 cells L^{-1} to mimic a heavy bloom condition (generally over 1×10^7 cells L^{-1}). At designated time points (0h and 24h), 1 mL subsamples were collected and preserved with formaldehyde for bacterial abundance analysis, and the rest were filtered through 0.2 μm filters. Filtrates were preserved at -20 ºC for later chemical analysis.

^{15}N-NH_4^+ and ^{15}N-urea Analysis

Total ammonium concentrations and atom % ^{15}N-NH_4^+ were analyzed using Ammonium Isotope Retention Time Shift High Performance Liquid Chromatography (AIRTS-HPLC; Gardner et al., 1995). Note that the AIRTS-HPLC cation exchange column isolates NH_4^+ and $^{15}NH_4^+$ from organic N forms, so that the latter compounds (i.e., urea and other DON) normally have minimal effects on results.

Measurement of the ^{15}N atom % enrichment of urea could be a problem in isotope dilution model (Hansell and Goering 1989), but this problem was solved by the application of AIRTS-HPLC. For ^{15}N-urea analysis, urea was first hydrolyzed to NH_4^+ enzymatically (McCarthy 1970), as modified by Parsons et al. (Parsons et al. 1984) and Dai et al.

(unpublished data). Briefly, 20 μL purified urease (in glycerol solution; Sigma Aldrich, P/N U1875) was added into 20 mL samples. Samples were then incubated in a water bath at 55ºC for 20 min. The total ^{15}N concentration and ^{15}N atom % were analyzed with AIRTS-HPLC. ^{15}N-urea concentration was calculated by subtracting the ^{15}N-NH_4^+ from total ^{15}N after hydrolysis. The recovery rate of this urea analysis method is close to 100% based on pre-experiments (Dai et al, unpublished data).

Here the disappearing rate of urea-N is defined as "removal rate", rather than "uptake rate" because conclusive evidence is not available about whether urea is hydrolyzed extracellularly before being taken up or intracellularly after uptake in natural waters. The potential removal rate (i) and actual regeneration rate (d) of urea were calculated based on an isotope dilution model modified slightly from the original formula (Blackburn 1979):

$$\frac{dP_t}{dt} = d - i \tag{1}$$

$$\ln\left(R_t - {}^{15}n\right) = \ln\left(R_0 - {}^{15}n\right) - \frac{d}{d-i}\ln\left[\frac{P_0 + (d-i)t}{P_0}\right] \tag{2}$$

where P_0 is the initial urea-N concentration; P_t is the urea-N concentration at time t; R_0 is the initial urea-^{15}N ratio; R_t is the urea-^{15}N ratio at time t; ^{15}n (0.0037) is the natural abundance of ^{15}N. Equation 1 indicates that P_t changes linearly with t, with a slope of (d-i) and an intercept of P_0, while equation 2 suggests that $\ln(R_t\text{-}^{15}n)$ changes linearly with $\ln(P_t/P_0)$ with a slope of –d/(d-i) and an intercept of $\ln(R_0\text{-}^{15}n)$. Thus, "d" and "i" can be estimated easily.

Bacterial Community and Bioinformatics Analysis

Bacterial abundance analysis was performed following published protocols (Marie et al. 1997; Gasol and Giorgio 2000; Liu et al. 2013; Liu and Liu 2015c). Briefly, bacteria were enumerated using an Accuri C6 Flow Cytometer (FCM) System with a laser emitting at 488 nm. Formaldehyde-preserved samples (500 µL) were stained with 5 µL SYBR Green I (SYBR-I) working solution (1:100, v/v), and incubated under dark conditions for at least 15 min. Each cell was detected from their signatures in a plot of 90º side light scatter (SSC-H) versus green fluorescence (FL1-H). The discriminator was set on FL1-H, as it is proportional to the nucleic acid-SYBR I-complex. The counting error was estimated to be within 25%.

The 0.2 µm filters collected from 2014 incubations were sent to Research and Testing Laboratory (Lubbock, TX) for 16S rRNA pyrosequencing following the procedures described previously (Liu et al. 2013). Subsequent community structure analysis was performed using MOTHUR (Schloss et al. 2009). A further prediction of functional genes was made based on the 16S rRNA marker gene using the bioinformatics tool Phylogenetic Investigation of Communities by Reconstruction of Unobserved States (PICRUSt; (Langille et al. 2013)). Input file for PICRUSt was created in MOTHUR using the command "make.biom". PICRUSt predictions were conducted on closed OTUs at the 97% similarity level following a previous study (Liu et al. 2017a). Metabolic pathway and functional gene predictions on copy-number-normalized OTUs were made using the Galaxy server (Goecks et al. 2010) at http://huttenhower.sph.harvard.edu/galaxy/.

RESULTS

2014 Incubation Experiment

^{15}N Cycling

All reported urea concentrations are based on N concentrations (1 μmol L^{-1} urea equals to 2 μmol L^{-1} urea-N). A decreasing trend in urea-^{15}N concentration with incubation time occurred at all four stations regardless of the water depths (surface or bottom) and light conditions (light or dark; Figure 2). However, the decreasing patterns differed among stations and incubation parameters.

At station 1 urea-^{15}N concentration decreased from the initial value of ca. 67 μmol L^{-1} to 60.8 μmol L^{-1} and 62.5 μmol L^{-1} during the first 2 hours, and remained relatively constant throughout the incubation in bottom and surface natural light samples, respectively. Surface dark samples showed a different trend ($p < 0.05$), with urea-^{15}N concentration decreasing to 44.8 μmol L^{-1} by the end of incubation (Figure 2A). Surface samples at station 3 shared a similar pattern: urea-^{15}N decreased constantly from the initial concentration of 64.0 μmol L^{-1} to 17.4 μmol L^{-1} and 14.4 μmol L^{-1} in surface natural light and surface dark incubations over 48 hours, respectively. A decrease in urea-^{15}N also occurred in bottom samples at station 3, where it dropped to 53.8 μmol L^{-1} during the first 2 hours but remained constant for the rest of the incubation (Figure 2B).

The urea-^{15}N concentration from surface natural light incubation at station 7 decreased at a constant rate, reaching 9.46 μmol L^{-1} at the end of the incubation (335 hours) from the initial concentration of 59 μmol L^{-1}. In contrast, only minimal decreases occurred in surface dark and bottom incubations (from 61 μmol L^{-1} to 51 μmol L^{-1} in surface dark;

from 63 μmol L^{-1} to 54 μmol L^{-1} in bottom; Figure 2C). In contrast, at station 10 almost all urea-^{15}N was removed by the end of incubations at hour 335 for all three treatments (Figure 2D).

Based on the isotope dilution model, the urea-N regeneration rate varied from non-detectable to 1.37 μmol L^{-1} h^{-1}, whereas the potential urea-N removal rate varied from 0.04 μmol L^{-1} h^{-1} to 2.27 μmol L^{-1} h^{-1}. Note that the change of urea-^{15}N (Figure 2) does not necessarily reflect the urea cycling rate (because both the removal of urea-^{14}N is not reflected in Figure 2), and also that urea-N cycling rates of station 7 and 10 were calculated on different time scales compared with those of station 1 and 3. In terms of net quantity, more urea-^{15}N was removed at station 7 and 10, but the highest regeneration and removal rates occurred in the surface natural light incubation at station 3 (Table 1).

The fate of urea under different irradiation conditions was investigated, through $^{15}NH_4^+$ concentration and the percentage of NH_4^+-^{15}N versus removed urea-^{15}N measured. No significant difference between light and dark incubation were detected at stations 1 and 3. Although over 12% (station 1) and 72% (station 3) of initially spiked ^{15}N-urea was removed during the incubation (Figure 2A&B), low concentrations of $^{15}NH_4^+$ (less than 1.00 μmol L^{-1}, Figure 1S) occurred throughout the surface natural light and surface dark samples incubation conducted at stations 1 and 3, with NH_4^+-^{15}N generally accounting for less than 10% of removed urea-^{15}N (Figure 3 A&B). The percentage of NH_4^+-^{15}N recovered relative to the urea-^{15}N removed reached ca. 21% and 14% at station 1 and 3, respectively in the bottom samples, and they are not statistically different from surface samples (both p value > 0.05; t-test).

In contrast, significantly different trends in urea's fate were observed under light and dark conditions for stations 7 and 10 ($p < 0.05$; Figure S1 C&D; Figure 3 C&D). More urea-^{15}N was removed and more ^{15}N remained as NH_4^+, under dark than under natural light conditions. At station 7, the percentage generally increased in dark incubations, reaching the highest value of 87% at the last time point, whereas it remained relatively unchanged in natural light and bottom incubations. At station 10, all treatments followed a similar pattern, with the highest percentage observed shortly after T_0 followed by decreases to nearly zero. The highest NH_4^+-^{15}N: removed urea-^{15}N percentage (about 63%), was again observed in dark incubations.

Bacterial Community

The bacterial abundance fluctuated throughout the short incubations but changes were not significant. Station 1 and 3 have similar initial and final bacterial abundances, with initial values ranging from 2.9×10^{10} cells L^{-1} to 4.0×10^{10} cells L^{-1}, and the final values ranging from 2.3×10^{10} cells L^{-1} to 3.4×10^{10} cells L^{-1} (Figure 4A&B). Specifically, bacterial abundance at station 1 decreased for all three treatments. In contrast, bacterial abundance at station 3 surface water incubations often increased with time after an initial decline within the first 2 hours. The flow cytometry data shows that bacterial population, represented by DNA content, remained relatively unchanged for incubations at station 1 (Figure S2A). At station 3, however, distinct bacterial populations with higher DNA content (higher values in FL1-H axis) developed in the surface water as the incubation proceeded (Figure S2B). These bacteria with high DNA content represent the group that

may have used spiked urea to efficiently build their biomass during the incubation (Liu and Liu 2016).

During the long incubations, bacterial abundance at station 7 decreased from an initial abundance of 6.5×10^{10} cells L^{-1} to 4.0×10^{10} cells L^{-1} in surface natural light and to 1.4×10^{10} cells L^{-1} in surface dark, and from 6.2×10^{10} cells L^{-1} to 5.9×10^{10} cells L^{-1} in bottom water at the end of the incubation (14 days), respectively. The trends at station 10 are more complicated. Bacterial abundance in both dark incubations (surface dark and bottom) decreased, dropping from about 3.0×10^{10} cells L^{-1} at the beginning to 1.3×10^{10} cells L^{-1} and 1.9×10^{10} cells L^{-1} at the last time point in surface dark and bottom, respectively. Bacterial abundance in the surface natural light incubation, on the other hand, increased to more than 5.0×10^{10} cells L^{-1} during the incubation (Figure 4B). Change of the green fluorescence intensity reflects changes in DNA content. Bacterial population stayed relatively unchanged for incubations at station 7 (Figure S2C) but groups of bacteria with higher DNA content increased in surface incubations at station 10 (Figure S2D).

The bacterial community data (Figure 5, Phylum level; Figure S3, Genus level) reveal the change of community structure during long incubations. The initial community at both stations were dominated by *Proteobacteria* (ca. 40% for both stations), *Actinobacteria* (about 26% and 31% for stations 7 and 10, respectively), and *Cyanobacteria* (ca. 12% and 4% for stations 7 and 10, respectively; Figure 5). With incubation, the community structure remained constant for the surface light and bottom incubations at station 7, as well as for the surface dark and bottom incubation at station 10. In contrast, bacterial community changed significantly in the surface dark incubation at

station 7 and surface light incubation at station 10. *Firmicutes* developed from 0.5% to 26% in the surface dark incubation at station 7, and from 2% to 74% in the surface light incubation at station 10. While *Deinococcu-Thermuss* developed from nearly 0% to 28% in the surface dark incubation at station 7, and from 2% to 18% in the surface light incubation at station 10. On the other hand, *Actinobacteria* dropped to about 1% in the surface dark incubation at station 7, and *Proteobacteria* dropped to ca. 4% in the surface light incubation at station 10 (Figure 5). This pattern can be visualized further by Principle Coordinates Analysis (PCoA) on the bacterial genus data (Figure S4). *Microcystis* was present at all time points for all treatments across different stations at the beginning of the incubation (Figure S3) but was absent at the last time point (T = 335h) of surface dark at station 7 and surface light at station 10, where the most dramatic changes in bacterial community occurred. Regardless of its relatively low abundance (generally < 1.0%), *Microcystis* remained as an important species because it is the dominant toxin producers in Lake Taihu (Otten et al. 2012; Steffen et al. 2012).

2015 *Microcystis* Incubation Experiment

Bacterial abundance data for the 2015 *Microcystis* incubation is provided in the Supporting Information (Table S1). $^{15}NH_4^+$ concentration remained nearly undetectable in all controls without the initial addition of $^{15}NH_4^+$ (filtered lake water; filtered lake water + ^{15}N-urea; filtered lake water + *Microcystis*). For $^{15}NH_4^+$-added control (filtered lake water + $^{15}NH_4^+$), $^{15}NH_4^+$ concentration remained constant during the incubation regardless of irradiation conditions (data not shown). In contrast, the concentrations of $^{15}NH_4^+$ increased

to about 3 μmol L^{-1} in the filtered lake water + ^{15}N-urea + *Microcystis* incubation, with no significant difference detected between different light treatments (Figure 6A). The concentrations of $^{15}NH_4^+$ in filtered lake water + $^{15}NH_4^+$ + *Microcystis* incubations dropped from the initial concentration of ca. 11 μmol L^{-1} to ca. 2 μmol L^{-1} under natural light conditions and to ca. 6 μmol L^{-1} under dark conditions within 24 hours, respectively (Figure 6A). Overall, based on filtered lake water + $^{15}NH_4^+$ + *Microcystis* incubations, the natural light incubation had a higher NH_4^+ cycling rate than the dark incubation, with an actual regeneration rate of 0.09 μmol L^{-1} h^{-1} (natural light) and 0.06 μmol L^{-1} h^{-1} (dark), and a potential removal rate of 0.56 μmol L^{-1} h^{-1} (natural light) and 0.29 μmol L^{-1} h^{-1} (dark), respectively (Table 2).

Concentrations of urea-^{15}N for control groups without the addition of ^{15}N-urea (filtered lake water; filtered lake water + *Microcystis*) remained undetectable, and for urea-^{15}N-added control (filtered lake water + ^{15}N-urea) the urea-^{15}N remained unchanged throughout the incubation period, regardless of irradiation conditions (data not shown). Unlike control groups, the concentrations of urea-^{15}N decreased from the initial 64.0 μmol L^{-1} to 58.0 μmol L^{-1} and 59.9 μmol L^{-1} in the natural light and dark treatments, respectively. In contrast to the natural lake water incubations conducted in 2014, differences were not significant between light and dark treatments in xenic *Microcystis* incubations. Furthermore, no differences in the fate of urea (NH_4^+-^{15}N: removed urea-^{15}N percentage) were detected in the pure *Microcystis* incubation. Dark incubation cycling rates (regeneration rate: ca. 0.28 μmol L^{-1} h^{-1}; removal rate: ca. 0.52 μmol L^{-1} h^{-1}) were higher than in natural light incubations (regeneration rate: ca. 0.02 μmol L^{-1} h^{-1}; removal rate: ca.

0.41 μmol L^{-1} h^{-1}), but the difference is not significant perhaps due to the high variability in the dark treatment (Table 2).

A cross comparison between NH_4^+ and urea shows that the removal of NH_4^+ (ca. 0. 56 μmol L^{-1} h^{-1}) was comparable but higher than for urea-N (ca. 0.41 μmol L^{-1} h^{-1}) in the *Microcystis* incubation under natural light (Table 2). In contrast, the dark uptake rate of NH_4^+ (ca. 0.29 μmol L^{-1} h^{-1}) was lower than that of urea-N (ca. 0.52 μmol L^{-1} h^{-1}; Table 2).

DISCUSSION

Microcystis growth on urea

Urea represents a notable source of anthropogenic N, as its usage as fertilizer and feed additive continues to increase (Glibert et al. 2006; Solomon et al. 2010a). However, the internal dynamics of urea in polluted eutrophic tributaries are not well understood (e.g. Solomon et al., 2010; Bogard et al., 2012). For example, it is still not clear how much of the urea resulting from agricultural fertilizer runoff is processed directly by CyanoHABs, or whether the bloom is supported indirectly by rapid recycling of urea-N to NH_4^+ or other organic forms during transport (Gardner et al. 2017). Assessing the ability of cyanobacteria or other CyanoHAB organisms to use urea as a N source directly or indirectly is important to understanding the dynamics of CyanoHABs, especially for fresh water systems such as Lake Taihu that receive large loads of anthropogenic pollution and suffer from CyanoHABs dominated by *Microcystis* spp. We speculated that urea cycling is an important internal component in the development and success of CyanoHAB *Microcystis* spp., and that *Microcystis* spp. in turn plays a direct role in urea cycling in Lake Taihu.

Not all phytoplankton can use urea directly, mainly due to the lack of essential enzymes for urea catabolism (Solomon et al. 2010a; Sipler and Bronk 2015). Thus, the ability to use urea as an extra source of N source could be critical to the development and maintenance of non-N fixing CyanoHABs (Chaffin and Bridgeman 2014; Huang et al. 2014; Davis et al. 2015; Gobler et al. 2016; Belisle et al. 2016; Gardner et al. 2017). Our 2014 incubation experiments demonstrate that urea was used by the lake water microbial consortium (Figure 2). The decrease in urea concentration (Figure 6B) and the increase of *Microcystis* cell density (from 3.3×10^9 cells L^{-1} to 4.6×10^9 cells L^{-1} in 24 hours; about 40% increase; Table S1) in the follow-up *Microcystis* culture incubation further confirm that *Microcystis* can grow directly or indirectly on urea. The increase of cell density in urea-substrate pure culture incubation is at least at a similar level to that in the NH_4^+ incubation (from 2.7×10^9 cells L^{-1} to 3.3×10^9 cells L^{-1} in 24 hours, about 22% increase; Table S1). Together the 2014 and 2015 incubation results show that urea cycling is an important internal component in the development and success of *Microcystis* spp. dominated CyanoHAB.

Urea can be hydrolyzed either extracellularly (Skujiņš and Burns 1976; Saiya-Cork et al. 2002) or intracellularly after uptake (Solomon 2006; Solomon et al. 2010a). Hydrolysis of urea to NH_4^+ and CO_2 is mediated by either urease or ATP-dependent urea amidolyase (UALase). Our measured urea removal rates (0.04 μmol L^{-1} h^{-1} to 2.27 μmol L^{-1} h^{-1} in 2014 incubations; 0.20 μmol L^{-1} h^{-1} to 0.52 μmol L^{-1} h^{-1} in 2015 incubations; Table 1&2) and regeneration rates (non-detectable to 1.37 μmol L^{-1} h^{-1} in 2014 incubation; 0.02 to 0.28 μmol L^{-1} h^{-1} in 2015 incubation; Table 1&2) are much higher than those

reported for non-bloom water (e.g., Bronk et al., 1998; Lomas et al., 2002; L'Helguen et al., 2005), but are comparable to those measured previously under bloom conditions (e.g., Belisle, 2014; Belisle et al., 2016). A recent study suggests that non-N-fixing CyanoHABs may cause a high NH_4^+ deficiency and demand in the water (Gardner et al. 2017), which may, in turn, create a favorable situation for non-N-fixing CyanoHABs, because cyanobacteria such as *Microcystis* may use urea as a N source. The high turnover rate, especially the high removal rate of urea measured in this work is consistent with the previous conceptual model (Gardner et al. 2017), and provides another set of substrate that could potentially support *Microcystis* in Lake Taihu. Again, these results show that urea supports the development and success of CyanoHAB species *Microcystis*, but our *Microcystis*-culture experiments, shown in the following section, suggest that the effects are result of indirect rather than direct incorporation of the urea by *Microcystis.*

Effects of light on the fate of urea

Urea cycling rates in the 2014 lake water incubation varied with light conditions. Potential removal and regeneration rates were generally higher under natural light/dark cycles than in the dark (Table 1), supporting the idea that photoautotrophic processes are important to urea dynamics. The fate of urea-N also differed: in dark surface water, the added ^{15}N-urea was released as $^{15}NH_4^+$, while only sparse amounts of removed urea-^{15}N accumulated as $^{15}NH_4^+$ in the light throughout the incubation (Figure 3 C&D; Figure S1 C&D). The low recovery rate of removed urea-^{15}N to $^{15}NH_4^+$ under light condition

resembles the pattern observed in a similar urea incubation experiment conducted in the northern Gulf of Mexico (Dai et al., unpublished data).

Previous studies indicate that urea uptake is light-dependent, since the active transport of urea requires energy (Takamura et al. 1987; Solomon et al. 2010a). The energy may be obtained from photophosphorylation of phytoplankton and cyanobacteria under sun light (Rees and Syrett 1979; Siewe et al. 1998; Beckers et al. 2004), and from oxidative phosphorylation under dark (Cimbleris and Cáceres 1991). A diel pattern in urea uptake has been observed (e.g., Takamura et al., 1987; Bronk et al., 1998; Yang et al., 2017). We report here that in Lake Taihu during CyanoHABs not only the cycling rate of urea is light-dependent, but that the fate of urea is also affected by irradiation. The difference in urea fate during CyanoHAB under different irradiation conditions at Lake Taihu may have resulted mainly from the dominant cyanobacteria *Microcystis*, leading to our hypothesis that *Microcystis* spp. plays a direct role in the light-dependent urea cycling. Specifically, under natural light conditions, *Microcystis*, behaving like autotrophs, may have assimilated reduced N mainly for growth (no accumulation of NH_4^+ from urea in the water), while under dark conditions *Microcystis*, behaving heterotrophically, or other bacteria may have remineralized urea for energy and released NH_4^+ into the environment.

However, our follow-up *Microcystis* culture incubation in 2015 rejected this hypothesis. Differences in cycling rates and urea fate were not significant between different irradiation conditions (Figure 6B). Thus, *Microcystis* alone was not the main reason for the difference in urea fate. This conclusion is reinforced by bacterial community data, which can be further visualized by a "heat map" (Figure S5) constructed based on the 2014

incubation. The correlations between *Microcystis* abundance and $^{15}NH_4^+$ (NH_4^+ originated from the spiked ^{15}N-urea) as well as NH_4^+-^{15}N: removed urea-^{15}N percentage are not significant (Pearson correlation; p = 0.2222 and 0.5266, respectively; Figure S5). In contrast, heterotrophic bacteria such as *Actinobacteria*, *Proteobacteria*, and *Deinococcus-Thermus*, not only contributed to the majority of the community (Figure 5), but also correlated significantly to the NH_4^+-^{15}N: removed urea-^{15}N percentage (Pearson correlation; *Actinobacteria*, p = 0.04573; *Deinococcus-Thermus*, p = 0.02104; *Proteobacteria*, p = 0.03282; Figure S5). This data indicates that heterotrophic bacteria are crucial to urea metabolism in Lake Taihu. Furthermore, the fact that heterotrophic bacteria, rather than cyanobacteria, play an important role in urea metabolism is consistent with published studies (Wilhelm et al. 2011; Li et al. 2011; Steffen et al. 2012). We conclude that urea cycling is related closely to the success of the CyanoHAB, but that the role of *Microcystis* in urea cycling is likely indirect.

The rejection of our hypothesis returns to the question about the unexpected fates of urea under different light conditions, if it cannot be attributed to *Microcystis*. One possible explanation is the high affinity of cyanobacteria to NH_4^+ (Takamura et al. 1987; McCarthy et al. 2009; Paerl et al. 2011; Gardner et al. 2017). Under light conditions, the $^{15}NH_4^+$ generated from urea hydrolysis is taken up quickly by cyanobacteria or other phytoplankton, which leads to a low NH_4^+-^{15}N concentration relative to removed urea-^{15}N. This tight coupling has been proposed to explain the low level of individual amino acids during peptide hydrolysis in certain coastal environments, where amino acids are taken up immediately after peptides are hydrolyzed (Kuznetsova and Lee 2002; Liu et al. 2013).

Under dark conditions, however, the NH_4^+ from urea cannot be assimilated efficiently in the absence of light required for phytoplankton growth. This speculation is supported by the NH_4^+ cycling rates under different irradiation conditions (Table 2). NH_4^+ removal rate in light (0.56 μmol L^{-1} h^{-1}) is almost double of that in dark (0.29 μmol L^{-1} h^{-1}). Together, these results suggest that the *Microcystis* spp. plays an indirect role in urea cycling in Lake Taihu.

The bioinformatics tool PICRUSt utilizes the functional gene abundance and the metabolism pathways based on 16s rRNA data (Langille et al. 2013), providing more insights into interactions between urea cycling and the bacterial community in Lake Taihu. Urea transporter abundance generally decreased with incubation time (Figure 7A), as did urease for most treatments, with the exception of the surface dark treatment at station 7 (Figure 7B). The increasing urease abundance at station 7 surface dark treatment coincides with the drastic change of bacterial community as well as the high percentage of NH_4^+-^{15}N: removed urea-^{15}N, and the correlation between urease abundance and NH_4^+-^{15}N: removed urea-^{15}N percentage is significant (p = 0.0496). Urea amidolyase (urea carboxylase and allophanate hydrolase), on the other hand, shows a strong irradiation-dependent pattern, in the natural irradiation incubations (surface light at stations 7 and 10) decreasing with time, while increasing (surface dark and bottom) during dark incubations (Figure 7C&D). This result indicates that urea amidolyase may play a role in the observed diel pattern in urea cycling, and further supports the idea that heterotrophic bacteria may play a key role in the cycling of urea in the lake, since *Microcystis* spp. do not process urea amidolyase (Solomon et al. 2010a).

CONCLUSIONS

A series of microcosm incubations were conducted in Lake Taihu to investigate the metabolism of urea and how it interacts with *Microcystis* spp. during 2014 and 2015. Our data showed that urea is used by the lake bacterial consortium and supports the growth of pure *Microcystis* culture at a comparable rate to that of NH_4^+ as a N source. We demonstrate that a diel pattern of urea metabolism exists in blooms, with higher cycling rates (potential removal and actual regeneration) of urea under natural irradiation condition, but a higher fraction of the urea removed was recovered as NH_4^+ under dark conditions. This difference may result from NH_4^+ being taken up quickly by *Microcystis* and/or other phytoplankton in light, but less efficient uptake in the dark. Interestingly, the bacterial community and predicted functional genes data suggest that the direct role of *Microcystis* in urea cycling is not as important as that of heterotrophic bacteria associated with the bloom, even though *Microcystis* is the dominant cyanobacteria species in the bloom. Overall, this work provides valuable insights into the cycling of urea in Lake Taihu and other lakes experiencing CyanoHAB. It highlights the direct or indirect importance of urea in the formation and proliferation of CyanoHABs in the lake.

Table 2.1. Urea-N cycling rate calculated from 2014 incubation (SL: surface light incubation; SD: surface dark incubation; Bot: bottom incubation)

	Urea-N Regeneration Rate ($\mu mol\ L^{-1}\ h^{-1}$)	Urea-N Removal Rate ($\mu mol\ L^{-1}\ h^{-1}$)
Station1 SL	0.000 ± 0.000	0.897 ± 0.010
Station1 SD	0.000 ± 0.000	0.676 ± 0.009
Station1 Bot	0.000 ± 0.000	0.289 ± 0.047
Station3 SL	1.371 ± 1.275	2.272 ± 1.413
Station3 SD	0.355 ± 0.165	1.332 ± 0.211
Station3 Bot	0.155 ± 0.155	0.201 ± 0.041
Station7 SL	0.073 ± 0.006	0.237 ± 0.034
Station7 SD	0.002 ± 0.002	0.044 ± 0.004
Station7 Bot	0.033 ± 0.033	0.042 ± 0.029
Station10 SL	0.345 ± 0.055	0.560 ± 0.010
Station10 SD	0.341 ± 0.251	0.534 ± 0.264
Station10 Bot	0.308 ± 0.007	0.525 ± 0.044

Table 2.2. NH_4^+ and urea cycling rates calculated from 2015 *Microcystis* incubation

	NH_4^+ cycling rate (μmol L^{-1} h^{-1})		Urea-N cycling rate (μmol L^{-1} h^{-1})	
	Regeneration	Removal	Regeneration	Removal
Natural Light	0.092 ± 0.017	0.557 ± 0.008	0.024 ± 0.024	0.409 ± 0.024
Dark	0.059 ± 0.015	0.289 ± 0.016	0.277 ± 0.277	0.517 ± 0.260

Figure 2.1. Map of Lake Taihu. Sampling stations (Stations 1, 3, 7, and 10) are shown as red dots.

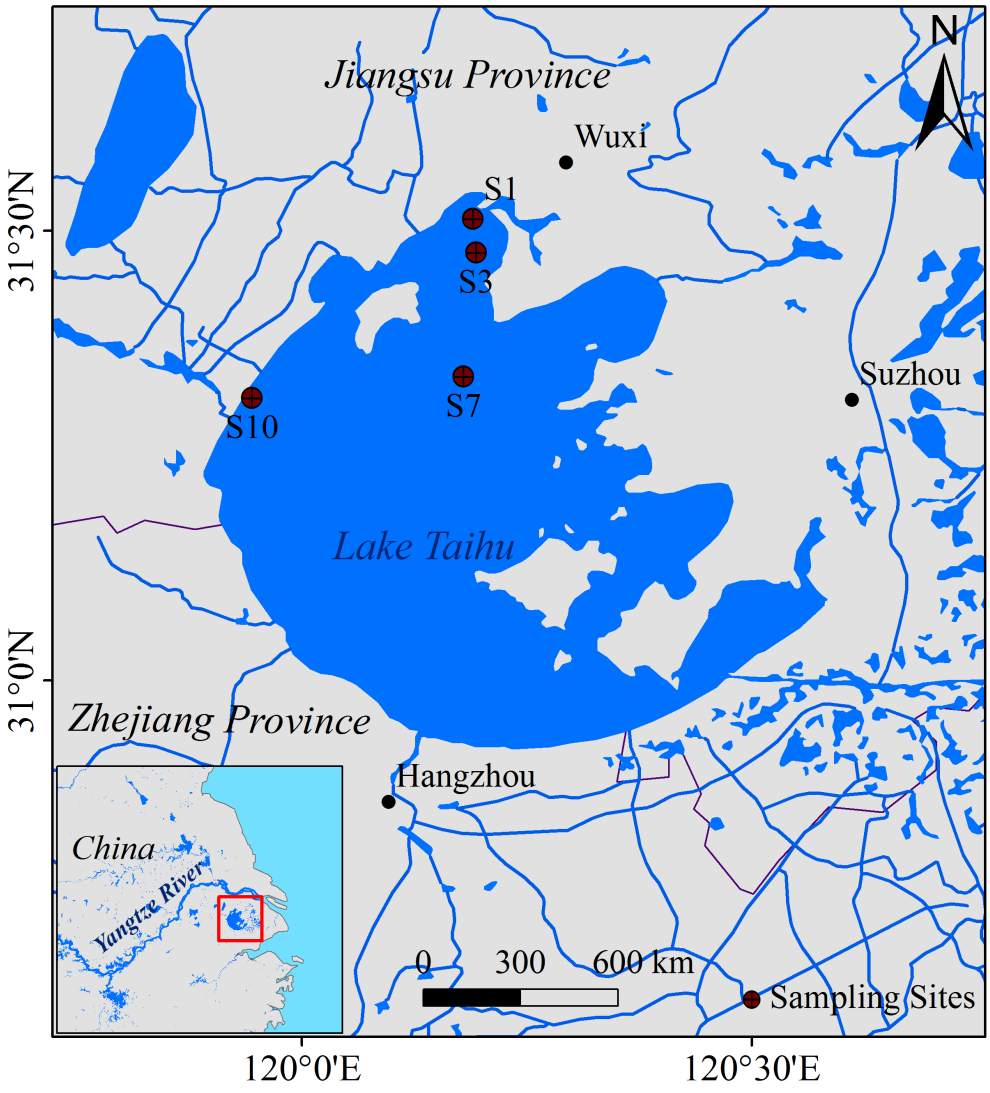

Figure 2.2. Change of urea-^{15}N concentration with time at Station 1 (A), Station 3 (B), Station 7 (C) and Station 10 (D) during the 2014 microcosm incubations. Surface Light: natural light condition; Surface Dark: dark incubation; Bottom: bottom incubation.

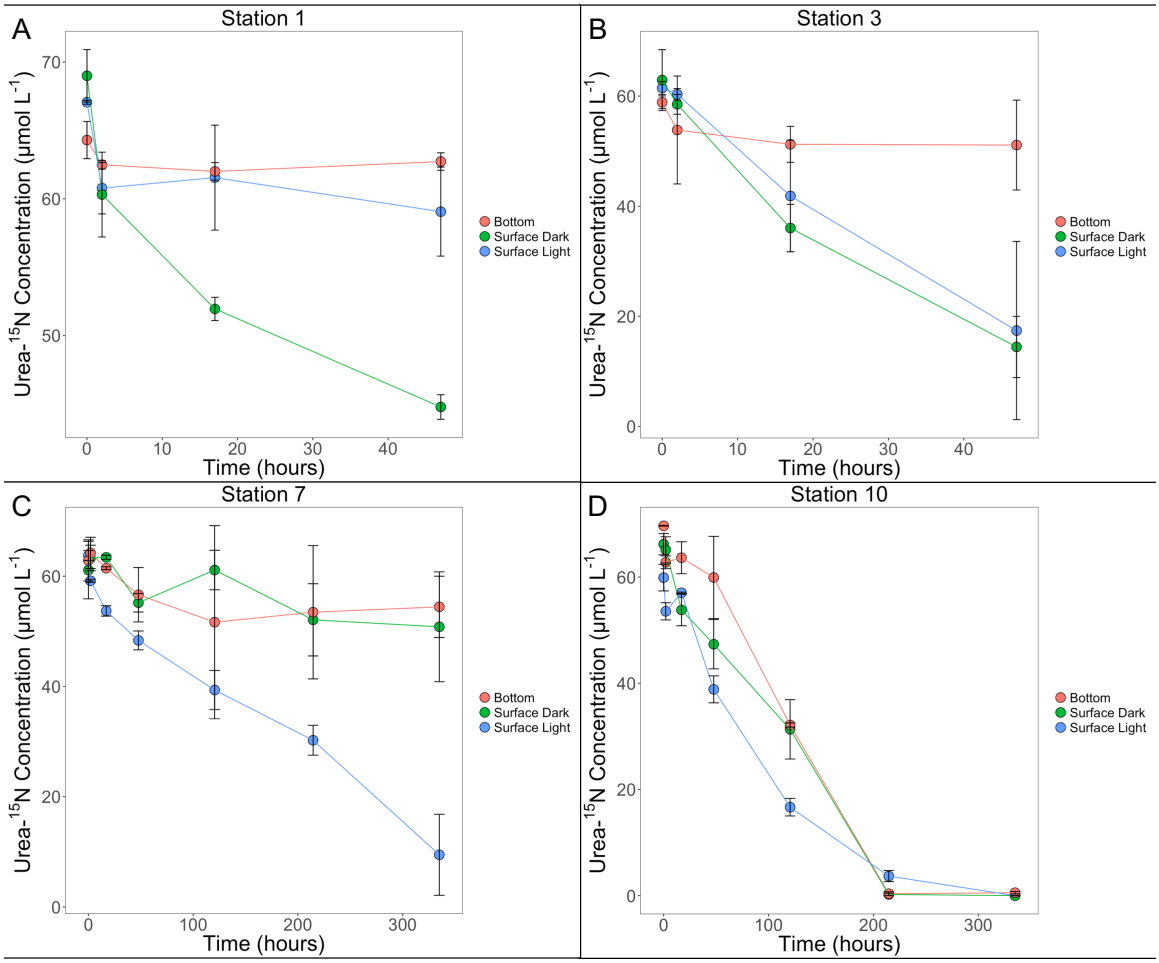

Figure 2.3. Change of NH_4^+-^{15}N: removed urea-^{15}N ratio with time at Station 1 (A) and Station 3 (B), Station 7 (C) and Station 10 (D) during the 2014 microcosm incubations. Surface Light: natural light condition; Surface Dark: dark incubation; Bottom: bottom incubation.

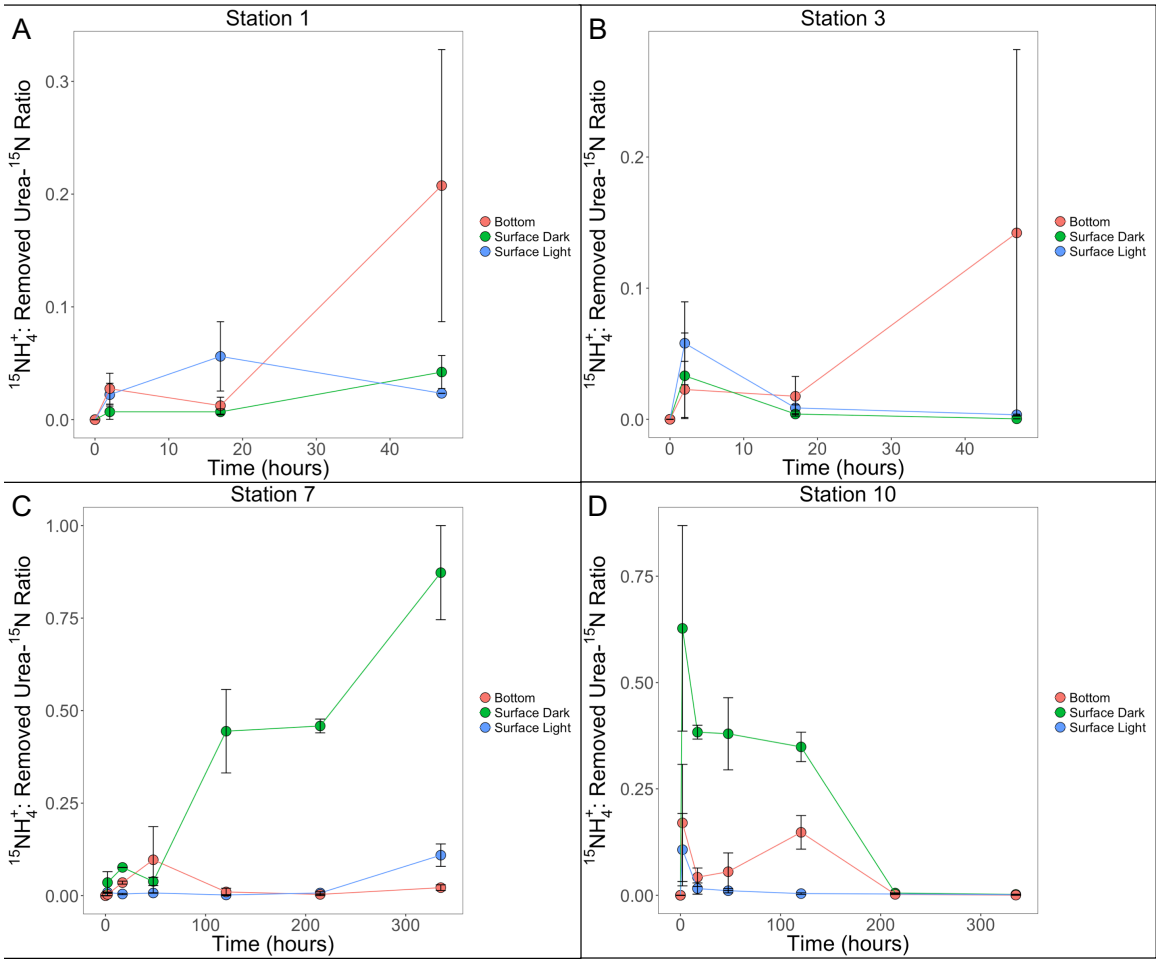

Figure 2.4. Bacterial abundance over time for short incubations: Station 1(A) and Station 3 (B); long incubation: Station 7 (C) and Station 10 (D) during the 2014 microcosm incubations. Surface Light: natural light condition; Surface Dark: dark incubation; Bottom: bottom incubation.

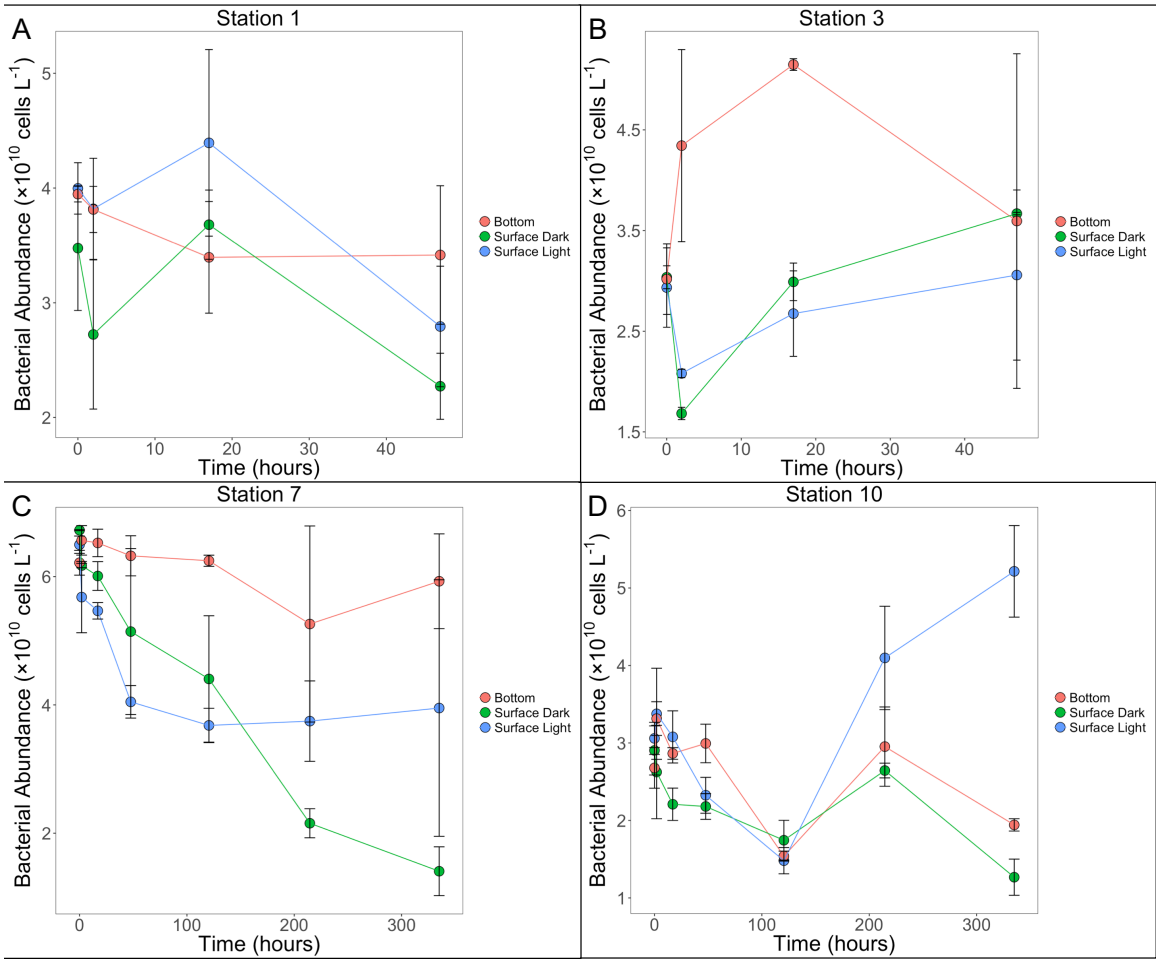

Figure 2.5. Bacterial community structure (phylum level) for incubations conducted at Stations 7 and 10 during the 2014 microcosm incubations (only 0h, 47h, and 335h samples were chosen for bacterial community analysis). Phyla that contribute less than 3% were combined together.

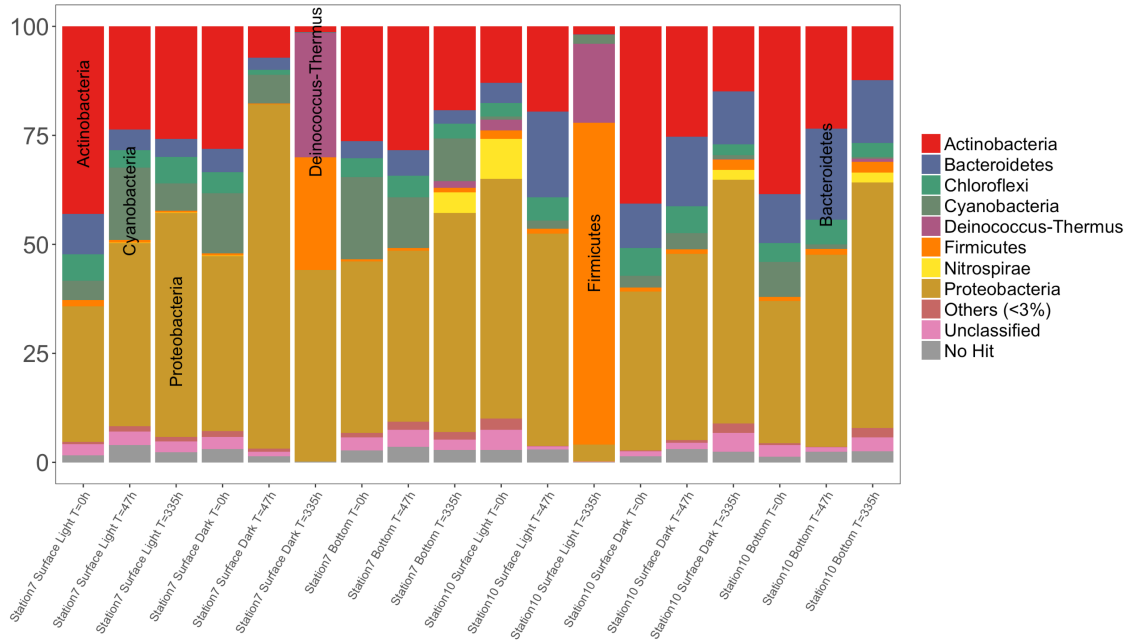

Figure 2.6. $^{15}NH_4^+$ (A) and urea-^{15}N concentration (B) with time during the 2015 *Microcystis* incubations. Control groups (filtered lake water; filtered lake water + $^{15}NH_4^+$; filtered lake water + ^{15}N-urea; filtered lake water + *Microcystis*) are not shown in the figure.

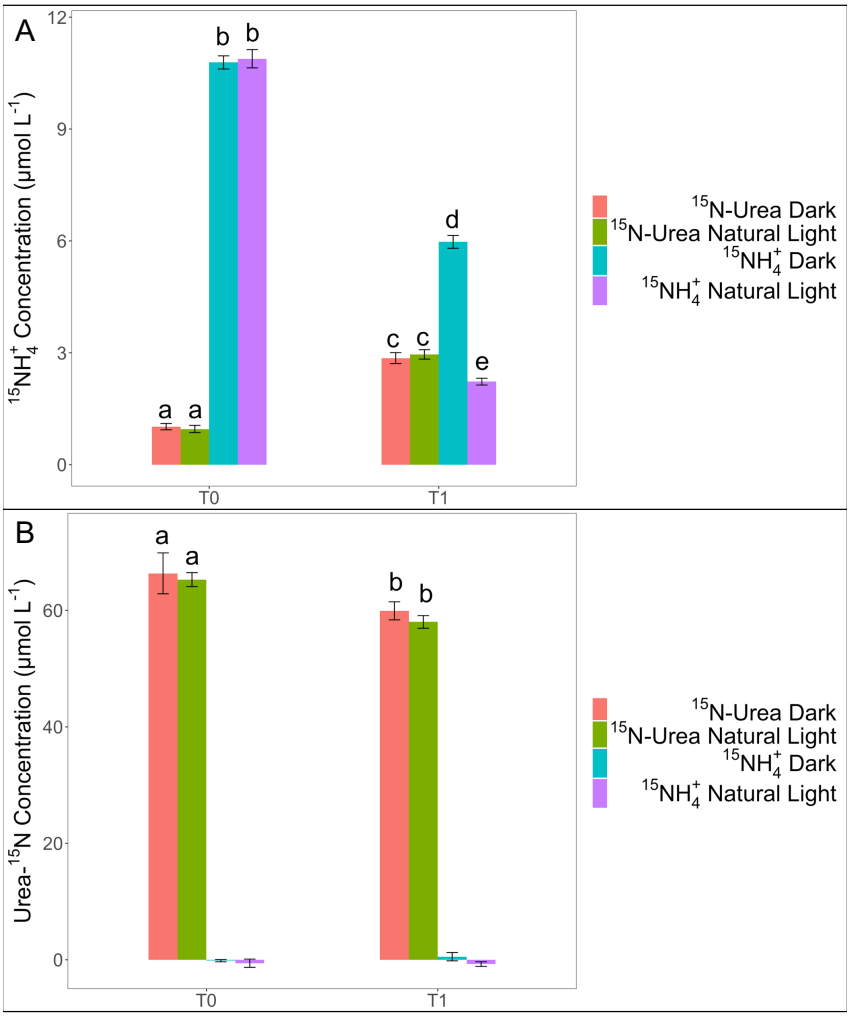

Figure 2.7. Predicted function gene abundance (normalized with *RecA*): urea transporter (A); urease (B); and urea amidolyase (urea carboxylase, C; allophanate hydrolase, D). Surface Light: natural light condition; Surface Dark: dark incubation; Bottom: bottom incubation.

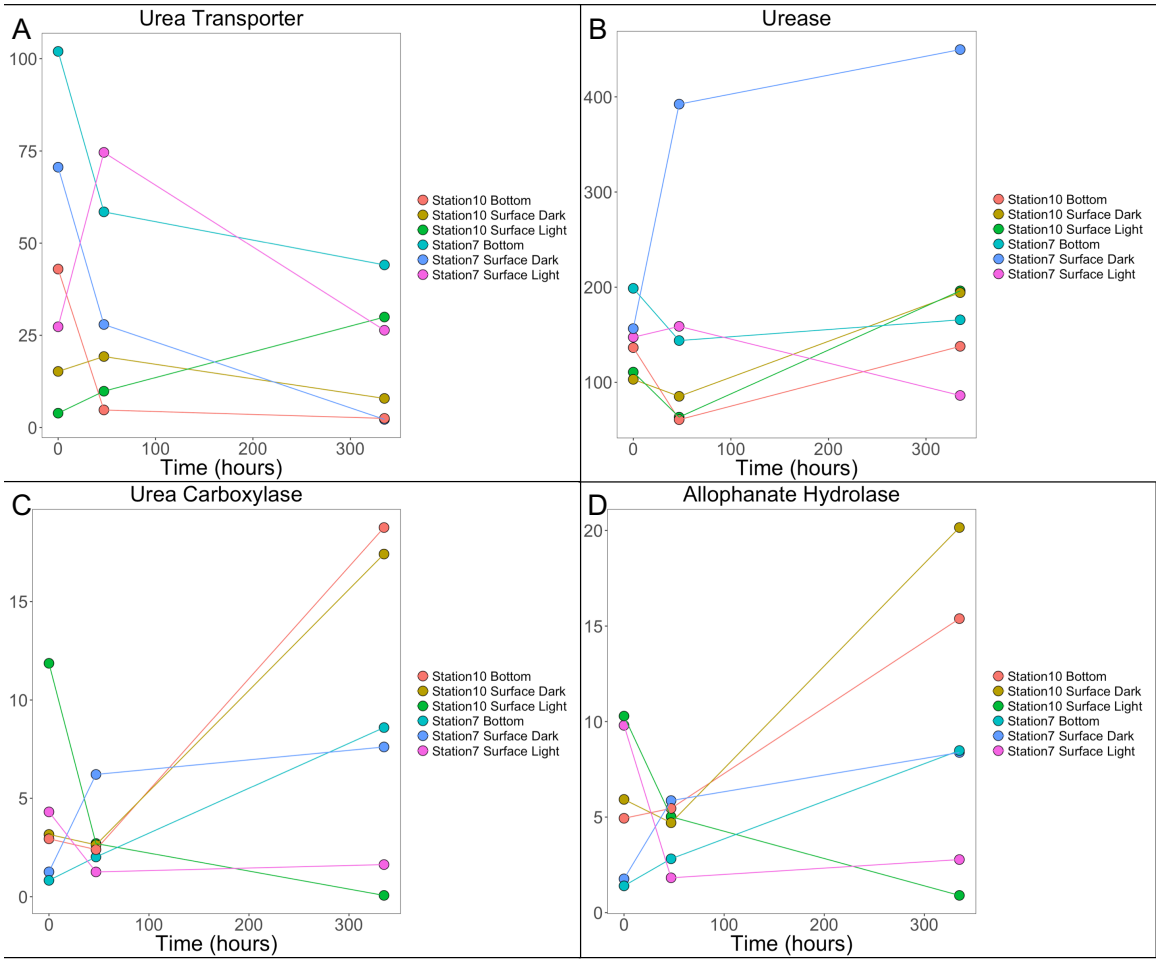

Chapter 3. A new holistic analytical method for quantifying the fates of amended ^{15}N labeled amino acids and peptides in seawater

ABSTRACT

Understanding the fate of organic nitrogen in aquatic systems is important as it relates to its recycling efficiency to inorganic forms and the long-term preservation as refractory organic forms. The fate of organic nitrogen can be investigated through ^{15}N labeling techniques, whereby the ^{15}N in different chemical forms, including ammonium, nitrite/nitrate and organic nitrogen, need to be quantified. However, it is analytically challenging to differentiate and measure ^{15}N in these forms, often with lengthy procedures and large analytical errors. We develop a new holistic method based on combining ammonium retention time shift high performance liquid chromatography (AIRTS-HPLC) with zinc reduction, UV oxidation, and ammonium oxidation membrane inlet mass spectrometry (OX-MIMS) analysis to minimize the required sample volume and simplify the overall procedure for determining concentrations of ^{15}N in different forms. This method does not require removal of inorganic nitrogen from the system, which is time-consuming. For a total ^{15}N concentration of ca. 4 μmol N L^{-1}, about 50 mL of sample is required for ^{15}N analysis of different forms, and analysis of a batch of 12 samples takes 3 days. We applied the developed method to investigate the short-term fate of ^{15}N during the degradation of a ^{15}N-labeled amino acid and peptide. With recovery rates ranging from 93% to 120%, our results show that as spiked ^{15}N labelled alanine and a peptide (Ala-Val-Phe-Val) disappeared, a fraction of ^{15}N (from ca. 13% to ca. 66% of initial ^{15}N added) was

transformed to non-amino acid or non-peptide DON. This holistic method, therefore, offers an effective and efficient way of determining the fate of labile organic nitrogen in aquatic environments.

INTRODUCTION

Dissolved organic nitrogen (DON) constitutes the largest pool of combined N (N covalently bonded to C, O, or H) in almost all marine environments, accounting for 58-77% of the total dissolved nitrogen (TDN) pool except in the deep-ocean and Southern Ocean (Berman and Bronk 2003; Sipler and Bronk 2015). DON is important to microorganisms, considering that one molecule of DON can provide them with both N and carbon (C), particularly in surface waters that are often nutrient limited (Bronk 2002; Sipler and Bronk 2015). Despite their importance, DON transformations are not well understood in nature. Systematic studies into DON dynamics has lagged far behind those of its C counterpart, dissolved organic carbon (DOC), primarily due to the substantial analytical challenges inherent in DON research. Also, isolating organic from inorganic forms of N is more complicated than for C which only requires simple acidification to remove inorganic forms.

Controlled incubation experiments are applied widely for studying DOM dynamics (e.g., Brophy and Carlson 1989; Moran and Hodson 1989; Heissenberger and Herndl 1994; Ogawa et al. 2001; Gruber et al. 2006). By tracking the disappearance of spiked substrate (generally labile DOM) and the production of "new" DOM, controlled incubation experiments provide a way to examine mechanisms of DOM metabolism: how DOM is utilized, how it is produced, and most importantly why some DOM can persist over millenary time scales (e.g., Ogawa et al. 2001; Arrieta et al. 2015).

Applying controlled incubations to DON studies could be challenging. Unlike C, dissolved N often occurs in various forms (NH_4^+, NO_2^-, NO_3^-, and DON) in aquatic

environments. A better understanding of the fate of N during incubation requires a quantitative measurement of different N forms in natural waters. In addition, rapid turnover rates of N caused by high biological demand indicates that simple measurements of N compound concentrations are not sufficient to reflect the production or consumption rates of DON because both processes often occur simultaneously (Isobe et al. 2011; Gardner et al. 2017). Under this scenario, researchers often have to rely on the ^{15}N labelling technique to determine the dynamics of DON in natural waters. ^{15}N enrichment techniques are essential to quantify the transformation rate of N from source to sink and trace the fate of N through the N cycle (Knowles and Blackburn 1993; Bedard-Haughn et al. 2003; Leinweber et al. 2013). The common approach to determine ^{15}N in different forms is to use elemental analyzer-isotope ratio mass spectrometry (EA-IRMS) after converting the target N compound(s) to a gaseous N-species (usually N_2). This technique is robust and reliable, but is labor-intensive (Bronk 2002). It requires a number of complex preparation process prior to mass spectrometer analysis and also requires sample sizes of hundreds of mL (Toshihiro et al. 2005; Isobe et al. 2011) for sufficient analytical sensitivity in ^{15}N-spiked studies, due to the high background concentration of N_2 gas.

Alternative methods for ^{15}N analysis are needed to simplify sample preparation and handle samples with limited volume. Toshihiro *et al.* (2005) developed a method for ^{15}N analysis by derivatizing NO_3^- with pentafluorobenzyl bromide (PFB-Br) and analyzing the nitric acid ester of PFB-alcohol (PFB-ONO_2) using gas chromatography mass spectrometry (GC-MS). With different forms of ^{15}N was transformed into $^{15}NO_3^-$ prior to analysis, concentration of each ^{15}N form can be determined. This method does not require a

measurement of $^{15}N_2$ gas, and thus has reduced the required volume for DON analysis to 10 mL or less, and has achieved a sensitivity of as low as 0.015 μmol ^{15}N L^{-1}. Likewise, Isobe *et al.* (Isobe et al. 2011) introduced another new method for ^{15}N analysis by applying a special gene-knockout denitrifying bacteria to reduce NO_3^- to N_2O gas (Sigman et al. 2001), which is subsequently analyzed via GC-MS. This method has greatly reduced the amount of laboratory work and is applicable to a rather wide range of N concentration (1 to over 150 $\mu mol \cdot L^{-1}$).

Most current methods for $DO^{15}N$ analysis require an isolation of NH_4^+ from the original sample by converting NH_4^+ to NH_3 at a high pH followed by purging and subsequent acidic trapping of NH_3. Alkaline removal of NH_4^+ is time consuming (takes 7 to 14 days to complete; e.g., Slawyk and Raimbault 1995; Toshihiro et al. 2005; Isobe et al. 2011), and may be affected by sample salinity. Isolation of NH_4^+ at elevated temperature under alkaline conditions may also potentially lead to degradation or hydrolysis of labile organic nitrogen such as peptides and amines (Toshihiro et al. 2005). Furthermore, concern has been raised about the incomplete removal and the subsequent carry-over of inorganic NH_4^+ into other N pools (Slawyk and Raimbault 1995). To overcome these issues, an analytical method without the need for prior NH_4^+ isolation from the rest of the sample is needed.

The goal of this study is to develop a new holistic method to quantitatively determine concentrations of different forms of ^{15}N, including NH_4^+, NO_2^- and NO_3^-, and DON efficiently. We improved conventional ^{15}N analytical methods by applying AIRTS-HPLC (Gardner et al. 1991, 1995). With this new overall protocol, we can (1) quantify

$^{15}NH_4^+$ in sample/standard without isolation via the conventional alkaline method; (2) measure ^{15}N in different forms in small-volume samples (≤ 50 mL required in total); and (3) quantify the fate of N in laboratory incubations.

MATERIALS AND METHODS

A comprehensive scheme depicting the procedures for the measurements of different forms of ^{15}N is presented in Figure 3.1. Briefly, $PO^{15}N$ on the GF/F filter is analyzed with EAIRMS. $^{15}NH_4^+$ is analyzed with AIRTS-HPLC; $^{15}NO_x$ is analyzed with AIRTS-HPLC after Zn reduction; and $DO^{15}N$ is analyzed with AIRTS-HPLC or OXMIMS after UV-oxidation and Zn reduction. Error propagation is a potential problem, as $^{15}NO_x$ and $DO^{15}N$ concentration is calculated by the difference between $DI^{15}N$ and $^{15}NH_4^+$, and the difference between $TD^{15}N$ and $DI^{15}N$, respectively. However, a direct measurement of each component will require pre-isolation steps (i.e., removal of NH_4^+), which could be even more problematic as mentioned above. In this case, we choose to calculate the concentration of different ^{15}N forms by mass balance.

Reagents

Reagents for HPLC analysis of NH_4^+ and NO_2^- + NO_3^- (NO_x^-) were prepared following the protocols of Gardener et al. (1993, 1995). Reagents for membrane inlet mass spectrometry (MIMS) analysis of NH_4^+ were prepared following Yin et al. (2014). A hydrogen peroxide solution (H_2O_2; 30%) was used to facilitate the UV oxidation process. Standards including NH_4Cl (natural abundance), $^{15}NH_4Cl$ (≥ 98 atom %), $NaNO_3$ (natural

abundance), $Na^{15}NO_3$ (≥ 98 atom %), ^{15}N-urea (98 atom %) and ^{15}N-L-Alanine (98 atom %) were purchased from Sigma Aldrich.

A boric acid mobile phase buffer for AIRTS-HPLC was prepared following a published protocol (Gardner et al. 1993, 1995). Briefly, 24 g of NaCl, 24 g of boric acid and 1.6 g of EDTA were dissolved in 2 L deionized water (DI water). 10 mL Brij 35 was added to lubricate the HPLC pump seals (Gardner et al. 1993). The pH of the buffer was adjusted to 9.41 using 50% NaOH solution. The buffer was filtered through 0.2 μm pore size nylon filter to maintain steady chromatographic conditions.

The OPA reagent for AIRTS-HPLC measurement was modified from previous studies (Gardner et al. 1991, 1995). Sixty grams of boric acid were dissolved in DI water and the volume was adjusted to 2 L. It was then mixed with a solution of 1 g of OPA dissolved in 20 mL ethanol and 1 mL 2-mercaptoethanol. 10 mL Brij 35 was added for pump-seal lubrication, and the pH of reagent was adjusted to 7.00 with KOH. The reagent was filtered through a 0.45 μm pore size nylon filter before use. This OPA reagent was good for ca. one week.

The hypobromite iodine solution used in MIMS measurement was prepared following published protocol (Yin et al. 2014). A volume of 600 mL 16 mol L^{-1} NaOH solution was mixed with 100 mL Br_2 at a temperature below 5 °C. NaBr crystals that precipitated were removed from the solution by filtration after one-week settling at 4 °C. Filtered solution was then mixed with an equal volume of KI solution (0.2%, w/v) to maintain stability. The oxidant solution can last for months if kept at -20 °C.

Particulate organic ^{15}N ($PO^{15}N$) analysis

A known volume (ca. 50 mL) of water sample was filtered through a pre-combusted 0.7 μm GF/F filter. The filter was placed in plastic petri-dish and treated with HCl via acid fumigation to remove inorganic carbon, and the filtrate was preserved for subsequent dissolved N analysis. $PO^{15}N$ on the filter was measured with an elemental analyzer coupled with a mass spectrometer (EA-IRMS) the main campus of UT Austin as described previously (e.g. Mercado et al. 2010). Peach leaves (NIST SRM 1547) served as the standard, and helium was used as the carrier gas. The total amount of $PO^{15}N$ was calculated by comparing the peaks of $^{29}N_2$ and $^{30}N_2$ with the standard. The precision (repeatability) for PON was within 1 % of the mean value.

$^{15}NH_4^+$ and $^{15}NO_x^-$ analysis

$^{15}NH_4^+$ was analyzed using the ammonium isotope retention time shift high performance liquid chromatography (AIRTS-HPLC) technique (Gardner et al. 1991, 1993, 1995). The brief principle is that $^{15}NH_4^+$ passes through a cation exchange column slightly slower than $^{14}NH_4^+$. The cation exchange column efficiency is not sufficient to completely separate $^{15}NH_4^+$ from $^{14}NH_4^+$, but the ratio of $^{15}NH_4^+$: total NH_4^+ is reflected in the shift in retention time, with larger retention time delay representing higher ratio of $^{15}NH_4^+$ (Gardner et al. 1991). Thus, "retention time shift" is defined as the difference between the sample retention time shift relative to that of a natural abundance internal standard. Organic N normally has minimal effects on results, because the cation exchange column isolates NH_4^+ and $^{15}NH_4^+$ from other primary amines and amino acids.

Less than 5 mL of sample is required for the $^{15}NH_4^+$ analysis, and each sample was run in triplicate. Sample was filtered immediately before analysis with a micro sample-filtering device (Gardner and Vanderploeg 1982). The fluorometric response of OPA-NH_4^+ derivative was measured by a fluorimeter (Gardner et al. 1991). Concentration of total NH_4^+ is calculated by comparing peak area of sample with peak area of internal NH_4^+ standard, and the ratio of $^{15}NH_4^+$ is calculated by comparing the retention time shift with a calibration curve established for each batch run using standard solutions with the same salinity as the samples.

NO_x^- (NO_2^- + NO_3^-) in the sample/standard was reduced to NH_4^+ by reacting with Zn under acidic conditions (Gardner et al. 1995; Carini et al. 2010). Briefly, 15 mL of sample/standard was acidified with 2 M H_2SO_4 (ca. 140 μL) to reach a pH of 2. An excessive amount of Zn powder (ca. 150 mg) was added. This approach was convenient and avoided the potential problem of NH_4^+ carry-over when sample volume is small (ca. 15 mL; Gardner et al. 1995) compared with the traditional Zn column method (over 200 mL; Axler and Reuter 1987). The vial was then capped and shaken vigorously before incubation at room temperature on a shaker table at 75 rpm for at least 30 min (Carini et al. 2010). To avoid potential matrix effects, 3 mL of boric acid mobile phase buffer (pH 9.41) was added to the vial to increase the pH. A precipitate of $Zn(OH)_2$ formed as pH increased. The vial was then shaken and allowed to settle for at least 15 min. The sub-sample was ready for AIRTS-HPLC analysis after it was passed through a 0.2 μm pore size nylon filter. NO_x^- concentration and $^{15}NO_x^-$ isotopic ratio were calculated after subtracting

NH_4^+ and $^{15}NH_4^+$ concentration from the total dissolved inorganic N pool, respectively. No fractionation was detected in the Zn reduction process.

Dissolved organic ^{15}N ($DO^{15}N$) analysis

DON in the water sample was oxidized to NO_3^- using a constructed UV-oxidation apparatus following the design in a published study (Armstrong and Tibbitts 1968). The 1200 W mercury vapor lamp (P/N: PC122.120) and the ballast (P/N: 34966001) were purchased from Hanovia. ^{15}N-Ala and ^{15}N-urea served as reduced organic N standards in this work, as recommended previously (Bronk et al. 2000).

Briefly, 20 mL of sample or standard was transferred into a quartz tube, and 200 μL of H_2O_2 (30%) was added to facilitate the oxidation process (Armstrong and Tibbitts 1968; Bronk et al. 2000). The tube was capped and shaken vigorously and was irradiated for 24 h. To avoid potential issues in the subsequent reduction reaction, oxidized sample or standard was kept in a 4 ºC fridge for at least 24 h before further reducing to NH_4^+ via Zn reduction as described above. No fractionation was reported in the UV oxidation process so far.

The reduced sample or standard was analyzed via AIRTS-HPLC as described above, in which DON concentration and $DO^{15}N$ isotopic ratio were calculated after subtracting the DIN ($NH_4^+ + NO_x^-$) measured in previous steps from the total N pool. As an alternative choice, $TD^{15}N$ concentration can be analyzed with MIMS using the OX-MIMS technique (Yin et al. 2014). After UV oxidation and subsequent Zn reduction, samples were oxidized with ca. 0.2 mL hypobromite iodine solution. All ^{15}N was

transformed into N_2 gas ($^{30}N_2$ and $^{29}N_2$), which can be measured with a MIMS as $TD^{15}N$. Concentration of $DO^{15}N$ was calculated by subtracting $DI^{15}N$ from measured $TD^{15}N$.

Incubation experiment

Two controlled incubation experiments were conducted to test the proposed N analytical method, and to investigate the fate of N over a short incubation time (< 4 days). Coastal water samples were collected from (1) a Ship Channel site (27.84° N, 97.05° W) in Port Aransas, Texas, connected to the open Gulf of Mexico (GOM), and (2) a northern GOM (28.85º N, 90.37º W) site in the Mississippi River plume in June 2015 and May 2016, respectively. ^{15}N-alanine (^{15}N-Ala; $C_3H_7{}^{15}NO_2$) was used in the 2015 incubation experiment, while ^{15}N-tetrapeptide Alanine-Valine-Phenylalanine-Alanine (^{15}N-AVFA; $C_{20}H_{30}{}^{15}N_4O_5$) was used for the 2016 incubation experiment. AVFA is a fragment of RuBisCO, and its decomposition and hydrolysis in coastal waters have been well studied (Liu et al. 2013; Liu and Liu 2015b, 2016). The initial concentration of ^{15}N-Ala was ca. 10 $\mu mol \cdot L^{-1}$ in the 2015 incubation experiment. The initial concentration of ^{15}N-AVFA was ca. 1 $\mu mol \cdot L^{-1}$ in the 2016 experiment, equivalent to a ^{15}N concentration of 4 $\mu mol \cdot L^{-1}$. In the Ala incubation, $DO^{15}N$ was measured using AIRTS-HPLC while in AVFA incubation, $DO^{15}N$ was measured using OX-MIMS.

Aliquots of collected water were transferred into pre-combusted amber glass bottles. Samples were incubated in the dark at near *in situ* water temperature. Subsamples were taken for ^{15}N analysis at designated time points (0 h, 12 h, 24 h, and 48 h for the Ala incubation; 0 h, 24 h, 43 h, and 86 h for the AVFA incubation).

ASSESSMENT

AIRTS-HPLC analysis of $^{15}NH_4^+$ and $^{15}NO_x^-$

Using AIRTS-HPLC to measure $^{15}NH_4^+$ and Zn-reduction with subsequent AIRTS-HPLC to measure $^{15}NO_x^-$ in ^{15}N-amended samples was described previously (i.e., Gardner et al. 1995; McCarthy et al. 2007, 2015; Carini et al. 2010; Lin et al. 2011). The assessment section here will focus on the oxidation of DON to NO_3^-.

Persulfate oxidation of DON

Three commonly applied conventional methods to convert DON to NO_3^- include: persulfate oxidation (PO), UV-oxidation, and high temperature oxidation (Bronk et al. 2000), and each of them has its own advantages and disadvantages. Persulfate oxidation provides the highest recovery rate, but has high blank values and cannot oxidize refractory DON effectively (Bronk et al. 2000). In contrast, UV-oxidation generates very low blanks, but recovery rates are sometimes inconsistent (Bronk et al. 2000). Persulfate oxidation and UV-oxidation were both evaluated in this effort.

Persulfate oxidation was performed following the published protocols (Valderrama 1981; Bronk et al. 2000). The standard solution was autoclaved for 30 min at 121 ºC and a pressure of 15 $lb \cdot in^{-2}$. After oxidation, Zn reduction was performed following the procedure described above. However, the results showed that concentrations of total N obtained from AIRTS-HPLC were much higher than the amount spiked, and no relationship between retention time shift and ^{15}N ratio could be established (data no shown).

It remains unclear what could have caused this inconsistency, but atmospheric N_2 might interfere with the N analysis, even though the oxidation of N-N triple bond is not

very efficient (Nydahl 1978; Valderrama 1981). Atmospheric N can react with persulfate reagent, thus producing NO_3^- during autoclaving (Hagedorn and Schleppi 2000). Conversion of N_2 into NO_3^- may explain why the measured N concentration was much higher than the amount spiked. It also offers a reasonable explanation to the lack of linear relationship between ^{15}N ratio and RTS in HPLC. The amount of ^{15}N spiked in the standard was negligible compared with the amount of ^{14}N in the atmosphere, resulting in an actual ^{15}N ratio close to natural abundance, which is beyond the detection limit of AIRTS-HPLC. Besides the interference from atmospheric N, matrix may be another factor. An alkaline environment is required for persulfate oxidation of N, which might have conflicted with the subsequent Zn reduction that occurs in an acidic environment.

Finding out the exact reason of the failure in persulfate oxidation for $DO^{15}N$ analysis is beyond the scope of this work. Nevertheless, it shows us that persulfate oxidation is not appropriate for the purpose of this work.

UV oxidation of DON

UV oxidation is much cleaner than persulfate oxidation in terms of matrix, as H_2O_2 is the only chemical added. A clean matrix is critical to the analysis of $^{15}NH_4^+$ using AIRTS-HPLC (Gardner et al. 1991, 1995).

Though previous studies suggested that the oxidation of organic matter by UV is completed generally within 2 to 3 h with a 1200 W lamp (Armstrong and Tibbitts 1968), our samples were oxidized in the UV chamber for 24 h to ensure a complete conversion of all N to NO_3^- (Gardner and Stephens 1978). To test oxidation efficiency, a natural DOM

sample collected from a plant leachate experiment with known DON concentration was diluted to make a standard with salinity of 35‰ (by addition of NaCl). The recovery efficiency was evaluated by comparing the "measured concentration" of NH_4^+ produced after UV oxidation and subsequent Zn reduction, with the "actual concentration". The recovery rate for the natural DON we tested was about 78% (Figure 3.2). At low concentrations ($N < 8$ $\mu mol \cdot L^{-1}$), our method often overestimated the DON concentration in the sample, while at high concentrations ($N > 20$ $\mu mol \cdot L^{-1}$), the method often underestimated the DON concentration. The calculated recovery rate was lower than for other methods (i.e., ca. 95% in Toshihiro et al. 2005), but comparable to the reported recovery rate for UV oxidation method (Bronk et al. 2000). In addition, the linearity of the calibration curve ($R^2 = 0.997$; Figure 3.2) indicates that the concentration of N in samples can be calculated accurately if calibration standards are run together with samples in the same batch. Since AIRTS-HPLC requires standards for the calculation of isotopic ratios, adding standards in the run does not increase the work load or increase the analysis time.

We also examined recovery of several other organic N compounds in nanopure water with salinity adjusted to 35‰ by NaCl. Organic N standards were prepared with: (1) tetrapeptide AVFA, (2) bovine serum albumin (BSA), (3) a natural DOM sample with known DON concentration, and (4) urea. Recovery rates for different compounds ranged from 89.9% to 101.1%, with the lowest recovery rate for AFVA, and the highest for urea (Figure 3.3). The tendency to underestimate high concentration was apparent. In contrast to our results, urea was only partially oxidized by UV in early studies (Armstrong and Tibbitts 1968). This problem was overcome by the application of a high-power mercury

arc lamp (1200 W) and an extended oxidation time (24 h) in our method. Using persulfate oxidant solution to replace H_2O_2 could increase the oxidation efficiency of UV (Bronk et al. 2000), but was not suitable for our system due to the matrix issue concern for HPLC analysis.

As mentioned above, the isotopic ratio of ^{15}N in the sample/standard by AIRTS-HPLC is calculated by comparing the retention time shift with a calibration line established in each batch run. To examine the linearity of the calibration line, ^{15}N-urea and ^{15}N-Ala were used as known isotopic ratio standards. Both of these standards generated a robust calibration line, with R^2 of 0.9994 for ^{15}N-urea (Figure 3.4A) and R^2 of 0.9998 for ^{15}N-Ala (Figure 3.4B). The high linearity of the calibration line indicates that the oxidation of organic N using UV does not further fractionate the N.

Overall, this UV oxidation with subsequent Zn reduction and AIRTS-HPLC analysis provides a reliable and accurate measurement of the ^{15}N concentration in the sample.

Application to incubation experiments

The proposed method, as shown in Figure 3.1, was applied to incubation experiments to (1) test its application in field studies further, and (2) investigate the fate of N during the decomposition of amino acids and peptides. Incubations of alanine were conducted using unfiltered surface water (salinity ca. 20‰) collected from the Ship Channel near the University of Texas Marine Science Institute, and the initial concentration of added ^{15}N-Ala was 10 $\mu mol \cdot L^{-1}$ (equivalent to 10 $\mu mol\ N\ L^{-1}$). Our preliminary

experiments illustrated that $PO^{15}N$ generally constituted only a minor fraction (≤ 2%) of the total ^{15}N pool (data not shown). This low $PO^{15}N$ percentage observed is consistent with the low PON concentrations and percentages reported in other studies (Bronk et al. 2007; Sipler and Bronk 2015). During the incubation, alanine disappeared within 12 h, as indicated by the quick concentration drop (Figure 3.5A). Rapid accumulations of $^{15}NH_4^+$ and uncharacterized $DO^{15}N$ (DON other than alanine) were detected with the decrease in ^{15}N-Ala concentration, indicating that the spiked Ala-^{15}N was transformed to other forms. On the other hand, the concentration of $^{15}NO_x^-$ was < 4% of the initial spiked ^{15}N in the system. This observation is consistent with previous incubation experiments (e.g., Liu et al. 2013), in which the fate of N was calculated based on mass balance. The $DO^{15}N$ detected in the sample, about 50% of the initial ^{15}N-Ala added, is not alanine, as no free alanine was detected with HPLC fluorescence detention (Lee et al. 2000; Liu et al. 2013). One possible explanation may be that these $DO^{15}N$ originated from the modification of original spiked alanine, and that these amino acid-derived molecules were structurally altered and no longer captured by the amino acid analysis, as suggested by a previous molecular level dissolved organic matter study (Liu et al. 2011).

A tetrapeptide (AVFA) incubation was conducted using unfiltered surface seawater collected from station C6 in the northern GOM, and the initial concentration of AVFA was 1 $\mu mol \cdot L^{-1}$ (equivalent to 4 $\mu mol\ N\ L^{-1}$). Unlike amino acid alanine, AVFA disappeared at a much slower rate (Figure 3.5B), with total peptide and amino acid fragments gone by 87 hours. Similarly, the $^{15}NH_4^+$ and uncharacterized $DO^{15}N$ (DON other than peptide or amino acid) represented 55% and 45% of added ^{15}N at the end of the incubation, and very low

percentage of added ^{15}N (less than 7% at 24 h and 0 in the rest time points) was recovered as $^{15}NO_x^-$ throughout the incubation. The early appearance of other DON in the alanine and AVFA incubation is consistent with previous findings (Liu et al. 2017b). The structure of these other DON compounds is unknown. Further studies are needed to elucidate the molecular level information and long-term fate of these newly formed DON compounds.

The overall recovery rate of two sets of incubation experiments varied from 93.4% to 120.0%. These incubation experiments showed that the fate of ^{15}N can be accurately quantified by our method.

COMMENTS AND RECOMMENDATIONS

The proposed method is generally more cost-effective and timesaving than the conventional methods for determining ^{15}N in different forms (e.g., Axler and Reuter 1987; Slawyk and Raimbault 1995; Hasegawa et al. 2000). Conventional methods, and even newly developed methods (Toshihiro et al. 2005; Isobe et al. 2011), require complex preparation processes, such as the alkaline isolation of NH_4^+ as NH_3 and subsequent trapping of NH_3 to ammonium salt, which not only is the rate-limiting step (Toshihiro et al. 2005; Isobe et al. 2011), but also is problematic in terms of NH_3 carry-over to other N pools (Slawyk and Raimbault 1995), and the potential loss of labile organic N such as amino sugars, amino acids and amines (Toshihiro et al. 2005).

Our method offers an alternative way to analyze $^{15}NH_4^+$ in the sample through HPLC. Each sample takes about 40 min to run. With the current set-up in the lab, 6 samples (each sample run in triplicate, and a three-point standard curve is required for either batch)

can be handled by HPLC in one day. The high throughput OX-MIMS method recently developed (Yin et al. 2014) can be used in TD^{15}N/DO^{15}N analysis, but is not applicable to analyze $^{15}NH_4^+$ alone. The hypobromite iodine solution is capable of oxidizing some labile organic N along with NH_4^+, which could cause potential error to the analysis.

Rate-limiting step in the proposed method is the oxidation of DON and triplicated measurements of samples by AIRTS-HPLC. Our constructed UV oxidation apparatus now is capable of oxidizing 6 samples per day but it could be upgraded to 12 samples per day with modification. However, this number is still quite low compared with persulfate oxidation. One possible way to overcome this issue is to combine with high throughput method. For instance, DI^{15}N could be analyzed with this method, while DO^{15}N can be measured using a combination of persulfate oxidation (oxidize all N to NO_3^-), Zn reduction (reduce all NO_3^- to NH_4^+) and OX-MIMS (oxidize all NH_4^+ to N_2 gas).

Overall, the methodology we developed in this work provides an effective way to analyze the ^{15}N in different forms in aqueous samples. Compared with conventional approaches, this proposed method eliminates the need of the time-consuming pretreatments for NH_4^+ isolation, and requires a much smaller volume of sample to analyze different forms of ^{15}N. Furthermore, using HPLC to analyze NH_4^+ and NO_x^- in the sample provides a foundation that can be expanded for future research, and the merit of the experiment will be enhanced. This method is particularly useful in evaluating the fate of N from labile organic nitrogen, and the formation mechanisms of semi-labile and refractory DON in aquatic environments.

Figure 3.1. A scheme showing all the steps of the process.

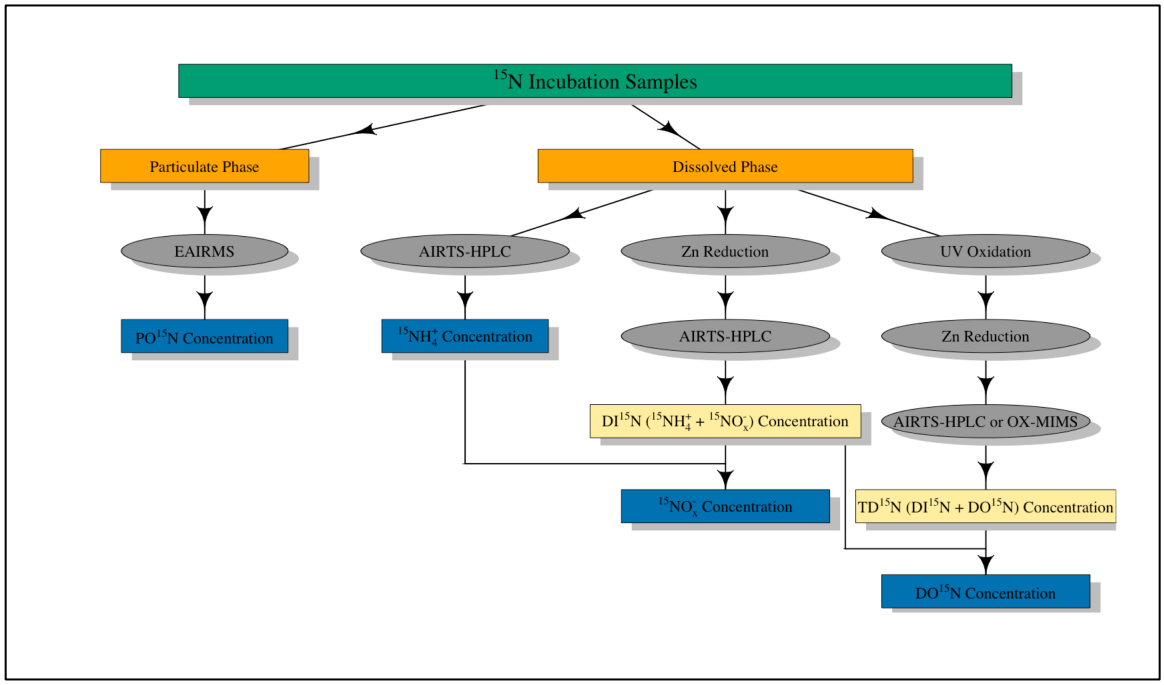

Figure 3.2. Calibration curve established using a natural DON sample as standard.

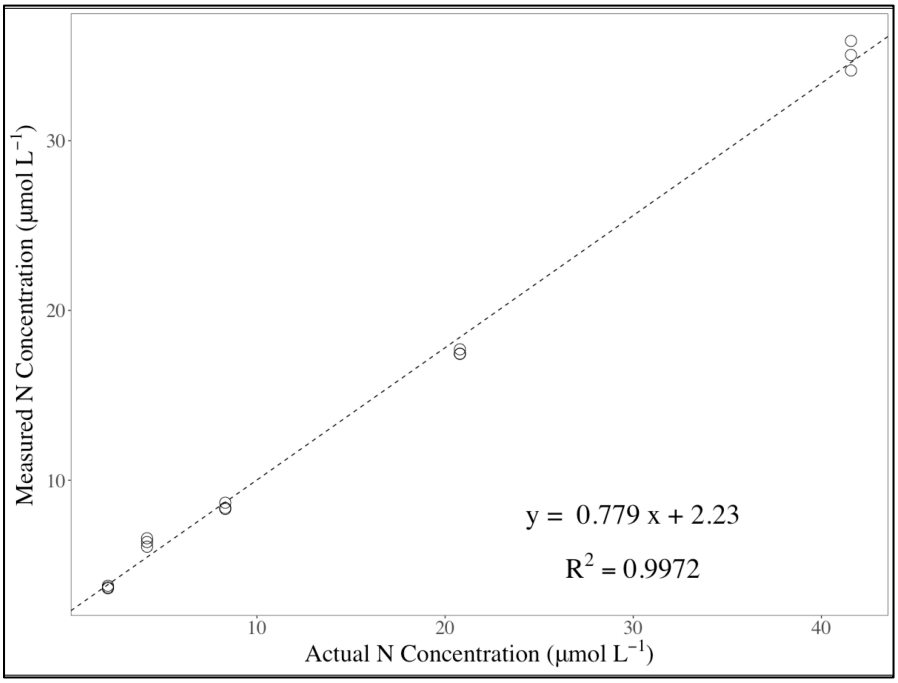

Figure 3.3. Recovery rates of different DON compounds. Open circles represent concentration from each measurement. Grey circles represent the mean of the individual measurements, with error bars as SE. Red circles represent the actual concentration. The numbers are recovery rates (%).

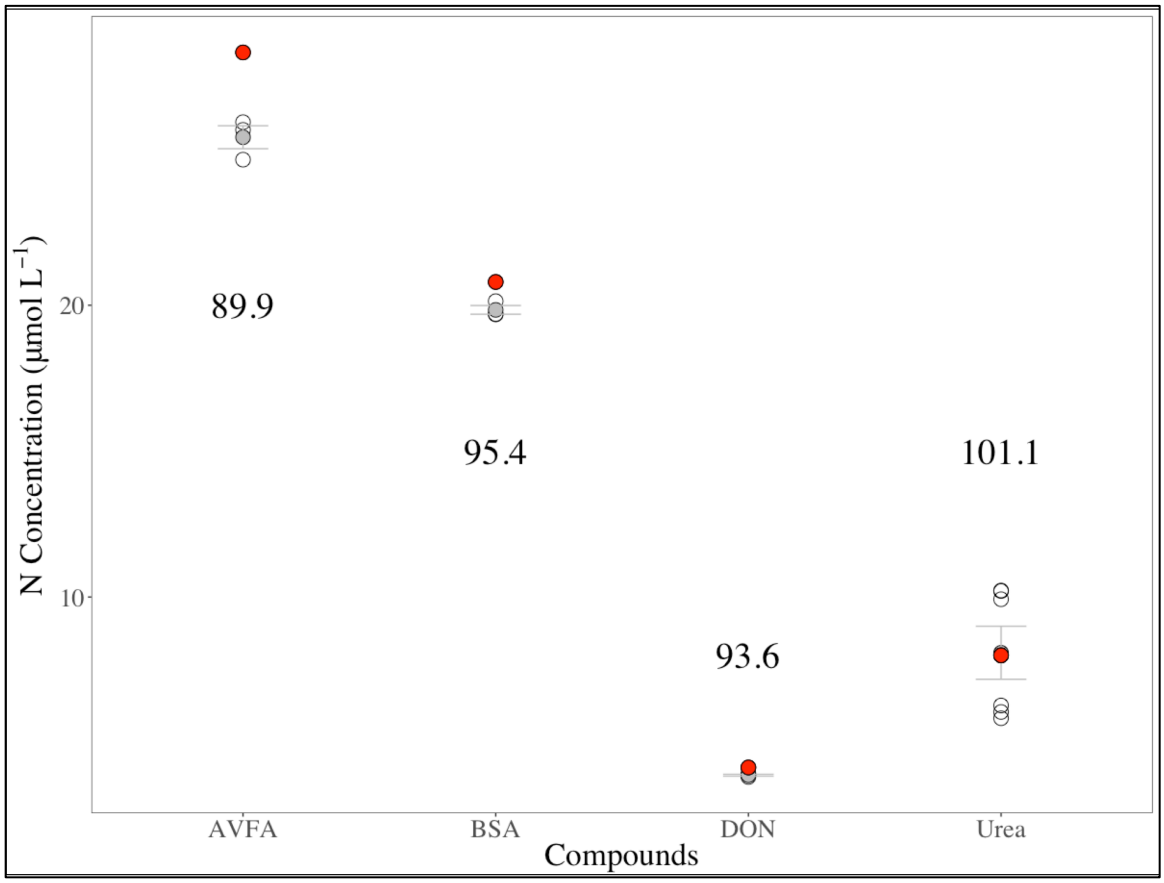

Figure 3.4. Calibration curve for isotopic ratio vs. retention time shift, (A) using urea as the standard; (B) using alanine as the standard.

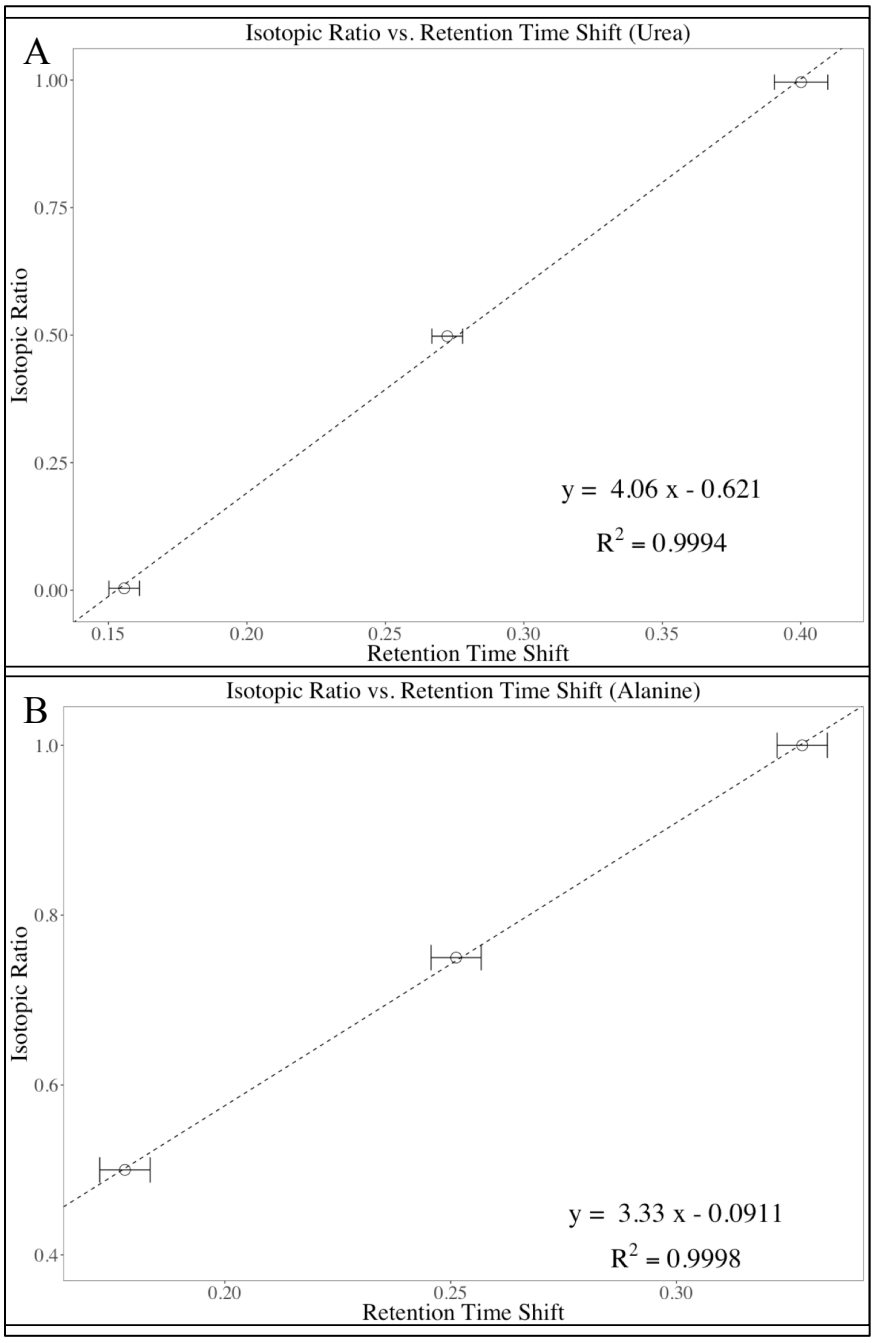

Figure 3.5. Fate of N in short-term from (A) ^{15}N-Ala incubation and (B) ^{15}N-AVFA incubation.

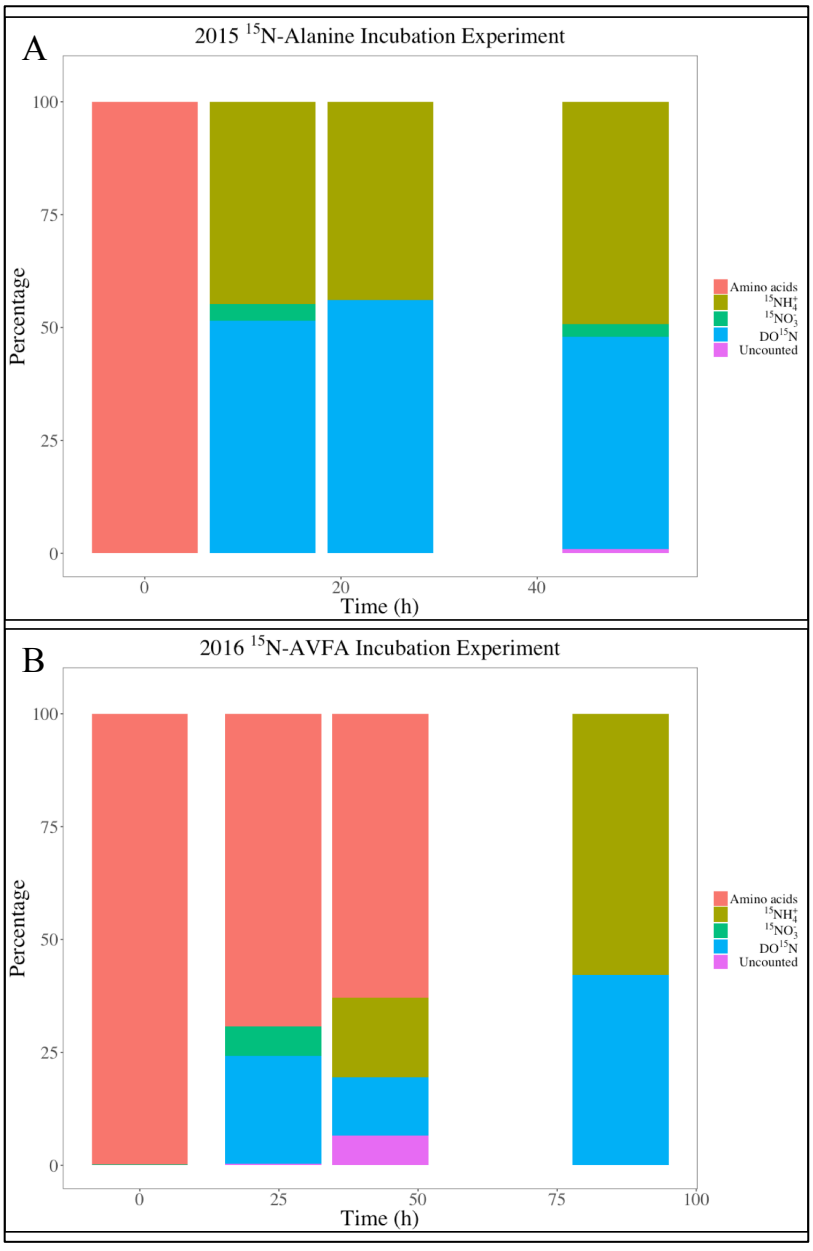

Chapter 4. Using a ^{15}N labeled peptide to trace the fates of nitrogen after degradation: The rapid formation of dissolved organic nitrogen in coastal seawater

ABSTRACT

Dissolved organic nitrogen (DON) represents a major N reservoir in aquatic systems. However, our understanding of this N pool is still limited due to our inability to identify DON at the molecular level. Controlled simplified incubation experiments with known substrates offers a helpful angle to reveal information about initial dynamics of DON formation. Here we used a ^{15}N-labeled tetra-peptide, Ala-Val-Phe-Ala, as a "typical" organic substrate, to monitor the fate of ^{15}N during incubation periods of up to 60 d with northern Gulf of Mexico waters. NO_x (NO_2^- + NO_3^-) was the dominant form of dissolved inorganic nitrogen (DIN) at the end of the incubations. Contrary to previous DOC studies, a large fraction (over 40-60%) of peptide N was transformed into uncharacterized DON within a time scale of one month. However, when using ^{15}N-Ala as substrate, only a minor fraction (< 7%) of the initially spiked ^{15}N was transformed into DON. We speculate that small peptide-like structure, in particular Val and Phe containing structures, may be important precursors of the refractory DON in marine waters.

INTRODUCTION

Dissolved organic nitrogen (DON), by definition, is the subset of the dissolved organic matter (DOM) pool that contains nitrogen (N). The DON pool is important to microorganisms, because one "metabolic drive" through DON may provide them with needed structural N and carbon (C) and energy (Bronk 2002; Sipler and Bronk 2015). However, systematic studies into DON dynamics have lagged far behind those of the its C counterpart, dissolved organic carbon (DOC), primarily due to the substantial analytical challenges inherent in DON research (Bronk 2002).

DON is considered among the most complex molecular mixtures on earth. Due to its chemical complexity, our lack of insight into its cycling, and the analytical limitation in molecular level characterization, the marine DON pool has long been considered a "black box", with less than 14% of the marine DON identified at the molecular level (Worsfold et al. 2008; Cao et al. 2017), leaving the majority of compounds comprising the DON pool uncharacterized (Sipler and Bronk 2015). This "black box" of DON can be categorized further into three subsets based on its global distribution: (1) a large refractory pool of unidentified components; (2) a semi-labile pool including compounds such as proteins, dissolved combined amino acids (DCAAs), and amino polysaccharides; and (3) a small labile pool containing labile forms such as urea, dissolved free amino acids (DFAAs), peptides and proteins, and nucleic acids (Bronk et al. 2007), with turnover times ranging from minutes for DFAAs (e.g., Fuhrman 1987) to days for urea (e.g., Bronk et al. 1998) and DNA (e.g., Jørgensen et al. 1993). DON can transfer from one subset to the other through different abiotic or biotic processes (e.g., Amon and Benner 1996; Dittmar 2015),

and bacteria may play an important role in the transformation of labile DON to semi-labile or refractory DON (Brophy and Carlson 1989; Tranvik 1993; Heissenberger et al. 1996; Ogawa et al. 2001). In this work, we specifically define that DON with a turnover time over a year as "refractory DON"; DON with a turnover time less than a few days as "labile DON"; and DON with an intermediate turnover time ranging from days to a year as "semi-labile DON".

To date, the molecular structure and dynamics during the early stage of DON formation still remains elusive. Thus, information on the smaller molecular subunits could provide important hints on the source and turnover of DON. Under this scenario, controlled incubation experiments with known labile substrate could be a preliminary but important step in DON studies. Amino acids and small peptides are key intermediate products in the decomposition of labile organic nitrogen. For instance, dissolved combined amino acids (DCAA), presumably in forms of peptides and proteins, are relatively abundant (0.2 to 4 μmol L^{-1}) in the water (Bronk 2002; Aluwihare and Meador 2008). Short-term decomposition of peptides and amino acids were studied systematically with synthesized peptide or peptide analogs (e.g., Hoppe 1983; Hoppe et al. 1988; Pantoja et al. 1993, 1997; Pantoja and Lee 1999; Liu et al. 2013, 2015; Liu and Liu 2015b, 2018). However, the long-term dynamics and fate of amino acid-N and peptide-N have not been extensively addressed.

In this study, mechanisms of DON decompositions and production by marine bacteria were studied in marine coastal waters using relatively long-term (months) incubation experiments with added ^{15}N-labled peptide and ^{15}N-amino acid as substrates.

We hypothesized that (1) the fate of N differs between different environments (i.e., oxic water vs. hypoxic water); and (2) a small fraction of the substrate N will be transformed into uncharacterized DON by the end of the incubation. The specific objectives of the present study are to: (1) investigate how semi-labile DON is formed from simple biomolecules in marine system by tracing the fate of the tetrapeptide (Alanine-Valine-Phenylalanine-Alanine, AVFA; $C_{20}H_{30}N_4O_5$) and amino acid (Alanine, Ala; $C_3H_7NO_2$); and (2) examine and quantify the fate of the peptide- and amino acid-N over short (hours) to long (month) time periods. To achieve these goals, ^{15}N labeled peptide and amino acid were added to seawater and incubated for at least one month. The concentrations and percentages of ^{15}N in ammonium, nitrate/nitrite, particulate organic nitrogen (PON) and DON were monitored over time using a combination of mass spectrometry and HPLC techniques, as described in Chapter 3.

MATERIALS AND METHODS

Peptide synthesis and sampling sites

^{15}N labeled AVFA (≥ 99%) was custom-synthesized (CS BIO) using isotope labeled amino acids with an automated solid phase peptide synthesizer, as described in a previous study (Liu et al. 2010). ^{15}N labeled alanine was purchased from Sigma-Aldrich (P/N 332127-500MG).

The peptide incubation experiment was conducted aboard the *R/V Pelican* in the northern Gulf of Mexico in May 2013 and May 2016. Water was collected using Niskin

bottles mounted on a CTD rosette at Station C6 (28.85º N, 90.37º W) (Rabalais et al. 2001). The C6 site has a depth of about 18 m, and is subject to seasonal hypoxia in bottom waters (Rabalais et al. 2002). Hypoxia was observed during sampling in both years. The amino acid incubation experiment was conducted using surface water collected from Ship Channel near UTMSI (27.84° N, 97.05° W).

Experiment design

Seawater for the 2013 AVFA incubation experiment was collected from two depths, surface (2 m) and bottom (ca. 16 m) at C6 station. Seawater aliquots (25 mL) were transferred into 30 mL pre-combusted amber glass bottles. ^{15}N labeled AVFA was added into each bottle to provide a final concentration of ca. 1 μmol L^{-1} (4 μmol L^{-1} ^{15}N). Samples were incubated in the dark at 25 ºC (near *in situ* water temperature). At time intervals of 0, 1, 2, 5, 14 and 30 d, one incubation bottle from each depth was sacrificed for sampling at each time point.

Seawater for the 2016 AVFA incubation experiment, again at C6, was collected from surface (2 m) and bottom (ca. 14 m) at C6 station. Aliquots of seawater (50 mL) were transferred into 60 mL pre-combusted amber glass bottles. Each bottle was spiked with ^{15}N labeled AVFA with a final concentration of ca. 1 μmol L^{-1} (i.e. 4 μmol L^{-1} ^{15}N) and incubated in the dark at ca. 25 ºC. One incubation bottle from each depth was sacrificed at designated time points (0, 1, 2, 4, 6, 9, 13, 19, 28, and 60 d).

For the 2015 Ala incubation experiment, surface water was collected (ca. 0.5 m), and aliquots (100 mL) were transferred into 125 mL pre-combusted amber glass bottles.

^{15}N labeled Ala was added into each bottle to provide a final concentration of ca. 10 μmol L^{-1} (10 μmol L^{-1} ^{15}N). Incubated in dark at ca. 25 ºC, one incubation bottle was sacrificed at designated time points (0, 0.5, 1, 2, 4, 7, 14, 21 d).

At each time point, 1 mL subsample was transferred into a 1.5 mL centrifuge tube, preserved with 90 μL formaldehyde, and stored at 4 ºC for bacterial abundance measurements. The remaining water sample was filtered through pre-combusted 0.7 μm glass fiber (GF/F) filter (2013 AVFA incubation) or 0.7 μm GF/F and 0.2 μm nylon filter (2016 AVFA incubation and 2015 Ala incubation). The filters and filtrate were stored in a freezer at -20 ºC until analysis.

Bacterial enumeration

Bacterial abundance was measured following published protocols (Marie et al. 1997; Gasol and Giorgio 2000; Liu et al. 2013; Liu and Liu 2015c). Briefly, bacteria were enumerated using an Accuri C6 Flow Cytometer (FCM) System with a laser emitting at 488 nm. Formaldehyde-preserved samples (500 μL) were stained with 5 μL SYBR Green I (SYBR-I) working solution (1:100, SYBR-I: water, v/v), and incubated under dark conditions for at least 15 min. Microbes were detected from their signatures in a plot of 90º side light scatter (SSC-H) versus green fluorescence (FL1-H). The discriminator was set on FL1-H, as it is proportional to the nucleic acid-SYBR I-complex. The counting error was within 25%.

^{15}N ammonium ($^{15}NH_4^+$) and nitrate/nitrite ($^{15}NO_x^-$) analysis

Analysis of ^{15}N in different forms follows the methods described in Chapter 3. Briefly, total ammonium (NH_4^+) concentrations and atom % ^{15}N-NH_4^+ were analyzed using Ammonium Isotope Retention Time Shift High Performance Liquid Chromatography (AIRTS-HPLC; Gardner et al. 1991, 1995). The AIRTS-HPLC cation exchange column specifically isolates NH_4^+ and $^{15}NH_4^+$, so that organic forms of N (amino acids, peptide and other DON) do not affect results in natural waters.

Total nitrate/nitrite (NO_x^-) concentrations and atom % $^{15}NO_x^-$ were analyzed after all NO_x^- was reduced to NH_4^+ using Zn powder under acidic conditions (Carini et al. 2010). After reduction, the NH_4^+ concentrations and atom % $^{15}NH_4^+$ were measured by AIRTS-HPLC. The NO_x^- concentrations and isotopic ratio were calculated by subtracting the NH_4^+ measured in $^{15}NH_4^+$ analysis from the total pool of DIN after Zn reduction (Carini et al. 2010).

^{15}N particulate organic nitrogen ($PO^{15}N$) analysis

The preserved 0.7 μm GF/F filters were treated with trace metal grade HCl to remove the inorganic carbon before particulate organic matter (POM) analysis. Particulate organic ^{15}N ($PO^{15}N$) concentration was measured with an elemental analyzer, which is connected to a mass spectrometer as described previously (i.e., Mercado et al. 2010). Peach leaves (NIST SRM 1547) served as the standard for calculating $PO^{15}N$.

DO^{15}N analysis

Peptide and amino acids concentrations were analyzed by HPLC following previous studies (Liu et al. 2010, 2013). Briefly, mobile phase A was 0.05 mol L^{-1} NaH_2PO_4 (pH 4.5), and mobile phase B was methanol. Going through a C18 column and a photodiode array detector (PDA) at a flowrate of 1 mL min^{-1}, mobile phase B (methanol) was ramped from 0% to 80% in 20 min, and then to 100% in 5 min. AVFA was quantified based on UV absorbance at 206 nm of the PDA detector. Individual amino acids were measured directly using HPLC with fluorescence detection after pre-column *o*-phthaldialdehyde derivatization (Liu et al. 2013). Total hydrolyzable amino acids (THAA) were measured after hydrolysis into individual amino acids using 6 mol L^{-1} HCl under nitrogen at 110 °C for 20 h following a published protocol (Liu et al. 2013).

Bulk DON in the water sample was first oxidized to nitrate (NO_3^-) using an assembled UV-oxidation apparatus generally following the published design (Armstrong and Tibbitts 1968). The 1200 W mercury vapor lamp (P/N: PC122.120) and the ballast (P/N: 34966001) were purchased from Hanovia. Oxidized samples were kept refrigerated at 4 ºC for at least 24 h before subsequent reduction of amino acid-N to NH_4^+ with Zn. Due to the limited amount of samples, total dissolved ^{15}N concentration was only measured in the 2015 ^{15}N-Ala incubation and 2016 ^{15}N-AVFA incubation. In ^{15}N-Ala incubation, $^{15}NH_4^+$ was analyzed with AIRTS as described above, and in ^{15}N-AVFA incubation, $^{15}NH_4^+$ was analyzed using the OX-MIMS technique following Yin et al. (Yin et al. 2014). The DO^{15}N concentrations were calculated by subtracting the DI^{15}N measured in previous steps from the TD^{15}N.

RESULTS

Peptide and amino acid concentrations

Concentrations of incubation substrates dropped rapidly in both AVFA and Ala incubations (Table 4.1). AVFA dropped to non-detectable level within 2 d in surface water and within 1 day in bottom water in 2013; and were below the detection limit within 4 d in both depths in 2016. Peptide degraded faster in bottom water than in surface water in 2013, but the degradation rates were not significantly different in 2016 (t = -0.759, p > 0.05). The rapid degradation rates in bottom water vs. surface water in 2013 agrees with previous reported results (Liu et al. 2010, 2013). In the 2016 incubation, THAA concentration quickly dropped to less than 3 μmol L^{-1} within 4 d in surface, and within 13 d in bottom with some fluctuations (Figure B1). Meanwhile, total Ala, Val, and Phe concentrations (free amino acids + combined amino acids) quickly dropped to less than 0.2 μmol L^{-1} within 6 d in both depths (Figure B2). In the 2015 Ala incubation, Ala concentration dropped below detection limit within the first 24 hours of the incubation (Table 4.1).

Bacterial abundance

Changes of bacterial abundance with time in the two AVFA incubations followed a similar pattern corresponding to the change of peptide (Figure 4.1). Bacterial abundance experienced an ascent during the beginning stage of the incubation when peptide or amino acid was still present, increasing from 8.7×10^5 cells mL^{-1} to 9.5×10^5 cells mL^{-1} during the first 48 hours in surface and from 9.2×10^5 cells mL^{-1} to 1.8×10^6 cells mL^{-1} during the first 24 hours in bottom in 2013 incubation (Figure 4.1A); from 1.2×10^6 cells mL^{-1} to 1.3×10^6 cells mL^{-1} during the first 48 hours in surface and from 7.2×10^5 cells mL^{-1} to 1.4×10^6 cells

mL^{-1} during the first 24 hours in bottom in 2016 incubation (Figure 4.1B); and from 1.2×10^7 cells mL^{-1} to 1.7×10^7 cells mL^{-1} during the first 12 hours in 2015 incubation (Figure 4.1C)

Bacterial abundance started to decline after peptide or amino acid was depleted. The abundance dropped to about 1.6×10^6 cells mL^{-1} in the 2015 Ala incubation, only about 10% of the original abundance (Figure 4.1C). In 2013 and 2016 incubations, small increases towards the end of the incubation were observed after the sharp decline. The abundance dropped to 1.5×10^5 cells mL^{-1} at both depths in the 2013 incubation (Figure 4.1A). In 2016 incubations, it dropped to 3.5×10^5 cells mL^{-1} before increasing to 1.1×10^6 cells mL^{-1} in surface samples, and to 2.6×10^5 cells mL^{-1} before increasing to 6.4×10^5 cells mL^{-1} in bottom ones (Figure 4.1B).

^{15}N in inorganic form: $^{15}NH_4^+$ and $^{15}NO_x$

It is reasonable to assume that all the dissolved inorganic ^{15}N measured in this study originated from the added ^{15}N labeled AVFA because the natural abundance of ^{15}N in seawater is low. The $\delta^{15}N$ in nitrate relative to air is lower than 5‰, as compared to a negative value for $\delta^{15}N$ in nitrite and about 10‰ for ammonium (Sigman and Casciotti 2001).

$^{15}NH_4^+$ concentration exhibited a similar three-stage pattern in all incubations, regardless of the water depth or time or location of incubation (Figure 4.2). At the beginning of the incubation, $^{15}NH_4^+$ accumulated quickly. $^{15}NH_4^+$ concentration increased from 0 μmol L^{-1} to 1.7 μmol L^{-1} within the first 5 d in surface and to 1.1 μmol L^{-1} within

the first day in 2013 incubation (Figure 4.2A), to ca. 2.4 μmol L^{-1} within the first 4 d in both depths in 2016 incubation (Figure 4.2B), and to ca. 4.5 μmol L^{-1} within the first 12 hours in 2015 incubation (Figure 4.2C). A slow increasing or steady stage followed. In this stage, $^{15}NH_4^+$ either remained relatively steady (from day 5 to day 14, surface 2013, Figure 4.2A), increased slowly (from day 1 to day 14, bottom 2013, Figure 4.2A; from day 4 to day 28, surface 2016, Figure 4.2B; from day 0.5 to day 7, 2015, Figure 4.2C), or decreased slightly (from day 4 to day 28, bottom 2016, Figure 4.2B). Finally, the incubation water experienced a sharp decrease in $^{15}NH_4^+$. For all incubations, the concentration of $^{15}NH_4^+$ was either close to 0 μmol L^{-1} or below detection limit by the end of the incubation (Figure 4.2).

$^{15}NO_x$ had a much simpler trend than $^{15}NH_4^+$. A monotonic increasing trend of $^{15}NO_x$ was observed in all incubations with the exception of the 2013 bottom experiment, in which the $^{15}NO_x$ concentration fluctuated during the incubation but followed an increasing trend. Specifically, in the 2013 incubation no $^{15}NO_x$ was detected in surface water until day 14. Within the last 16 d, $^{15}NO_x$ concentration in surface water accumulated quickly to ca. 0.6 μmol L^{-1} (Figure 4.2A). $^{15}NO_x$ appeared much earlier in the bottom water. On day 2, ca. 1.1 μmol L^{-1} $^{15}NO_x$ was detected. At the end of incubation, ca. 2.4 μmol L^{-1} of peptide-^{15}N was transferred into NO_x forms (Figure 4.2A). A similar trend was observed in the 2016 incubation. No $^{15}NO_x$ was detected in the samples until day 28 in surface water and day 19 in bottom water. About 1.4 μmol L^{-1} and 1.7 μmol L^{-1} $^{15}NO_x$ was detected at the end of the incubation in surface and bottom, respectively (Figure 4.2B). The appearance of $^{15}NO_x$ in 2015 Ala incubation was the earliest among all three incubations. Within the

first week of incubation, the conversion of peptide-N to nitrite/nitrate-N was detected (Figure 4.2C), and the concentration of $^{15}NO_x$ increased rapidly since then, ending up with over 8 μmol L^{-1} ^{15}N stayed in the form of NO_x on day 21.

To summarize, $^{15}NH_4^+$ was the dominant form of dissolved inorganic ^{15}N ($DI^{15}N$) during the initial stage of the incubation. As the incubation proceeded, $^{15}NH_4^+$ decreased while $^{15}NO_x$ increased. By the end of the incubation, $^{15}NO_x$ dominated the $DI^{15}N$ pool, while $^{15}NH_4^+$ either was below detection limit, or only accounted for a small fraction.

^{15}N in organic form: $PO^{15}N$ and $DO^{15}N$

$PO^{15}N$, measured only for the 2013 incubation, constituted only a minor fraction of the total ^{15}N pool. The changes of $PO^{15}N$ resembled the patterns of bacterial abundance at both depths, particularly in bottom water (Figure B3). In surface water the $PO^{15}N$ concentration fluctuated slightly throughout the incubation (Figure B3). It increased from 0.07 μmol L^{-1} at the beginning of the incubation to only 0.09 μmol L^{-1} at the end, with the highest concentration (0.10 μmol L^{-1}) observed at the time point of 2 weeks. In bottom water sample (16 m), $PO^{15}N$ increased sharply from 0 h (0.08 μmol L^{-1}) to 24 h (0.58 μmol L^{-1}) but then decreased from 24 h to 48 h (0.18 μmol L^{-1}), resembling the changing pattern of bacterial abundance observed at the same depth (Figure 4.1). After 48 h, $PO^{15}N$ concentrations decreased slowly to a concentration of 0.09 μmol L^{-1} at the end of the incubation. In summary, $PO^{15}N$ generally accumulated only about 2% of the total ^{15}N pool. This low PON percentage observed is consistent with the low PON concentrations and percentages reported previously (Bronk et al. 2007; Sipler and Bronk 2015).

Assuming that all PON was from bacteria, based on $PO^{15}N$ concentration and bacterial abundance, the amount of ^{15}N per bacterium cell ranged from 1.2×10^{-15} g (day 0 and day 2) to 8.7×10^{-15} g (day 14) in surface waters, and 1.2×10^{-15} g (day 0) to 1.2×10^{-14} g (day 5) in bottom water. These values are consistent with the average content of carbon and nitrogen for oceanic bacteria (Lee and Fuhrman 1987; Fuhrman 1992; Fukuda et al. 1998).

Due to the inadequacy of sample volumes of the 2013 incubation, $DO^{15}N$ was measured only in the 2016 AVFA incubation and 2015 Ala incubation. $DO^{15}N$ decreased gradually during the incubation (Figure 4.3). The high $DO^{15}N$ concentration early in the incubation was from the added ^{15}N-AVFA or ^{15}N-Ala (Table 1). As the incubation proceeded, the concentration of $DO^{15}N$ gradually dropped to ca. 2.0 μmol L^{-1} in surface and ca. 1.5 μmol L^{-1} in bottom on day 4 in the 2016 incubation, and to ca. 1.0 μmol L^{-1} on day 14 in the 2015 incubation. The observed "uncharacterized" $DO^{15}N$ concentrations (ca. 2.6 μmol L^{-1} in surface and ca. 1.9 μmol L^{-1} in bottom in 2016 incubation; ca. 0.9 μmol L^{-1} in 2015 incubation) remained constant during the incubation (Figure 4.3). Note that even though the concentrations remained constant, the DON compounds may still change.

Fate of ^{15}N

The fate of ^{15}N was visualized with bar graphs (Figures 4.4, 4.5, and 4.6). The percentage of $DO^{15}N$ in the 2013 AVFA incubation was calculated through mass balance, assuming that ^{15}N loss during the incubation was negligible. The recovery rate ranged from

83.5% to 120.2% with an average of 98.0% for ^{15}N in 2016 AVFA incubation, and ranged from 88.2% to 127.8% with an average of 104.2% for ^{15}N in 2015 Ala incubation.

Overall, a large fraction of peptide N was transformed into "uncharacterizable" N. At the end of the 2013 incubation (day 30), 86.3% and 66.8% of peptide-N was transformed to DON in surface and bottom, respectively (Figure 4.4). At the end of the 2016 incubation (day 60), 63.7% and 47.3% of peptide-N was transformed to DON in surface and bottom waters, respectively. In both incubations, the percentage of DON was higher in bottom hypoxic water than that in surface oxic water. Compared with DON, DIN constituted a minor component. NH_4^+ was near the detection limit and NO_x accounted for 11.1% and 32.0% in the 2013 incubation, and 34.4% and 43.3% in 2016 incubation.

In contrast, NO_x is the dominant form of N for the alanine incubation, accounting for 82.4% of total N at the end of incubation (Figure 4.6). Similar to the peptide incubation, NH_4^+ is almost undetected. DON, on the other hand, was much lower compared with the peptide incubation, only representing 6.6% of the total N pool by the end of the incubation.

DISCUSSION

We hypothesized that (1) the fate of N differs between different environments (i.e., oxic water vs. hypoxic water); and (2) a small fraction of the substrate N would be transformed into uncharacterizable DON by the end of the incubation.

Our result supports Hypothesis 1 that the fate of N depends on the location and biotic characteristics of the water (i.e., oxic water vs. hypoxic water). The 2013 peptide incubation experiments indicate that the labeled tetrapeptide degraded more efficiently in

the bottom water than in the surface water. With a much higher phosphate concentration (ca. 1.0 μmol L^{-1} in bottom vs. ca. 0.4 μmol L^{-1} in surface), the decomposition rate of peptide in the bottom water was about double that in surface in 2013. The fact that organic matter decomposes faster under hypoxic than oxic conditions, which is consistent with recent studies in this area (e.g., Liu and Liu, 2015b; Liu et al., 2013), suggests that organic matter decomposition in the hypoxic zone is more complicated than recognized previously, and nutrient levels, especially phosphate, in water play an important role in controlling the degradation rate of labile organic matter (Liu and Liu 2015c). The data suggest that organic matter degradation in the hypoxic zone is more complicated than a simple linear transition between oxic and anoxic conditions.

For the AVFA incubation conducted in GOM, the change of $^{15}NH_4^+$ and $^{15}NO_x$ concentrations with time showed that ammonification/remineralization and nitrification occurred at different stages in surface and bottom waters. In surface water, ammonification was dominant early in the incubations, with no sign of nitrification, until day 14 in the 2013 incubation and day 27 in the 2016 incubation, when it started to dominate (Figure 4.2). In comparison, nitrification in bottom water occurred not only faster but also in a higher magnitude. This result is in consistent with previous findings (Carini et al. 2010), in which nitrification rate was higher in the lower water column. The observed discrepancies between surface and bottom water can be attributed to differences in the bacteria community at different depths. Nitrifiers, such as *Nitrosomonas*, *Nitrobacter*, and marine ammonia oxidation archaea (AOA) like *Thaumarchaeota,* are more abundant in bottom than in near-surface waters. This speculation is supported by a recent study of AOA

pointing out that *Thaumarchaeota* was more abundant in deep and less oxygenated water in the northern Gulf of Mexico (Tolar et al. 2013, p. 2). It is also possible that high phosphate level in the bottom water enhanced the growth of nitrifiers and thus the nitrification rate (e.g., Purchase 1974). Further study is needed to elucidate the exact cause of this intriguing phenomenon.

The second hypothesis that only a small fraction of substrate N is transformed into uncharacterized DON, however is only supported by our amino acid incubation result, but not peptide incubation results. In the peptide incubation, the DON result was inconsistent with several other studies of DOC. Previous studies investigated the formation of DOC by marine bacteria using different substrates such as glucose (e.g., Gruber et al. 2006; Lønborg et al. 2009), leucine (e.g., Heissenberger and Herndl 1994), glucose and leucine (e.g., Brophy and Carlson 1989), glucose and glutamate (e.g., Ogawa et al. 2001), and detrital lignocellulose (e.g., Moran and Hodson 1989; Bergbauer and Newell 1992). Only a small fraction of the original labile substrate, ranging from 1.4% when using leucine as the substrate (Brophy and Carlson 1989) to 7.3% when using glucose as the substrate (Lønborg et al. 2009), was transformed into unidentifiable DOM at the end of the incubation in terms of C. In our ^{15}N study, however, more than 60% and 40% of ^{15}N was detected as $DO^{15}N$ in the 2013 AVFA incubation and 2016 AVFA incubation, respectively (Figures 4.4 and 4.5); the newly formed DOM cannot be attributed to individual amino acids. These percentages in AVFA incubation are one order of magnitude higher than the reported numbers in DOC, 6% (^{14}C-DOM/initial added ^{14}C-leucine) after eight-day incubations (Heissenberger and Herndl 1994), and 5% (DOC/initial added glucose) and 7% (DOC/initial added glutamate)

after a one-year incubation in Ogawa et al. (2001), and the 3 to 5% (DOC/initial added glucose) after one-month incubation in Gruber et al. (2006).

The inconsistent results between C and N provide insights into the formation of semi-labile DON. During incubation, C from the labile organic substrate is probably used as an energy source to fuel and maintain the growth of the bacterial community and is remineralized quickly into inorganic form (CO_2), which explains why DOC concentration dropped rapidly (e.g., Ogawa et al. 2001; Lønborg et al. 2009). Unlike C, N from the substrate can be reused after remineralization. Unless removed from the system through processes like denitrification (DNF) and/or anaerobic ammonium oxidation (ANAMMOX), which were unlikely in our incubation due to the abundance of O_2, remineralized inorganic N can be re-assimilated into DON quickly.

A high yield of DON during short term peptide incubations was reported previously (e.g., Liu et al., 2013). During the three-day incubation, 21-26% of the N in added AVFA and VFA were incorporated into bacterial biomass and/or excreted as DON in surface water at C6 station in northern GOM, and the percentage increased to 50-60% in bottom water (Liu et al. 2013), but their results were based on mass balance rather than direct measurement. Our result through direct measurement confirms the high yield of DON when using peptide as the incubation substrate during a long-term incubation. Interestingly, a different fate of the spiked ^{15}N was detected in ^{15}N-Ala incubations. In ^{15}N-Ala incubation, the DON accounted for 6.6% of total N pool by the end of one-month the incubation (Figure 4.6), while the majority of spiked ^{15}N was in inorganic form. The

percentage of uncharacterizable DON from the amino acid incubation was low (< 7%) compared to peptide incubation but comparable to DOC data.

Causes for the differences between peptide-substrate incubation and amino acid-substrate incubation are intriguing, as one would expect amino acid and peptide to share a similar fate, since peptides are generally hydrolyzed before becoming available to microbes (Weiss et al. 1991; Arnosti 2011; Liu et al. 2013). One possible explanation is that the water from the Port Aransas ship channel was different from the northern Gulf of Mexico in terms of biological and chemical parameters, such as the bacterial community and nutrient concentrations. Alternatively, the metabolism pathways of Val and Phe may differ from that of Ala, which may contribute to the observed discrepancy (Amano et al. 1982). Val and Phe may be more readily transformed into DON rather than remineralized due to their physical (i.e., hydrophobicity) and/or chemical (i.e., branched chain and benzyl group) properties. THAA data in the 2016 incubation showed that, unlike Ala, excretion of Phe was detected during the incubation (Figure A4.2B & D). An incubation experiment conducted at station HO (28.60º N, 91.24º W) in the northern GOM in 2010 (unpublished data) supported this speculation. Not only was the excretion of Val and Phe detected, but the transformation percentage of individual amino acid Phe to NH_4^+ resembled that of peptide. About 50% of the added amino acid was transferred into NH_4^+ at the end of the incubation. More research is needed to differentiate these two possibilities.

Without further molecular characterization, our data could not annotate the detailed structure of the produced DON compounds. However, recent advancement in molecular-level characterization of DON could provide further insights into the structural detail of the

newly formed DON. ^{15}N-nuclear magnetic resonance (^{15}N-NMR) and Fourier transform ion cyclotron resonance mass spectrometry (FT-ICR MS) showed that a large proportion of the functional groups of the uncharacterized high molecular weight (HMW) DON are amide groups (Aluwihare and Meador 2008; Worsfold et al. 2008; Sipler and Bronk 2015). A recent study using advanced two-dimensional NMR further revealed that N-methyl amides are important components of the amide compounds in refractory HMW DON (Cao et al. 2017). Furthermore, peptides contain structure and/or precursor structure of N-methyl amides (McPhail et al. 2007; Tripathi et al. 2010; Cao et al. 2017). Thus, it is possible that peptide-like structures containing certain amino acids (i.e., Val and/or Phe) may play an important role in the formation of the N-methyl amides. Simple amino acids (i.e., Ala), on the other hand are more likely to be quickly assimilated by bacteria but less likely to be excreted, due to their simpler structure and its important role in almost all kinds of biochemical processes (Amano et al. 1982).

In conclusion, our results show that (1) peptide was degraded faster in hypoxic water than in oxic water, which indicates that hypoxia is not a simple intermediate between oxic and anoxic conditions in terms of organic matter degradation; (2) fates of the N from the peptide differed between surface and bottom water; and (3) when using peptide as the incubation substrate. A large proportion of the N can form new DON and these new DON compounds can persist at least for one month, meeting the criterion of semi-labile (at least) DON (Bronk 2002). However, when a single amino acid was used, less than 7% of the added ^{15}N was transformed into DON. We speculate that small peptide-like structures, in particular Val and Phe containing structures, may be important precursors of the refractory

DON. Overall, this study provides preliminary but intriguing insights to the formation of DON. In addition, our study is based on one peptide, AVFA. Cautions should be taken when extrapolating the results to other peptides and peptide homologs. The longer incubations with different peptides should be examined further.

Table 4.1. Concentrations of different forms of N at different times during the incubations.

Different Forms of N	Incubation																					
	2013 ^{15}N-AVFA Incubation Time Point (day)						2016 ^{15}N-AVFA Incubation Time Point (day)										2015 ^{15}N-Ala Incubation Time Point (day)							
	0	1	2	5	14	30	0	1	1.8	3.6	5.6	8.5	12.5	18.6	27.4	60	0	0.5	1	2	4	7	14	21
$^{15}NH_4^+$ (μmol L^{-1}) *	0.03	1.02	1.34	1.94	1.90	0.06	0.00	0.00	0.71	2.31	2.36	2.19	2.11	2.29	2.13	0.00	0.00	4.48	4.39	4.92	5.95	6.46	0.02	0.12
	0.03	1.12	1.08	1.22	1.78	0.00	0.00	0.33	0.71	2.37	2.49	2.17	2.77	2.67	2.28	0.00								
$^{15}NO_x$ (μmol L^{-1}) *	0.00	0.00	0.00	0.00	0.00	0.63	0.00	0.00	0.00	0.00	0.00	0.00	0.00	0.00	0.00	1.38	0.00	0.37	0.00	0.29	0.37	1.20	7.95	8.24
	0.25	0.17	1.14	1.72	0.41	2.35	0.00	0.00	0.00	0.00	0.00	0.00	0.00	0.00	0.31	1.73								
$PO^{15}N$ (μmol L^{-1}) *	0.07	0.10	0.08	0.08	0.10	0.09	-	-	-	-	-	-	-	-	-	-	-	-	-	-	-	-	-	-
	0.08	0.58	0.18	0.13	0.08	0.09	-	-	-	-	-	-	-	-	-	-								
Peptide/Amino acid-N (μmol L^{-1}) *	1.40	0.23	0.00	0.00	0.00	0.00	3.71	3.00	2.30	0.00	0.00	0.00	0.00	0.00	0.00	0.00	12.81	0.08	0.03	0.00	0.00	0.00	0.00	0.00
	1.75	0.00	0.00	0.00	0.00	0.00	3.77	3.27	2.53	0.00	0.00	0.00	0.00	0.00	0.00	0.00								
Non-peptide/amino acid $DO^{15}N$ (μmol L^{-1}) *	0.00	3.66	4.30	3.69	3.62	4.93	0.57	0.73	0.73	1.79	0.98	1.53	1.84	1.12	1.72	2.55	0.00	7.15	6.62	4.69	6.45	3.12	0.85	0.66
	0.00	5.50	4.97	4.29	5.09	4.92	1.04	0.47	0.46	1.11	1.68	1.89	1.32	1.50	1.34	1.89								

*: For 2013 and 2016 incubations, the upper row is surface water and the lower row is bottom water.

Figure 4.1. Bacterial abundance with time of 2013 AVFA incubation (a), 2016 AVFA incubation (b), and 2015 Ala incubation. The error bars represent standard error of duplications. Note the difference in timescales for the panels.

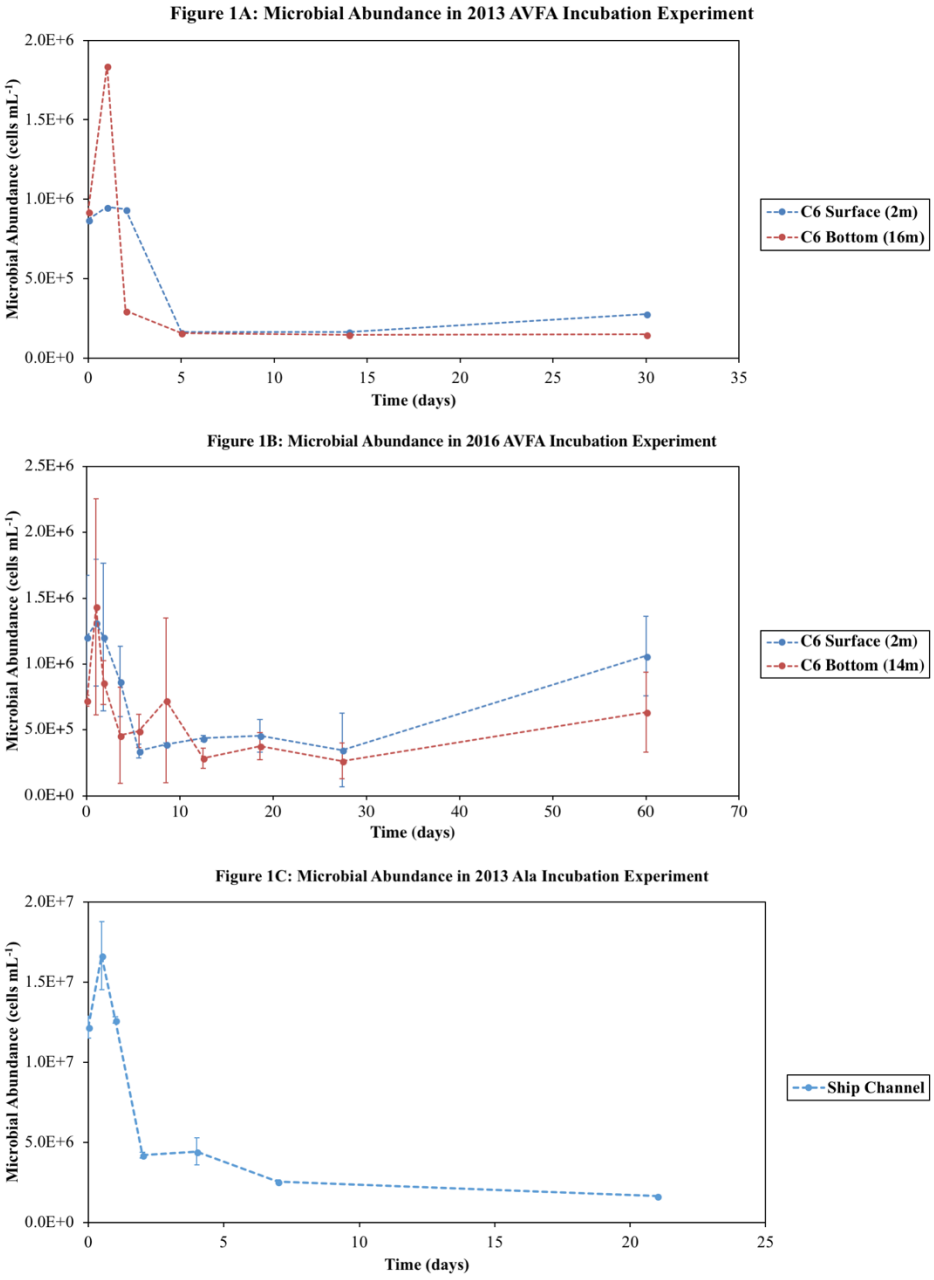

Figure 4.2. Change of DI^{15}N concentration with time in the 2013 AVFA incubation (a), 2016 AVFA incubation (b), and 2015 Ala incubation (c). A three-stage pattern in $^{15}NH_4^+$ was observed: $^{15}NH_4^+$ rapidly accumulated during the beginning stage of the incubation, stayed relatively unchanged for a while, and then dropped to undetectable level. $^{15}NO_x$ on the other hand, showed an increasing trend.

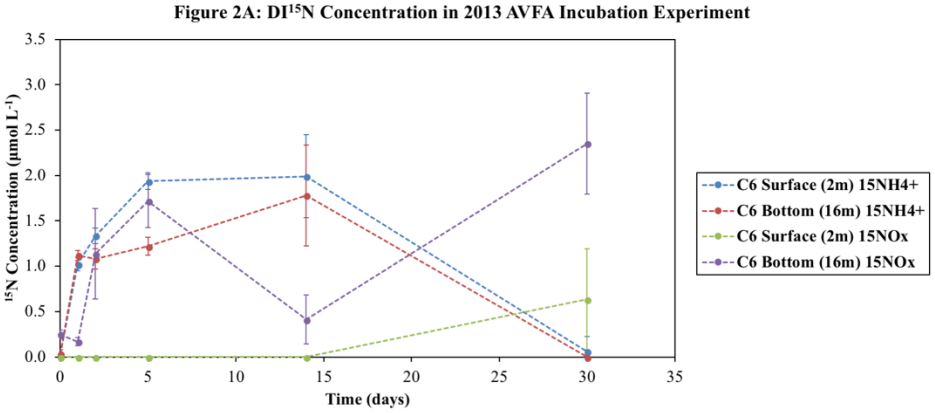

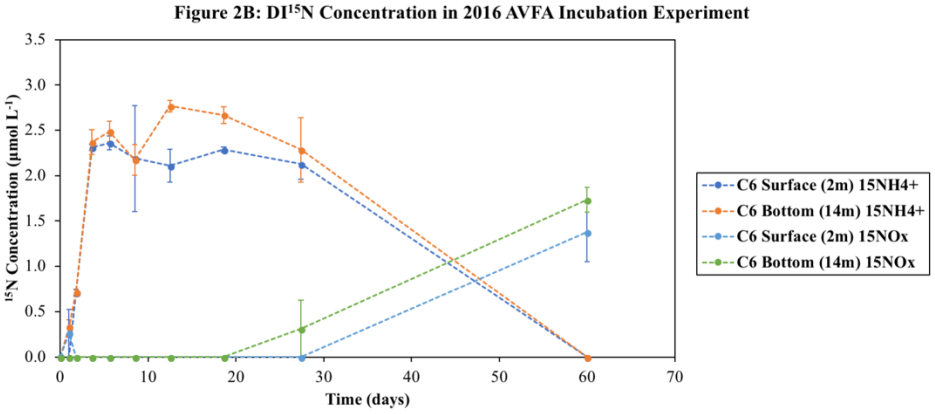

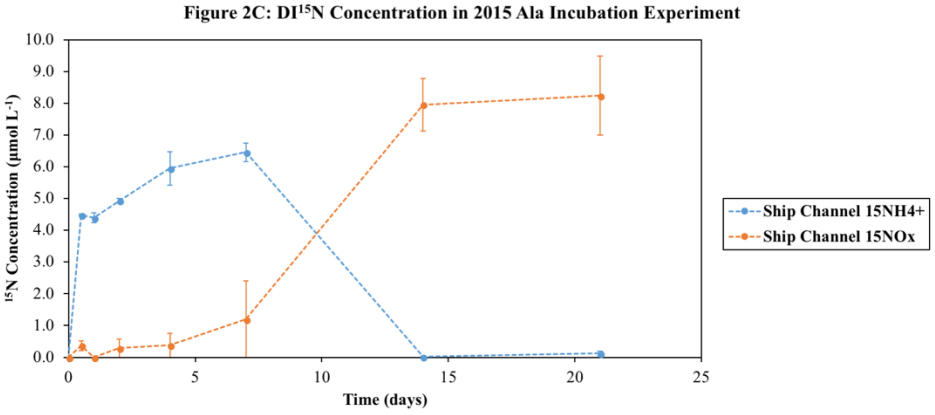

Figure 4.3. Change of $DO^{15}N$ concentration with time of 2016 AVFA incubation (a), and 2015 Ala incubation (b).

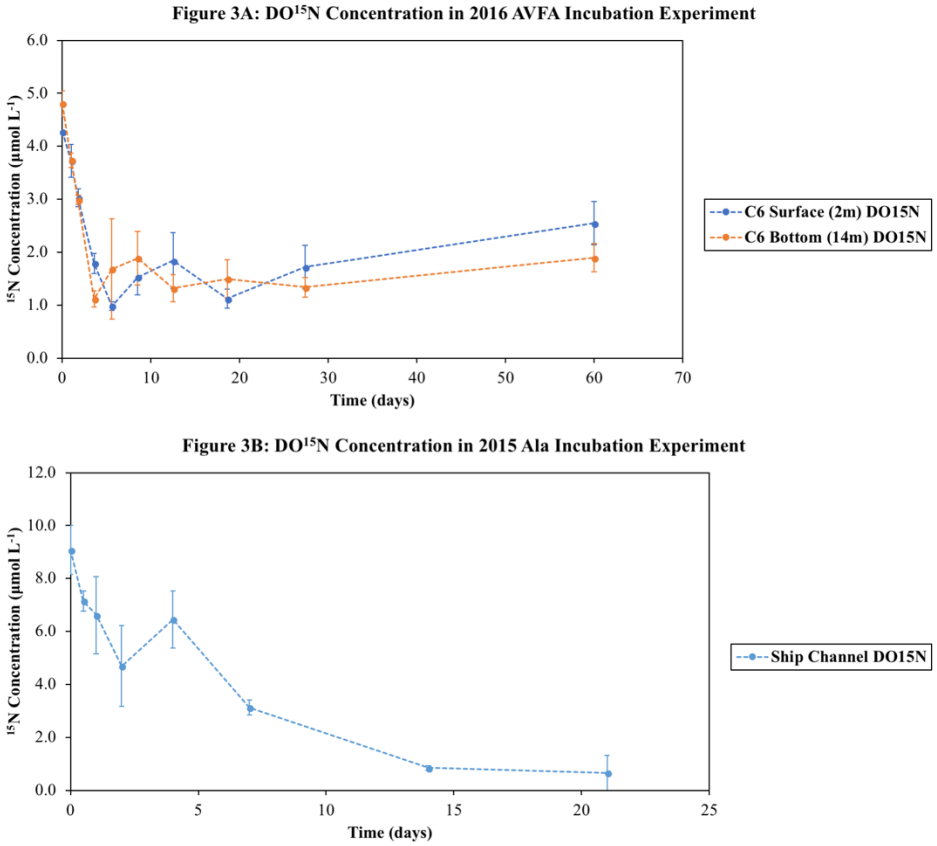

Figure 4.4. (a) Percentage of different ^{15}N constituents with time in surface (2 m) water of 2013 AVFA incubation; (b) Percentage of different ^{15}N constituents with time in bottom (16 m) water of 2013 AVFA incubation.

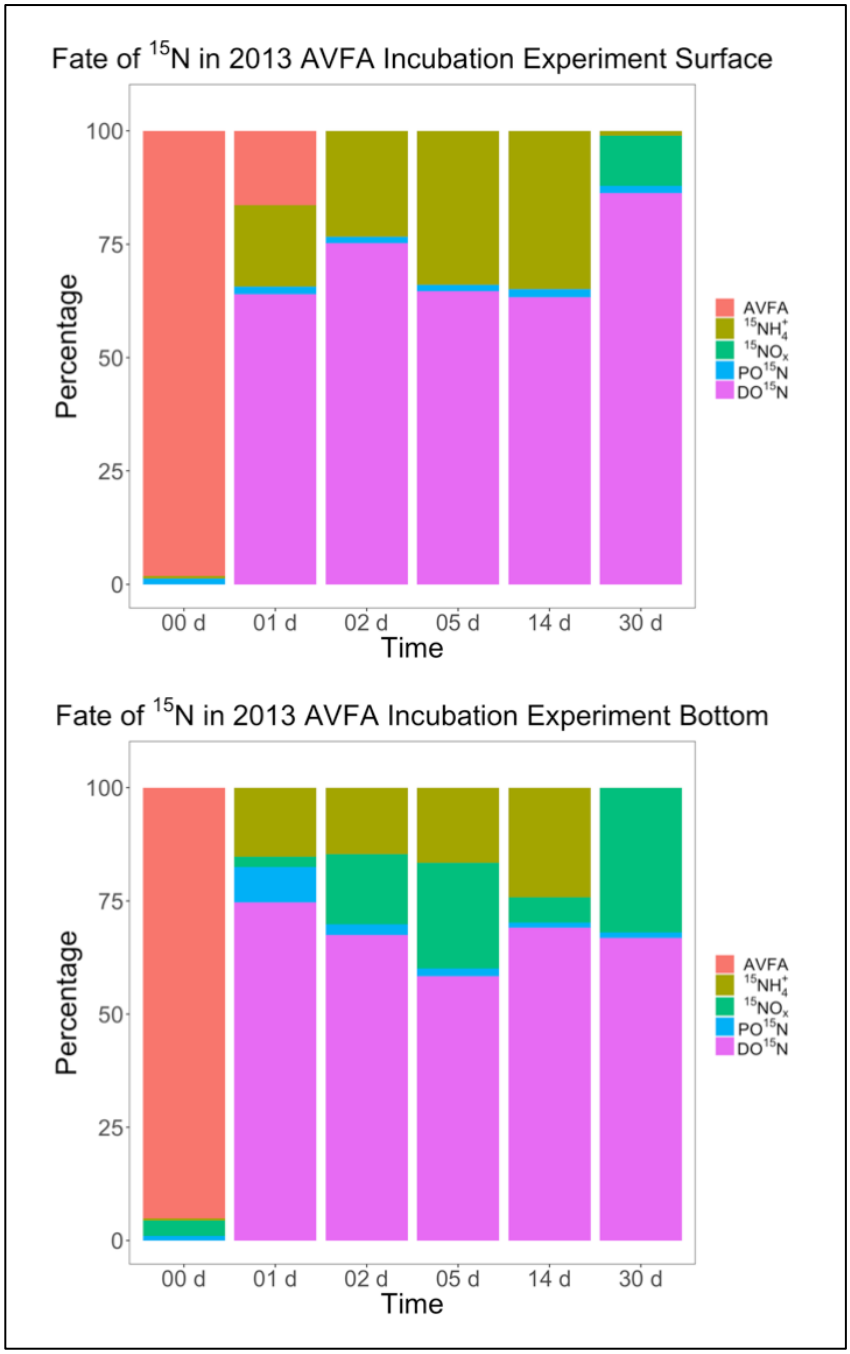

Figure 4.5. (a) Percentage of different ^{15}N constituents with time in surface (2 m) water of 2016 AVFA incubation; (b) Percentage of different ^{15}N constituents with time in bottom (16 m) water of 2016 AVFA incubation.

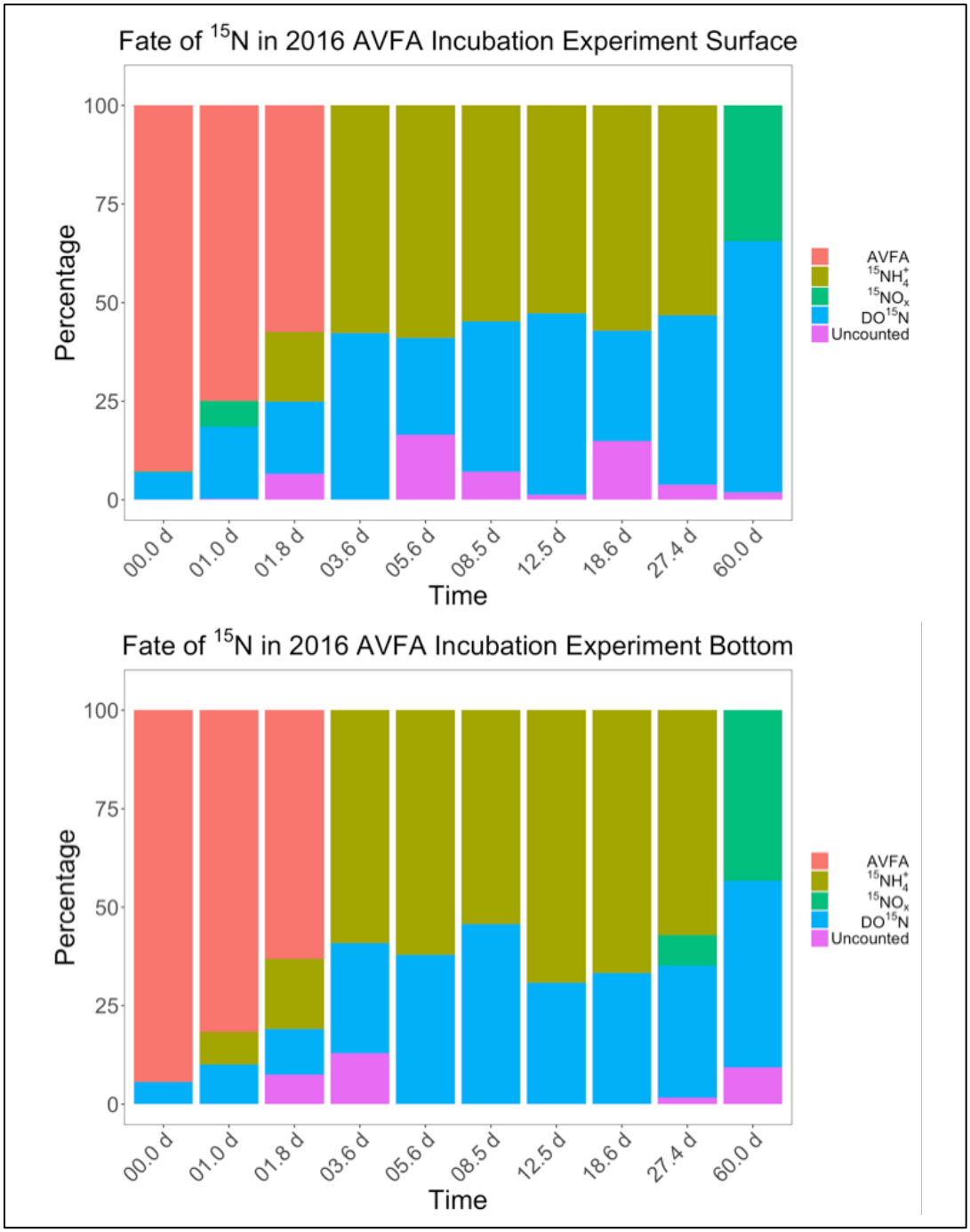

Figure 4.6. Percentage of different ^{15}N constituents with time of 2015 Ala incubation.

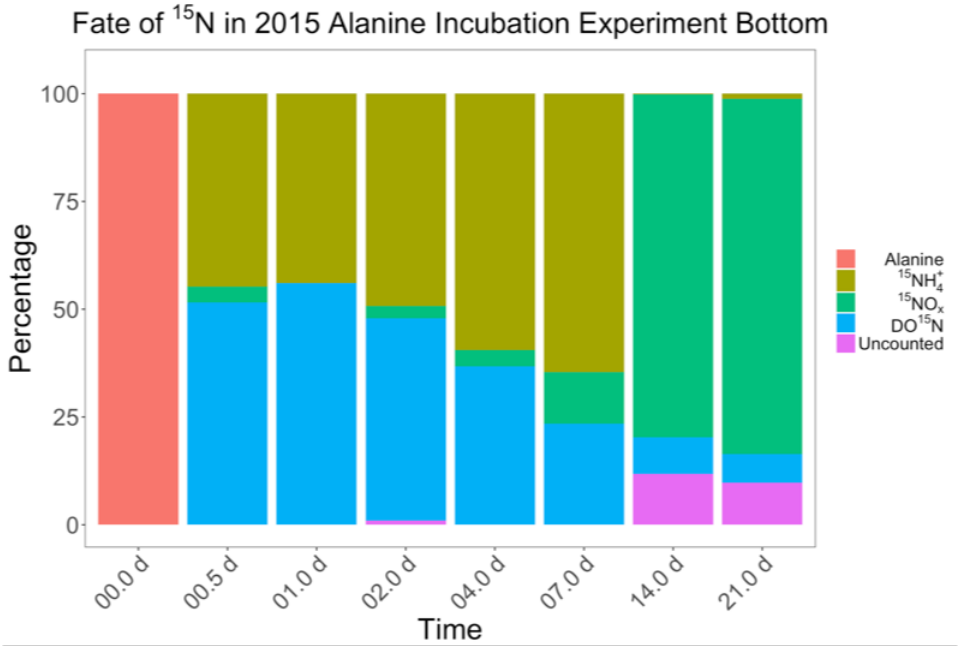

Chapter 5. Molecular structure characterization of riverine and coastal dissolved organic matter with ion mobility quadrupole time of flight LCMS (IM Q-TOF LCMS)

This chapter has been accepted for publication in *ES&T*.

Authors: Kaijun Lu, Wayne S. Gardner and Zhanfei Liu

The dissertator's contribution includes: sample collection, developing the analytical protocol, analyzing data, and writing the dissertation.

ABSTRACT

Deciphering molecular structures of dissolved organic matter (DOM) components is key to understanding the formation and transformation of this globally important carbon pool in aquatic environments. Such a task depends on the integrated use of complementary analytical techniques. We characterize the molecular structure of natural DOM using an ion mobility quadrupole time of flight liquid chromatography mass spectrometer (IM Q-TOF LC/MS), which provides multidimensional structural information on DOM molecules. Geometric conformation of DOM molecules is introduced into molecular-level analysis via the ion mobility (IM) in the system, and an actual measurement of isomers is achieved for the first time. Our data show that natural DOM molecules from several south Texas rivers and adjacent coastal waters have smaller geometric conformation compared with standard biomolecules. Furthermore, about 10% of all DOM molecules resolved within the detection limit of IM-MS had at least one but no more than four isomers. With acquired geometric and isomeric information, we established a multidimensional database

containing 89 natural DOM compounds. This database provides a foundation to expand further, or compare, with DOM data from different seasons and locations.

INTRODUCTION

Dissolved organic matter (DOM) is an important carbon pool in the ocean, containing 660×10^{15} grams of carbon, similar in magnitude to atmospheric carbon and over 1000 times more than all living organisms in the oceans combined (Dittmar 2015). This large marine carbon pool exchanges constantly with atmospheric carbon through processes such as photosynthesis and respiration. Therefore, small disturbances of the DOM pool could impact global climate substantially. Despite its potential climatic significance, molecular information of DOM is not well defined. Also unclear is why a major fraction of this reduced organic carbon persists in an environment enriched with electron acceptors for millennial time scales (Dittmar and Paeng 2009; Dittmar 2015). Given the small size ($\leq$ 1000 Da) of the most refractory DOM, an intriguing question is why is it not assimilated efficiently by bacteria (Dittmar and Kattner 2003)? This paradox relates to our limited understanding of DOM at the molecular level. In fact, less than 30% of DOM in the surface ocean and only about 5% in deep water has been characterized (Benner 2002). Deciphering molecular-level information of DOM is key to understanding this important carbon pool and its interactions with pollutants (Chiou et al. 1986; De Paolis and Kukkonen 1997) and greenhouse gases (Moran and Hodson 1989; Bouillon et al. 2012).

Precise molecular-level analyses of DOM rely on the integrated use of complimentary analytical techniques. The current capacity to resolve DOM at the molecular-level can be described in the form of a three-dimensional analytical space comprising 10^8 to 10^{14} individual voxels, which is constrained by the resolution of three

complementary techniques of (1) nuclear magnetic resonance (NMR; resolution 10^2 to 10^5), (2) ultrahigh-resolution Fourier Transform Ion Cyclotron Resolution Mass Spectrometry (FTICR MS; resolution 10^4 to 10^5), and (3) high-performance separation (resolution 10^2 to 10^4; (Hertkorn et al. 2007). However, our understanding is still not comprehensive even though thousands of distinct molecular formulas can be resolved from the intricate mixture of DOM with the combination of NMR and ultrahigh resolution MS (Hawkes et al. 2016).

An important deficiency is our limited knowledge of the isomeric information of DOM molecules, and thereby the total number of compounds in natural DOM. Knowing the total number of different structural units is crucial in exploring reasons behind the long-term stability of DOM, such as the recently-ignited dilution hypothesis (Dittmar 2015). Because high resolution MS only provides isomer-filtered information of complex DOM mixtures, estimation of the number of isomers in DOM mixture currently relies on calculation and modelling (Hertkorn et al. 2007, 2008; Zark et al. 2017), ranging from over a hundred thousand (Zark et al. 2017; Hawkes et al. 2018) to several million (Hertkorn et al. 2007; Dittmar and Stubbins 2014). A recent study calculated that the number of DOM isomers may be over 10-fold of the detected individual formulas by modelling based on intrinsic averaging theory (Zark et al. 2017). Another study further suggested that the total number of isomers in natural DOM could be over 10^7 because a maximum of theoretically possible structural isomers exists at the observed level of H-saturation in DOM, and the intensities of the mass spectral peaks are a function of the abundance of isomers (Hertkorn et al. 2007). However, modelling results alone cannot explain why the molecular size range

of DOM has a unimodal distribution with the maximum intensity reached at around 400 Da (Dittmar and Stubbins 2014). Based on this hypothesis, the mass spectra should have a monotonous increasing trend, as the number of isomers should increase exponentially with molecular size. The actual measurement of isomers in natural DOM, therefore, may be critical in explaining this paradox.

Ion mobility mass spectrometry (IM-MS) provides structural and isomeric information of molecules as a unique dimension in molecular-level DOM studies. Ions are separated in the IM chamber through low-energy interactions with inert buffer gas (N_2 or He) during the transit (May et al. 2014; May and McLean 2015), as ions with larger collision cross section (CCS) areas are delayed with longer drift times than smaller ones due to more frequent collisions with buffer gas molecules (McDaniel 1964; McDaniel and Mason 1973; Fenn et al. 2009). Molecular-level structural information in the form of CCS values can help characterize the target compound and differentiate isomers (May et al. 2014). The coupling of IM and MS in elucidating complex mixtures was reported during the past decade (e.g., Baker et al. 2007; Gaspar et al. 2009; Lanucara et al. 2014). However, the use of IM-MS focused mainly on either standard biomolecule mixtures or using drift time as a supportive tool (e.g., using IM to unravel the existence of multiple charged compounds in the standard Suwannee River Fulvic Acids; Gaspar et al. 2009). No calibrated CCS values were reported, which made these applications laboratory- and instrument-dependent. These limitations prevented accurate cross-lab comparisons to generate effective information in molecular-level DOM studies. With recent commercialization of traveling-wave IM-MS and drift tube IM-MS (Lanucara et al. 2014;

May and McLean 2015), IM-MS now offers a standardized measurement of compounds with calibrated CCS values using standards with high precision and confidency (Hines et al. 2016). However, to date, the system has not been applied to obtaining systematic structural and isomeric information of natural DOM.

The goal of this study is to provide multidimensional information for natural DOM from multiple coastal sites. We report the results of natural DOM analysis using an online combination of high-performance liquid chromatogram (HPLC), IM and Quadrupole Time-Of-Flight mass spectrometry (Q-TOF MS). Natural DOM samples were collected from five South Texas rivers and adjacent coastal waters near the University of Texas Marine Science Institute (UTMSI). We aim to explore a new dimension (geometric conformation or "shape" of DOM molecules) in molecular-level DOM analysis. More importantly, we use the IM-MS to obtain actual measurement of isomers in DOM which is not available otherwise (Hertkorn et al. 2007, 2008; Dittmar and Stubbins 2014; Dittmar 2015). Our results from respective riverine and coastal waters illustrate that natural DOM molecules have lower CCS values compared with standard biomolecules of same molecular weights, indicating that their geometric conformations are more compact. With actual measurement, we demonstrate for the first time that 4.7% to 12.3% (positive mode) and 6.4% to 13.1% (negative mode) of the detected natural DOM molecules have at least one isomer, but no more than four.

MATERIALS AND METHODS

Sampling sites and sample preparation

Samples were collected from 7 sites in five south Texas rivers (Aransas River, AR: N 28.13°, W 97.43°; Lavaca River 1, LR1: N 28.96°, W 96.68°; Lavaca River 2, LR2: N 28.83°, W 96.58°; Mission River, MR: N 28.29°, W 97.28°; Nueces Dam, DAM: N 27.88°, W 97.63°; San Antonio River 1, SR1: N 28.53°, W 97.04°; San Antonio River 2, SR2: N 28.48°, W 96.86°; Figure C1, Appendix C) in May 2016 using a 2-L Van Dorn sampler. Samples were also collected from the Ship Channel (SC: N 27.84°, W 97.05°; Figure C1, Appendix C) connected to the open Gulf in September 2016. One-L samples were filtered (0.2 μm pore size) to remove suspended particles. Bulk DOC concentration was measured on 20 mL of the filtrate. DOM was isolated from the rest of filtered water and prepared for LC/MS analysis by solid-phase extraction (SPE) using a PPL cartridge (Agilent Bond Elut PPL cartridge, P/N 12105006) following the established protocol (Dittmar et al. 2008). DOM extracts were eluted with methanol and stored at -20 °C until further analysis. They were diluted 10-fold with methanol prior to analysis. The recovery rate of DOM extraction ranged from 31% to 44% on a carbon basis. All solvents and chemicals were LC/MS grade (acquired from Fisher or Sigma Aldrich).

Instrumentation

The instrumentation includes an HPLC coupled with an IM-QTOF MS with an orthogonal electrospray ionization (ESI) source (Agilent 6560, see Figure C2, Appendix C). Ion mobility separation occurs in a 78-cm uniform field drift tube with high purity N_2 as the buffer gas. Ions traverse the drift tube under a weak electric field (10 to 20 $V \cdot cm^{-1}$;

May et al. 2014) to ensure that the mobility of ions depends solely on their structures and interactions with the buffer gas. The estimated resolving power (calculated as $t/\Delta t$, in which t is drift time and Δt is the peak width measured in milliseconds at half height) of ion mobility exceeds 60 at drift time of 30 ms (May et al. 2014). The TOF MS alone has resolving power greater than 40 000 at *m/z* of 1200 (May et al. 2014), while the whole instrument IM Q-TOF LC/MS can resolve up to 2 000 000 at *m/z* of 300.

The MassHunter LC/MS Data Acquisition (Version B.07.00) provided the LC/MS parameters setup and monitored the acquisition process. Both positive and negative ion ESI modes were applied. However, because the IM data of most biomolecules were acquired under ESI+ mode (Tao et al. 2007; Fenn et al. 2009; May et al. 2014), we focus on the ESI+ mode here for comparison with published data (details for ESI- data are provided in Appendix C). MS and MS/MS data were acquired with the acquisition mode of QTOF-Only, while IM data were acquired under the IM-QTOF mode.

HPLC settings

For ESI+ mode, mobile phase A was H_2O with 0.1% (v/v) formic acid, and B was acetonitrile. One-μL of each sample was eluted through a Stablebond C_{18} column (Poroshell 120 SB-C18; 2.7 μm, 2.1 × 100 mm; Agilent P/N 685775-902) at a flow rate of 0.5 $mL \cdot min^{-1}$. During the 21-min run, mobile phase B was increased from 3% to 90% during the first 15 min, and held at 90% from 15 min to 20 min, and then dropped to 3% from 20 min to 21 min. A post-run time of 4 min allowed the column to reach equilibrium.

The same C_{18} column used in ESI+ mode was tested in negative mode, but it offered inadequate resolution, with most of the compounds co-eluting in humps (data not shown). A hydrophilic interaction chromatography (HILIC) column, on the other hand, separates small polar analytes efficiently (Buszewski and Noga 2012). Thus, a HILIC column (2.7 μm, 15 cm × 4.6 mm SUPELCO, P/N 53981-U) was used in ESI- mode. Mobile phase A was H_2O with 10 mM ammonium acetate, and mobile phase B was acetonitrile. Formation of a stable aqueous layer on the surface of a HILIC column is crucial for achieving optimal separation power. Therefore, the column was equilibrated before analysis. At a flow rate of 0.4 $mL \cdot min^{-1}$, mobile phase B was increased from 80% to 97% during the first 15 min, dropped to 84% at 18 min, 72% at 21 min, and 60% at 24 min, increased back to 97% at 30 min and held at 97% until 60 min. For sample analysis, 1 μL of samples was eluted through the HILIC column at a flow rate of 0.5 $mL \cdot min^{-1}$. During the 10-min run, mobile phase B was held at 98% during the first 1 min, and dropped to 95% from 1 min to 10 min. A post-run period of 15 min allowed the column to reach equilibrium before injection of next sample.

Data acquisition

The MS, non-targeted MS/MS, and IM-MS acquisition parameters are detailed in Appendix C. Specifically, the MS acquisition rate was 4 spectra/s, and acquisition time was 250 ms/spectrum. The MS/MS acquisition rate was 2 spectra/s, and acquisition time was 500 ms/spectrum. This high frequency of acquisition ensures the application of non-targeted LC-MS/MS (Petras et al. 2017).

MS data analysis

Data analysis employed MassHunter Qualitative Analysis (Version B.07.00, Service Pack 2), MassHunter IM-MS Browser (Version B.07.01), and MassHunter Molecular Structure Correlator (Version B.07.00). The built-in function "Find by Molecular Feature" in MassHunter Qualitative Analysis identified compounds in the MS results. +H was allowed in positive data, while –H, +HCOO, and $+CH_3COO$ were allowed in negative data. A neutral loss of H_2O was enabled in both modes. The mass inaccuracy tolerance was set at ≤ 1.5 ppm (< 0.9 mDa at a mass range of 150-600 Da). Possible formulas were computed with the function "Generate Formulas", which takes the exact mass, ^{13}C isotope abundance and ^{13}C isotope spacing into account. Generated formulas were further screened manually with the following basic criteria (Kujawinski and Behn 2006; Stubbins et al. 2010; Liu et al. 2011; Hertkorn et al. 2013): (1) Double Bond Equivalent (DBE) = $1+ \frac{1}{2}(2C-H+N+P) \geq 0$; (2) O:C ≤ 1; (3) N ≤ 4 and N:C ≤ 1; (4) 0.333 ≤ H/C ≤ 2.25; (5) Nitrogen Rule; and (6) isotopic spacing and abundance (detail in Appendix C).

MS/MS data analysis

Compounds in MS/MS results were revealed by the function "Find by Auto MS/MS" in MassHunter Qualitative Analysis with the following settings: retention time window of 0.2 min, set to be comparable to the full width of a typical chromatogram peak (Figure 5.1 and C3); an MS/MS TIC threshold of 1,000 for both positive and negative modes; mass match tolerance of 0.05 *m/z*. Possible formulas were assigned to the found compounds using the function "Search Database". The +H, +Na, and $–H_2O$ ion species

were selected in positive data, while –H, +HCOO, +CH_3COO, and –H_2O were selected in negative data. The database used was a standalone version of METLIN Metabolites (Smith et al. 2005). MS/MS data were examined in detail using Molecular Structure Correlator, which provided fragmentation information by comparing results with ChemSpider and METLIN Metabolites database.

IM-MS data analysis

IM-MS data were analyzed with the IM-MS Browser. Drift times, which represent the total transit time of the ions, including the mobility drift time and the flight time through the interfacing IM-MS ion optics and MS (May et al. 2014), were acquired using the function "Find Features (IMFE)" with the following settings: isotope model common organic (no halogens); charge state ≤ 1; ion intensity ≥ 50. Compound drift times were calibrated with reference ions to determine the gas-phase momentum transfer collision cross section (CCS; Mason and Schamp 1958; May et al. 2014).

RESULTS AND DISCUSSION

LC for powerful preliminary separation of DOM molecules

HPLC is an important tool in molecular-level analysis of complex samples (Hertkorn et al. 2007), and has been used to isolate and identify biomolecules in many studies (Ogawa et al. 2001; Leenheer and Croué 2003; Rathgeb et al. 2017). Here, the C_{18} column provides a preliminary separation of natural DOM molecules based on their hydrophobicity. The retention mechanism of the HILIC column is still under debate (Hao et al. 2008), but may involve partitioning of analytes from the bulk eluent through multimodal retention mechanisms including ion-exchange, hydrogen-bonding, hydrophobic and hydrophilic interactions with the immobilized water-rich layer on HILIC stationary phases (Alpert 1990; Yoshida 2004; Guo et al. 2007; Hao et al. 2008). Figures 5.1 and C3 show typical chromatograms for our sampling sites (Rivers and Ship Channel) measured under both ESI modes. The HPLC chromatograms were highly reproducible, with retention times differing less than 0.05 min between replicate samples (data not shown). The chromatograms are divided further into different fractions (F1 to F5) based on mobile phase and the distribution of peaks. Note that signal intensity of the marine Ship Channel sample was higher than that of riverine samples in ESI+ mode, but lower in ESI- mode (Figures 1 and C3).

A complete MS dataset of both ESI+ and ESI- data was acquired (Appendix C). In order to compare with published IM data mainly in ESI+ mode, we here focus on the positive mode. ESI+ mode is not used as commonly in most DOM studies, based on the assumption that DOM primarily contains molecules with carboxyl groups that can be

ionized efficiently in negative mode (Ohno et al. 2016). However, neither ESI- mode nor ESI+ mode provides a holistic projection of the complex DOM mixture (Hertkorn et al. 2008). Our primary goal here is to demonstrate multidimensional information on the size, structure and composition of DOM.

Briefly, our data shows that compounds annotated in ESI+ mode generally have a higher average value of H/C (paired t test, $df = 7$, $t = 14.602$, $p < 0.05$) but lower O/C ratios (paired t test, $df = 7$, $t = -2.4629$, $p < 0.05$; Table C1, Appendix C). The most prominent difference in O/C ratios observed in marine samples agrees with the conclusion from previous literature that oxygenated molecules are preferentially ionized in negative mode (Hertkorn et al. 2008, 2013; Ohno et al. 2016). On average, 4959 and 2331 peaks are found in ESI+ and ESI- mode, with 2816 and 1629 formulas assigned, respectively. The formula assignment percentage in this work is 56.4% in ESI+ mode, and 68.4% in ESI-.

The van Krevelen diagrams are shown in Figure C4 (Appendix C). H/C = 1.5 is defined as the molecular lability boundary (MLB) to differentiate natural DOM into labile and less labile groups, with H/C ≥ 1.5 corresponding to more labile material (D'Andrilli et al. 2015). Using this standard, about one half of the compounds (43.4% in ESI+ and 67.9% in ESI-) were below the MLB in both ESI modes, indicating that DOM collected from rivers and coastal waters is an intricate mixture of relatively "labile" and "recalcitrant" constituents. Lipid-, protein-, cellulose-, and lignin-like biomolecules (Mopper et al. 2007; Hockaday et al. 2007; Hertkorn et al. 2008; Liu et al. 2011; Repeta 2015) are present in the van Krevelen diagrams, but overall very few compositions of natural DOM are observed in the specific sectors of the diagram anticipated for these biomolecules (Figure C4,

Appendix C). The majority of natural DOM is positioned between different groups of biomolecules (Figure C4, Appendix C). In agreement with previous studies (Hertkorn et al. 2002, 2007, 2008; Dittmar and Kattner 2003), this observation indicates that the covalent bonding between different classes of biochemical precursor molecules may be an important source of natural DOM (Hertkorn et al. 2008). Note that the van Krevelen diagrams in this work are different from those reported previously in direct infusion experiments, but consistent with a previous LC-MS study (Rathgeb et al. 2017).

Most previous DOM studies using ultrahigh resolution MS technique such as FTICR-MS have applied direct infusion. However, the application of HPLC prior to the DOM analysis is still desirable because combining HPLC with MS alleviates ion competition/suppression effects during ionization (Petras et al. 2017; Rathgeb et al. 2017). In the mixture of DOM, the ionization of the low efficiency compounds is suppressed by high efficiency compounds (Tang et al. 2004; Ohno et al. 2016). For instance, in ESI- mode carboxyl-rich alicyclic molecules (CRAM; Hertkorn et al. 2006) would be ionized preferentially due to their high carboxyl-group content, thus in direct infusion other types of compounds would be suppressed (Hertkorn et al. 2008). With the addition of HPLC, high ionization efficiency molecules can be separated from low efficiency molecules in a certain degree due to their different physical properties. Many compounds with higher H/C and/or O/C ratios were revealed in this work (Figure C4, Appendix C) compared with other direct-infusion DOM studies (Hertkorn et al. 2006; Liu et al. 2011; Repeta 2015; D'Andrilli et al. 2015). This result is consistent with previous findings that fractionated DOM covers a larger area of van Krevelen diagrams than non-fractionated (Hertkorn et al. 2008).

The other advantage of using HPLC is the separation of compound mixtures by the column and hence the enhanced resolving ability in annotating DOM molecules, even isomers, because it introduces a near-orthogonal dimension for molecular-level analysis (Hertkorn et al. 2007; Petras et al. 2017). When re-examining the van Krevelen diagram based on the retention time (Table C2, Figures C5, and C6, Appendix C), the H/C ratios increase and O/C ratios decrease progressively as the solvent shifts from hydrophilic to hydrophobic in ESI+ mode, while H/C ratios increase as the solvent becomes less hydrophobic in ESI- mode (Table C2, Appendix C). The retention time information can also differentiate structural isomers. For example, more than one peak with *m/z* of 437.1943 were detected in Ship Channel samples but not in riverine samples under ESI+ mode (Figure 5.2). Of the several m/z 437.1943 peaks, one compound eluted at about 11.3 min at fraction F3, as compared to ca. 18.5 min at fraction F4 for the other compound (Figure 5.2a). Although the two compounds had identical *m/z* and isotopic features (Figure 5.2b & c), their drastically different elution times indicate that they are isomers, with the second compound being more hydrophobic. MS/MS results further confirm that these two compounds had different fragments after collision, with the first compound having fragments with an *m/z* of 59, 87, and 421, as compared to fragments of 112, 114, 130 and 364 for the latter (Figure 5.2d&e). Note that this isomeric information would be buried without the previous separation by HPLC.

Molecular formula assignments based on non-targeted LC-MS/MS results

In the MS/MS mode, selected ions are fragmented automatically by the applied collision energy. Using targeted tandem MS to obtain detailed structural information of certain compounds is common in molecular-level DOM studies. Here we take advantage of the high acquisition speed (2 spectra/s, as mentioned above in Methods and Appendix C) to do a non-targeted full scan LC-MS/MS analysis of natural DOM. We use the fragment information as a holistic method to annotate the DOM molecules based on METLIN Metabolites database. This non-targeted LC-MS/MS approach has been reviewed extensively in metabolomics studies (Viant and Sommer 2013; Liesenfeld et al. 2013; Gika et al. 2014; Rubert et al. 2015), but was applied in DOM analysis only very recently (Petras et al. 2017). Additionally, the Molecular Structure Correlator (Version B.07.00) can calculate the likelihood of the fragmentation pathway. On average, in ESI+ mode, 176 and 224 compounds were assigned with a match based on the METLIN Metabolites database for riverine and marine samples, respectively. In ESI- mode, 180 and 74 compounds were assigned with a match, respectively. The assignment rate based on MS/MS ranged from 56.4% to 62.5% in ESI+ mode and from 68.4% to 70.4% in ESI- mode. The van Krevelen diagrams based on MS/MS data (Figure C7, Appendix C) resemble those generated from MS data. From these samples we assembled a database of 89 DOM molecules with holistic structures based on non-targeted LC-MS/MS in appendix, and two example molecules are further shown in Figure C8 (Appendix C).

The 3D size of DOM molecules from IM results: CCS-based characterization

Currently, ion mobility instrumentation is used mainly for structure-based characterization and differentiation of chemical isomers with high resolution, high sensitivity, and broad sample compatibility (May and McLean 2015). The existing IM database was acquired mainly under ESI+ mode (Tao et al. 2007; Fenn et al. 2009; May et al. 2014), so only ESI+ data of natural DOM is shown and discussed here to compare with the existing database. Species, *m/z*, drift time and CCS values of the biomolecules standards were obtained from published studies using the same model of IM instrument that is calibrated with standards (May et al. 2014). The number of compounds detected through IM-MS varies among different samples, but remains quite constant among replicates. The average number of features ranged from 46 in Lavaca River 2 (LR2) to 460 in Lavaca River 1 (LR1) under ESI+ mode (Table C3, Appendix C), and they are about one order of magnitude lower than those in MS and MS/MS due to the ion loss during IM. The fact that LR1 has the most features detected in IM-MS is consistent with HPLC chromatograms, in which LR1 has chromatogram peaks not detected in other samples at retention time of ~ 6.4 min and ~ 7.2 min (Figure 5.1). It remains unclear why such a great difference in the number of features occurred from the two sites of the same river (Figure C1, Appendix C). One possible explanation is that LR2 is on the downstream of LR1, the abiotic/biotic modifications during transportation may have caused this change, as the low flow is typical for south Texas rivers (Reyna et al. 2017). In addition, the downstream LR2 is influenced by a major stream branch sourced from Lake Texana from north, so the difference on the features between LR1 and LR2 is not surprising. Of the 266 compounds

in marine sample, 180 and 76 were assigned with a formula with MS and MS/MS, respectively. For riverine samples, the number varied from 27 to 293 with MS, and 4 to 20 with MS/MS (Table C3, Appendix C). The van Krevelen diagrams based on IM-MS data in ESI+ mode (Figure C9, Appendix C) again assemble those generated from MS data and MS/MS data.

IM separations are based on the ion's interaction with neutral buffer gas, which is proportional to "apparent ion surface area" (Fenn et al. 2009). When coupled with MS, IM can provide gas-phase separations in one dimension on the basis of structure, and a second dimension on the *m/z* value. The CCS data of standard biomolecules and tetraalkylammonium were acquired from published database (May et al. 2014). As shown by the CCS vs. *m/z* diagram (Figure 5.3), CCS increases with an increasing *m/z*. For standard biomolecules, the CCS value at a particular *m/z* increases in the order of carbohydrates < peptides < lipids < tetraalkylammonium (TAA) salts. The lower CCS values of carbohydrates and peptides show high efficiency of gas-phase packing due to their higher degrees of freedom in structures. In contrast, lipids exhibit the largest CCS values among biomolecules mainly due to their inability to form compact, self-solvated structures in the gas phase (May et al. 2014). TAA salts have the highest CCS values in the database because of the strong intramolecular repelling force between the positively charged alkyl groups.

Natural DOM showed the same trend in the CCS-*m/z* relationship: the CCS increased with *m/z* (Pearson correlation; $t = 95.005$; $df = 3851$; $p < 0.01$). The correlations between CCS and *m/z* in both standard biomolecules and natural DOM are depicted

adequately by a power-law relationship (for DOM: $y = 21.99x^{0.35}$, $R^2 = 0.7010$). The exponent of 0.35 for natural DOM is smaller than the exponents of biomolecules (0.55 for peptides, 0.47 for carbohydrates, and 0.60 for lipids; May et al. 2014), suggesting that CCS of natural DOM is small compared with biomolecules of the same molecular weight (e.g., comparing with carbohydrates: $t = 18.169$; $df = 3974$; $p < 0.01$). The difference of CCS between natural DOM and biomolecules becomes more apparent as molecular weight increases (Figure 5.3), implying that the change of CCS is less sensitive to molecular size in natural DOM. This result indicates that natural DOM compound structures are often more compact than biomolecules. This observation may result from abiotic and biotic modification of DOM during environmental degradation processes, assuming that they originated from biomolecules. Furthermore, the fact that natural DOM possesses different CCS values from biopolymers concurs with the MS findings in this work and other studies (Hertkorn et al. 2002, 2007, 2008; Dittmar and Kattner 2003), in which only few compositions of natural DOM can be attributed to known biopolymers. Note that the molecule geometric conformation as CCS value was derived in gas phase, and it may change in aqueous phase where natural DOM exists. However, since all the molecules were compared under the same conditions, the conformation differences among different molecules observed in gas phase should be consistent in aqueous phase (Tobias and Brooks 1992; Chipot et al. 1996; Hanus et al. 2004).

Statistical analyses show that within DOM molecules, CCS values are correlated positively with H/C ($R^2 = 0.0017$, Pearson correlation; Table C4, Appendix C) and O/C ($R^2 = 0.018$, Pearson correlation; Table C4, Appendix C), but negatively with N/C ($R^2 =$

0.0511, Pearson correlation; Table C4, Appendix C). The positive relationship between CCS and O/C within DOM molecules suggests that with CCS values increase, DOM molecules become degraded (O/C increases). Degraded DOM molecules have lower degree of freedom in their structure, which results in an increased CCS value. Thus, CCS values may characterize the oxidation and degradation level of natural DOM. Note that although statistically significant, the correlation between O/C ratio and CCS is weak. Further studies to investigate CCS changes among more DOM samples or through laboratory incubations are needed.

As mentioned above, a database containing 89 compounds, covering the annotated compounds from river and coastal regions, was established with our developed protocol, based on respective results from LC-MS, MS/MS, and IM-MS (Appendix C). This database contains multidimensional information on natural DOM, including retention times from LC, *m/z* from MS, CCS from IM-MS, and possible formula and structures based on MS/MS. This database provides a platform to seek specific DOM compounds, and will expand as more natural DOM samples are analyzed from other fresh and saline waters.

Isomers in DOM molecules from the IM results

Besides separating natural DOM molecules on the basis of structure, IM Q-TOF LC/MS helps elucidate the "unknown structural isomers" (Dittmar 2015) of DOM. The resolution of IM-MS is high enough to separate isomers with subtle changes in structure (Dwivedi et al. 2007; Zhu et al. 2009). For instance, Methyl-α-Glucopyranosides (α-MeGlc; Figure 5.4a) and Methyl-β-Glucopyranosides (β-MeGlc; Figure 5.4b) were

separated by IM with a difference of 0.47 ms in drift time (Dwivedi et al. 2007), while tertrasaccharide alditols cellobiitol (Glcβ1-4 Glcβ1-4 Glcβ1-4 Glc-ol; Figure 5.4c) and maltotetraitol (Glcα1-4 Glcα1-4 Glcα1-4 Glc-ol; Figure 5.4d) were separated with a difference of as much as 1.20 ms (Zhu et al. 2009). We show two typical examples of isomers detected in our DOM samples: (1) The *m/z* value of 249.1556 (± 1.5 ppm) clearly includes at least two isomers (Figure 5.4e), with drift times of 29.30 ms and 22.94 ms, respectively; (2) Compounds 340.2571 (± 0.3 ppm) have at least two isomers as shown in the drift time diagram (Figure 5.4f), with drift times of 21.11 ms and 24.31 ms, respectively. Structural isomers have the same elemental composition and very close elution times in HPLC. Even though many isomers, including enantiomers, can be separated via different combinations of columns and mobile phases, differentiating isomers in natural DOM samples by traditional MS and tandem MS methods is still quite challenging, if possible. The IM-MS offers a novel way of identifying DOM isomers as they have different drift times and CCS values.

From our IM-MS measurement, the percentage of compounds possessing isomers (defined as isomer percentage) for DOM in fresh and coastal waters remain relatively constant among different river samples, ranging from 4.7% to 12.3% under ESI+ mode, and from 6.4% to 13.1% under ESI- mode (Table 1), with the average percentage at about 10%. The highest isomer percentage under positive mode occurred in San Antonio River 1 (SR1) samples, while under negative mode it was found in Aransas River (AR) samples. Overall, ten percent of DOM molecules have at least one isomer (the largest isomer number is four). The isomer percentage calculated here is much lower than previous modelling

results (Hertkorn et al. 2008; Dittmar and Stubbins 2014; Zark et al. 2017). Moreover, the multiple-peak distribution of drift time peaks (Figure 5.4e and 5.4f) further suggests that the total number of isomers is far from the theoretical maximum value for every formula, since a large number of isomers tend to form one mono-peak Gaussian distribution in drift time. Also, the number of isomers (in form of CCS values) of a given molecule does not exponentially increase with increasing molecular weights (Figure 5.3), which otherwise would be expected if there are no constrains on isomer existence (Hertkorn et al. 2007; Dittmar and Stubbins 2014). Another important implication of the reported isomer percentage is that the total number of DOM molecules may not be high enough for the concentration of each individual molecule to reach the minimum threshold as claimed, which is the basis of so-called "dilution hypothesis" (Hertkorn et al. 2008; Dittmar and Stubbins 2014; Dittmar 2015; Arrieta et al. 2015).

However, the IM may not resolve all the isomers in DOM samples. Current resolving power of available IM instrument generally ranges from 50 to 100, and >100 resolving power is rarely reported (Dodds et al. 2017b). A similar system (LC-ESI-IM-TOF-MS) was capable of resolving over 70% of the constitutional isomers from a 4000-peptide mixture (Srebalus Barnes et al. 2002). A more recent study has reported that with a resolving power of 60, IM-MS alone (without LC) resolved over 30% of the isomers of leucine ($C_6H_{13}NO_2$), with most constitutional isomers (i.e., ethyl ester vs. tertleucine vs. norleucine) resolvable, but some diastereomers (i.e., L-allo-isoleucine vs. L-isoleucine) and most enantiomers (L-leucine vs. D-leucine and L-isoleucine vs. D-isoleucine) unresolvable (Dodds et al. 2017a). Nevertheless, our IM-MS result clearly demonstrates

that, in contrast to what modelling studies hypothesized, the number of isomers is lower than modelled in DOM molecules. While more work is needed to reconcile the discrepancy between our measurement and modelling data, this dataset provides the first quantitative information about DOM isomers based on actual measurements, and it opens a new direction in molecular-level DOM analysis.

IMPLICATION

This work shows that the IM Q-TOF LC/MS provides a multi-dimensional approach to annotate natural DOM, by combining HPLC, MS, tandem MS and ion mobility. With IM in the system, geometric conformation of DOM molecules is introduced into molecular-level analysis, and a direct measurement of isomers in natural DOM is achieved for the first time. Our data show that natural DOM molecules from several south Texas rivers and coastal waters are more compacted than standard biomolecules, and that higher oxidation state results in larger geometric conformation of DOM molecules. Moreover, of all DOM molecules resolved within the detection limit of IM-MS, from 4.7% to 12.3% under ESI+ mode, and from 6.4% to 13.1% under ESI- mode, respectively, had at least one isomer. The isomer percentage measured in this study is much lower than that reported in previous modelling efforts. A database containing 89 compounds was established with multidimensional information, including retention times, molecular weight, possible formulas and structures based on MS/MS, CCS, and isomeric information. This database provides a foundation to be further expanded, or compared, with data from different seasons and locations. We expect this preliminary study to serve as a "first spark"

to provoke other studies leading to new advancements on elusive organic compound identifications in natural DOM samples. The unique ability of IM-MS to separate isomers will increase our understanding of the complex structure of DOM and its interactions with light, natural ions, and/or contaminants in natural environments.

Table 5.1. Isomer percentages for different samples

Sites	ESI+	ESI-
Ship Channel	7.5 ± 0.1 %	6.4 ± 2.3 %
Aransas River	9.8 ± 0.2 %	13.1 ± 2.2 %
Lavaca River 1	9.8 ± 0.2 %	7.2 ± 1.8 %
Lavaca River 2	4.7 ± 2.3 %	9.4 ± 0.3 %
Mission River	10.2 ± 0.7 %	7.2 ± 2.16 %
Nueces Dam	10.2 ± 0.4 %	9.1 ± 2.5 %
San Antonio River 1	12.3 ± 1.6 %	10.0 ± 0.7 %
San Antonio River 2	9.5 ± 6.5 %	10.0 ± 2.5 %

Figure 5.1. Chromatograms of LC retention time vs. ion intensity under ESI+ mode. Different fractions (F1-F5) are determined based on the mobile phase (see the main text) and the distribution of chromatographic peaks. (a) Riverine samples under ESI+ mode; (b) Ship Channel sample under ESI+ mode.

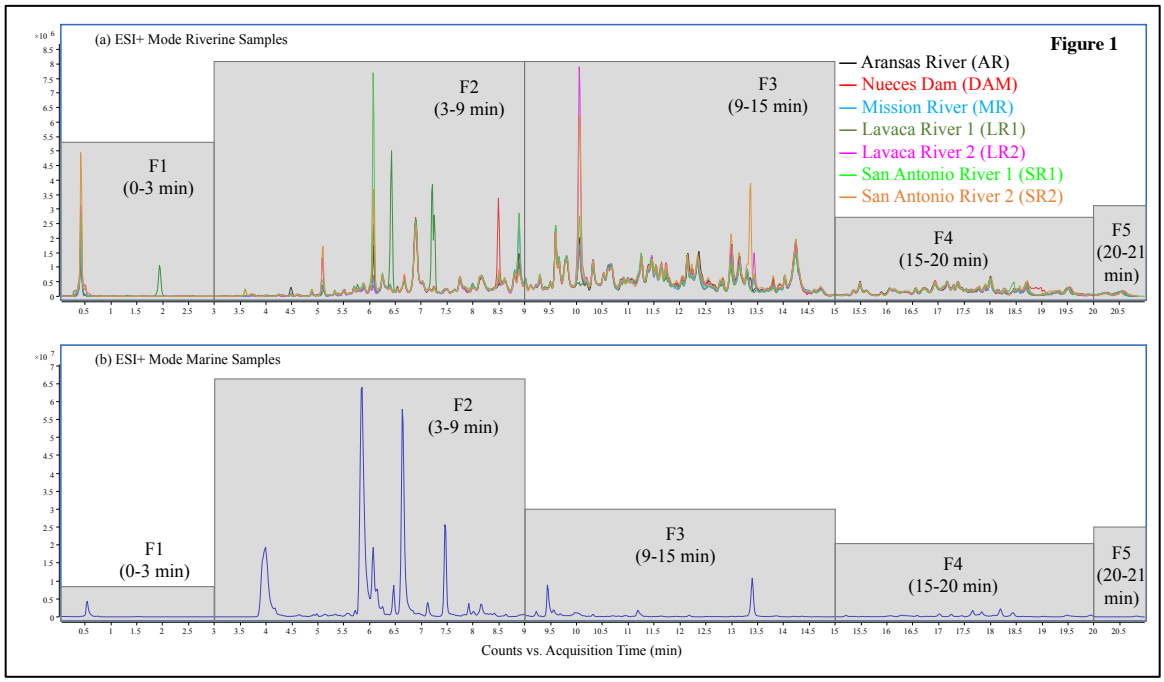

Figure 5.2. Chromatograms and spectra for ion 437.1943 (m/z). (a) Chromatogram of compounds with different elution times (Green: elution time 11.3 min; Yellow: elution time 18.5 min). (b) Parent ion spectrum of 437.1943 at 11.3 min. (c) Parent ion spectrum of 437.1943 at 18.5 min. (d) Product ions spectrum of 437.1943 at 11.3 min. (e) Product ions spectrum of 437.1943 at 18.5 min.

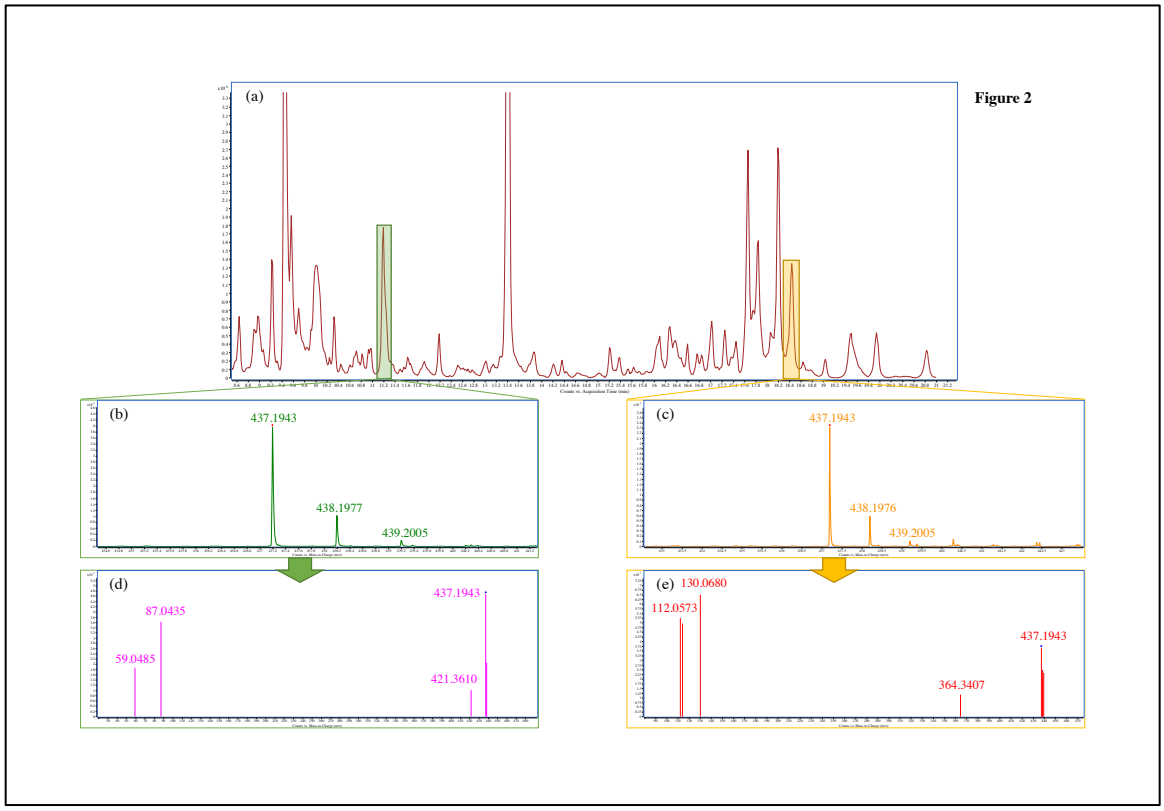

Figure 5.3. Scatter plot of CCS (Ω) vs. m/z. Squares represent published standard biomolecules (tetraalkylammonium salt cations, carbohydrates, peptides and lipids May et al. 2014). CCS generally increases with an increasing m/z for biomolecules, and the relationship can fit with a power-law function. Natural DOM showed the same trend in the CCS-m/z relationship but possess lower CCS values compared to the standard biomolecules given the same molecular weights ($p < 0.05$). The trend becomes clearer as molecular weight increases.

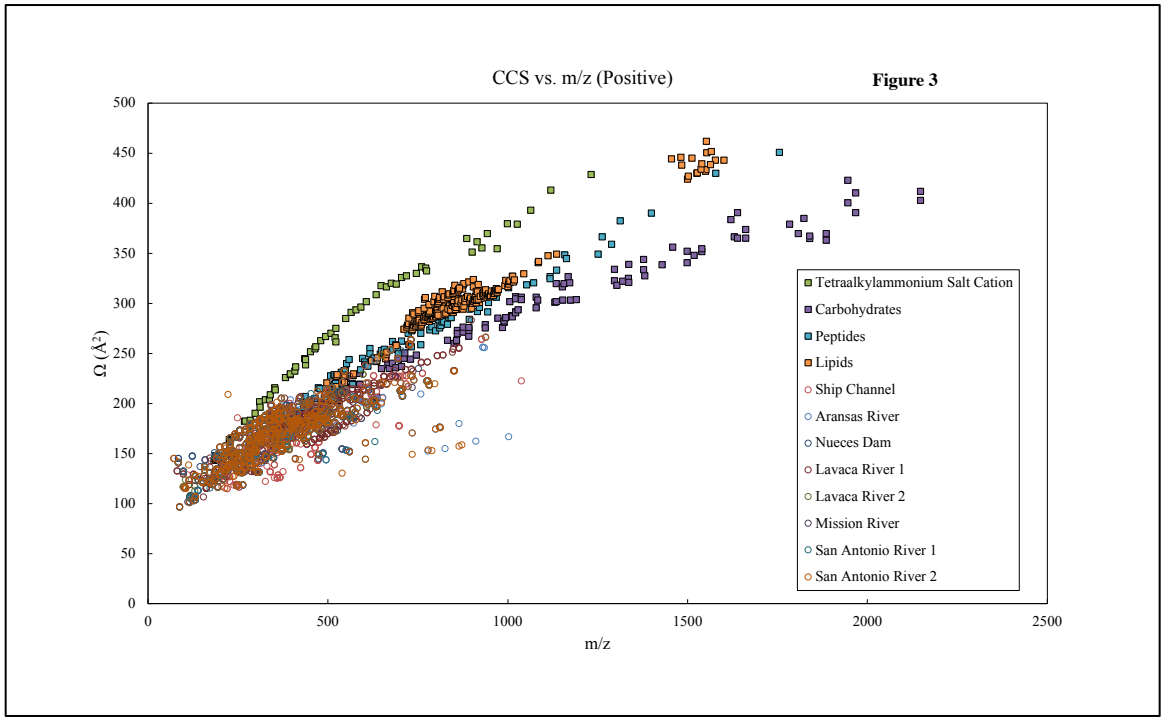

Figure 5.4. (a) Methyl-α-Glucopyranosides (α-MeGlc).(Dwivedi et al. 2007) (b) Methyl-β-Glucopyranosides (β-MeGlc).(Dwivedi et al. 2007) (c) alditols cellobiitol (Glcβ1-4 Glcβ1-4 Glcβ1-4 Glc-ol).(Zhu et al. 2009) (d) maltotetraitol (Glcα1-4 Glcα1-4 Glcα1-4 Glc-ol).(Zhu et al. 2009) (e) Compounds 249.1556 (± 1.5 ppm) shows two isomers with drift times of 29.3 ms and 22.94 ms. (f) Compounds 340.2571 (± 0.3 ppm) shows two isomers with drift time of 21.11 ms and 24.31 ms.

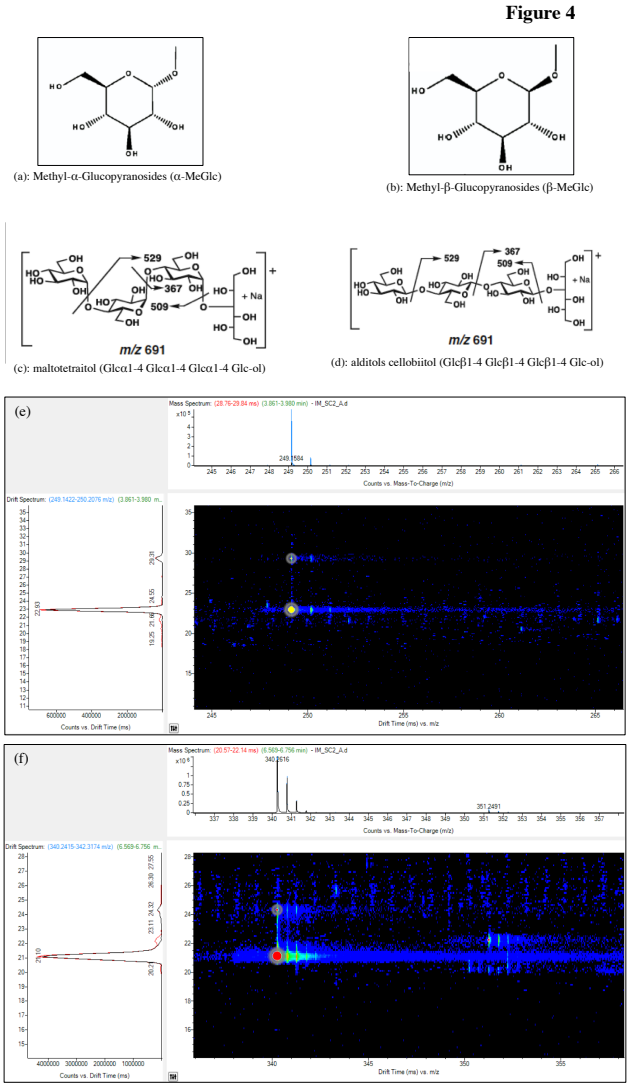

Chapter 6. Conclusions and implications

In this dissertation, we investigated the cycling, formation, and characterization of DON following an order of decreasing lability from labile small molecules such us urea and peptide to natural uncharacterized DON. The cycling of urea, the long-term fate of peptide, and the molecular-level information on previously uncharacterized DON are discussed in detail.

We conducted a series of microcosm incubations in 2014 and 2015 to study urea cycling the Lake Taihu and how it interacts with *Microcystis* spp. during CyanoHABs (Chapter 2). Our data showed that lake bacterial consortium uses urea and urea can support the growth of pure *Microcystis* culture at a rate comparable to NH_4^+. A diel pattern in urea metabolism was recognized previously (Solomon et al. 2010a). We demonstrate that the diel pattern in urea metabolism is not only reflected by the cycling rate of urea (higher cycling rates under natural irradiation), but also in the fate of urea, with a higher fraction of the removed urea recovered as NH_4^+ under dark conditions. We further demonstrate that the direct role of *Microcystis* in urea cycling is not as important as that of heterotrophic bacteria associated with the bloom, even though *Microcystis* is the dominant cyanobacteria species in the bloom. Overall, this chapter provides insights into urea dynamics in Lake Taihu labile DON cycling, and further addressed the relationship between urea and CyanoHABs. It potentially emphasizes that urea's role in CyanoHABs is likely indirect. The result from this study can be applied in other eutrophic or hypereutrophic lakes (i.e., Lake Erie in North America, Lake Victoria in Africa, etc.) for future CyanoHABs control.

In the following chapters, we studied the cycling of labile DON and the formation of semi-labile and refractory DON in controlled incubation experiments (amino acids and peptide; Chapter 4). A holistic analytical method of ^{15}N in different forms is developed to quantitatively determine the fate of N throughout the incubation (Chapter 3). Our data shows that peptide was degraded faster in hypoxic water than in oxic water, indicating that hypoxia is not a simple intermediate between oxic and anoxic conditions when investigating the degradation of organic matter. The faster degradation rate of peptide in low-oxygen water documented previously (Liu et al. 2013), corresponded directly to the fast-growing bacteria, such as *Roseobacter* (Liu et al. 2013; Liu and Liu 2016). Our data further estimated the long-term fate of amino acid N and peptide N by quantifying the different forms (NH_4^+, NO_x^-, PON, and DON) of N. Surprisingly, only a small fraction of the peptide N was transferred to inorganic form (NH_4^+ and NO_x) when using AVFA as the incubation substrate, while a large proportion of the peptide N (over 40% in bottom water and over 60% in surface water) stays as uncharacterized DON (not peptide or amino acid), persisting at least one month. On the other hand, when alanine was used as incubation substrate, DIN was the dominant form of N throughout the incubation (over 80% spiked N in NO_x). It remains unclear what caused the difference in the fate of N. One explanation is the presence of specific amino acids such as Val and Phe may have affected the production of new DON, as Phe and Val may possess a different metabolism pathways compared with Ala (Amano et al. 1982). We speculate that small peptide-like structure with certain amino acids (i.e., Phe and Val) may be important precursors of the refractory N-methyl amines and amides in DON, but further work is needed to test this hypothesis. Characterizing and

determining the fate of N is always challenging due to the analytical challenges mentioned above, yet the long-term fate of N is particularly important in DON research, as it serves as a bridge connecting two extremes (labile and refractory) in DON. These two chapters (Chapter 3 and 4) together introduce a simple but efficient holistic method for DON analysis and also provide preliminary but intriguing insights into the formation mechanism of unidentified semi-labile DON through controlled incubation.

In Chapter 5, we took a further step into the unidentified extreme of DOM and DON by introducing the geometric conformation of DOM molecules into its molecular-level characterization. With the combination of HPLC, MS, tandem MS and ion mobility, a multi-dimensional characterization of natural DOM was achieved by the IM Q-TOF LC/MS. The IM provides geometric information on natural DOM, and a direct quantitative measurement of isomers in natural DOM is made for the first time. IM data shows that biomolecules such as carbohydrate, peptide and lipid, and natural DOM molecules have a more compact geometric conformation in natural DOM than in pure compounds, as reflected by their smaller CCS values. Of all DOM molecules resolved within the detection limit of IM-MS, ca. 10% had at least one isomer. However, the percentages of isomer measured in this study were much lower than predicted by modelling results. The fact that a trend of increasing isomer abundance with increasing molecular weight was not detected further contradicts with the isomer abundance estimated by modelling efforts. In other words, the number of isomers present in natural DOM may not be sufficient to support the dilution hypothesis, in which researchers have argued that with a huge number of isomers the concentration of each molecule is too low to allow utilization by bacteria (Arrieta et al.

2015). The work presented in this chapter not only introduces a new dimension into the molecular-level characterization of natural DOM, but also provides insights into the long-term stability of DOM in aquatic systems.

To summarize our work, this dissertation provides systematic studies of DON, covering the dynamic of labile DON, transformation from labile DON to semi-labile DON, long-term fate of DON, and molecular-level information of DON. Fate of labile DON, which has not been studied extensively, was revealed with a ^{15}N technique. Geometric conformation and the isomeric information on natural DOM and DON are introduced into DOM studies in a quantitative manner. The new information provided in this dissertation potentially opens a new dimension in future DON studies. Therefore, the dissertation presented here has laid a solid foundation for future studies. Some future directions or questions related to our study may include:

1. Unique quantitative measurements of DOM and DON isomers are introduced into studies of DOC and DON. In Chapter 5 we focused on several south Texas Rivers and a central coastal GOM region. More studies, across different temporal and spatial scales, are necessary to explore these new dimensions of information further and address new questions. For example, does seasonality affect the geometric conformation and isomeric property of natural DOM? How would geometric conformation and isomer percentage of natural DOM change following a freshwater-ocean transect, and a depth profile? Does DOM in the deep ocean possess a higher isomer percentage? Samples of natural DOM from south Texas rivers across

different seasons were collected. Also collected are samples following a transect of: (1) Atchafalaya River to open GOM; (2) Mississippi River to open GOM; (3) several depth-profiles in open GOM. Future studies will be focused on the analysis of these samples, and other samples across different temporal and spatial scales. Data produced can also be used to expand the database mentioned in Chapter 5.

2. With the multi-dimension technique, we have annotated some interesting compounds in natural DOM in molecular level through MS and MS/MS. One of them appears as a tri-peptide not documented previously. Further studies are needed to further confirm the presence of these particular compounds by comparing with known standards. Subsequent studies to quantify the concentrations and even to trace the source of the present compounds are necessary if their presences are confirmed. This study would be among the first few that identify and quantify specific compounds in natural environment. When combined with controlled incubation experiments, this work will provide further insight into the formation of refractory DOM and DON.
3. Geometric conformation of natural DOM should be explored further. For instance, computational chemistry can estimate the structure of a specific molecule given its exact molecular weight (from MS), fragmentation patterns (from MS/MS), and CCS values (from IM). This idea was tested with a few compounds but larger systematic studies are needed.

4. Our peptide incubation experiment shows that, in contrast to C, a considerable fraction of labile DON is converted into uncharacterized DON at the end of month-long incubation. Converted DON is defined as "uncharacterizable" because they are not peptides or amino acids. However, molecular-level information of these DOM and DON molecules can be obtained with the application of IM Q-TOF LC/MS. With the combination of controlled incubation and state-of-art LC-MS, we can further investigate the content of DON compounds produced from the incubation. Furthermore, we can explore how DOM and DON change before and after incubation, and how these changes are related to the change in bacteria community. Previous studies of the changes of DOM communities throughout the incubation appears to be controversial but important. DOM diversity decreases as incubation proceeds, however the communities sometimes become more diverse, supporting the dilution hypothesis (as community becomes diversified, concentration of each molecule becomes diluted). IM function, helps define how isomers of natural DOM change. Samples were already collected from: (1) an incubation with the substrate of riverine DOM; and (2) a controlled incubation with fresh labile algae matter.

Appendices

APPENDIX A. SUPPORTING INFORMATION ON UREA DYNAMICS DURING LAKE TAIHU CYANOBACTERIAL BLOOMS IN CHINA

Figure A1. Change of $^{15}NH_4^+$ with time at Station 1 (A), Station 3 (B), Station 7 (C) and Station 10 (D) during the 2014 microcosm incubations.

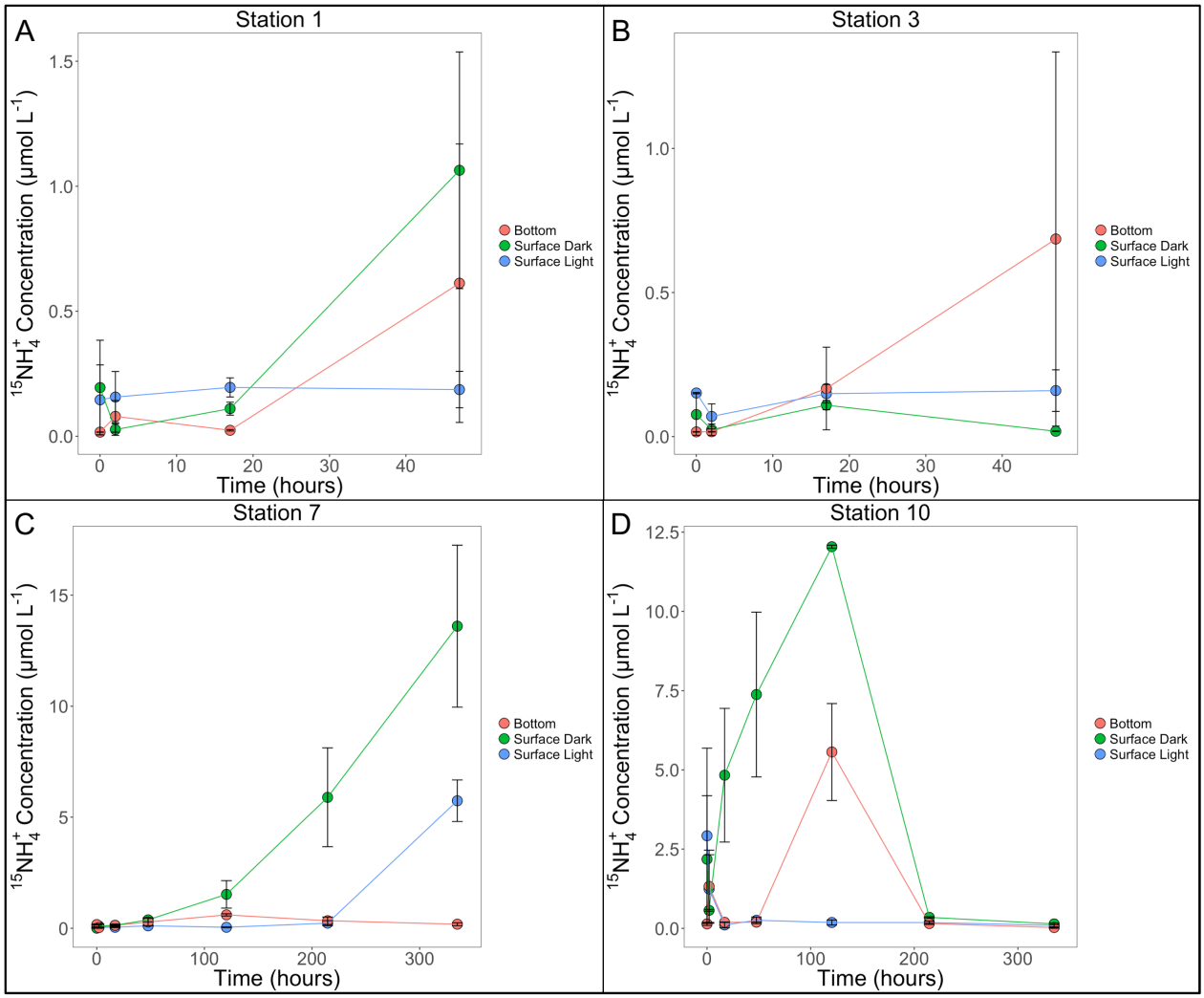

Figure A2. Bacterial fluorometry images with SSC-H (cell size; x axis) vs FL1-H (green fluorescence; y axis) during incubations at Station 1 (A), Station 3 (B), Station 7 (C), Station 10 (D). The images show that bacterial population, represented by DNA content, remained relatively unchanged for incubations at Station 1. At Station 3, however, distinct bacterial populations with higher DNA content developed in the surface water as incubations proceeded. For the long incubation, bacterial population stayed relatively unchanged for incubations at Station 7, but the DNA content of the bacterial population increased in surface incubations at Station 10.

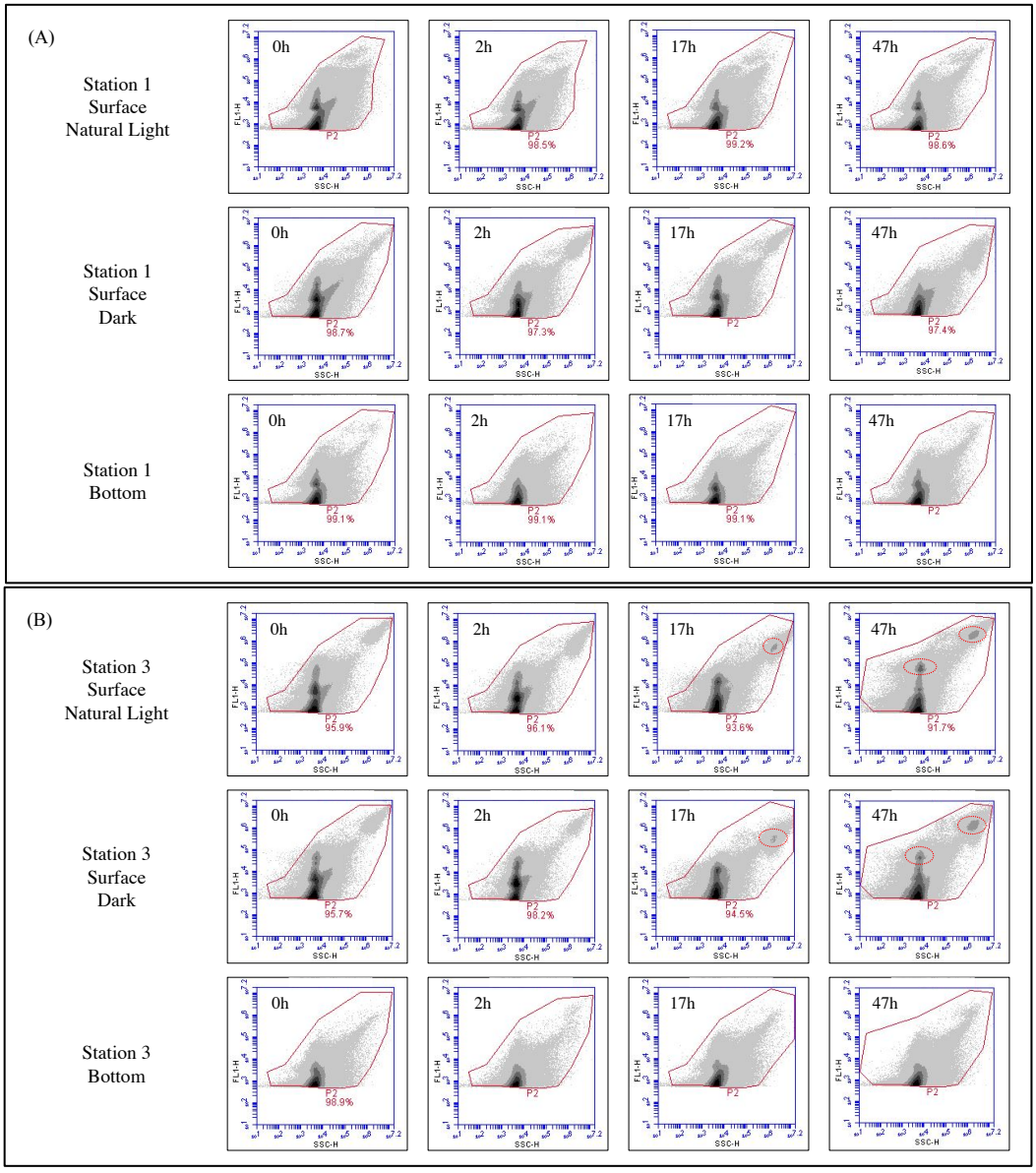

Figure A2, cont.

Figure A3. Bacterial community structure (genus level) for incubations conducted at Stations 7 and 10 during the 2014 microcosm incubations (only 0h, 47h, and 335h samples were chosen for bacterial community analysis). Genus contribute less than 3% were combined together.

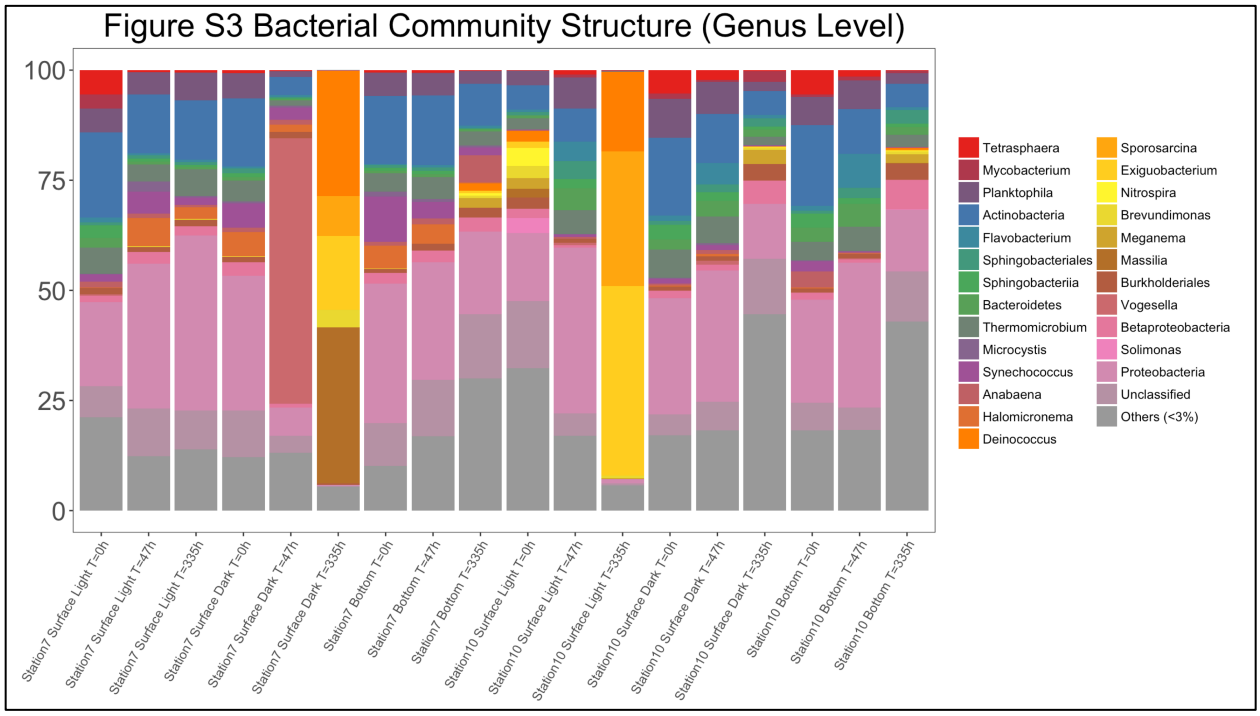

Figure A4. Principle Coordinates Analysis (PCoA) on the bacterial genus data. PC1 explains about 48% of the data variance and PC2 30%. Surface light treatments (0h, 47h, 335h) at Station 7, surface dark treatment (0h) at Station 7, bottom treatments (0h, 47h, 335h) at Station 7, surface light treatments (0h, 47h) at Station 10, surface dark treatment (0h, 47h, 335h) at Station 10, and bottom treatments (0h, 47h, 335h) at Station 10 were grouped together, indicating that these samples have similar bacterial community structure. Surface dark treatments (47h, 335h) at Station 7, and surface light treatment (335h) at Station 10 were isolated, indicating that their bacterial community is different. The fact that surface dark treatment (335h) at Station 7 and surface light treatment (335h) at Station 10 were grouped together further indicates that the similarity of bacterial community. Overall, PCoA suggests that drastic changes occured in the surface dark treatment at Station 7 and the surface light treatment at Station 10.

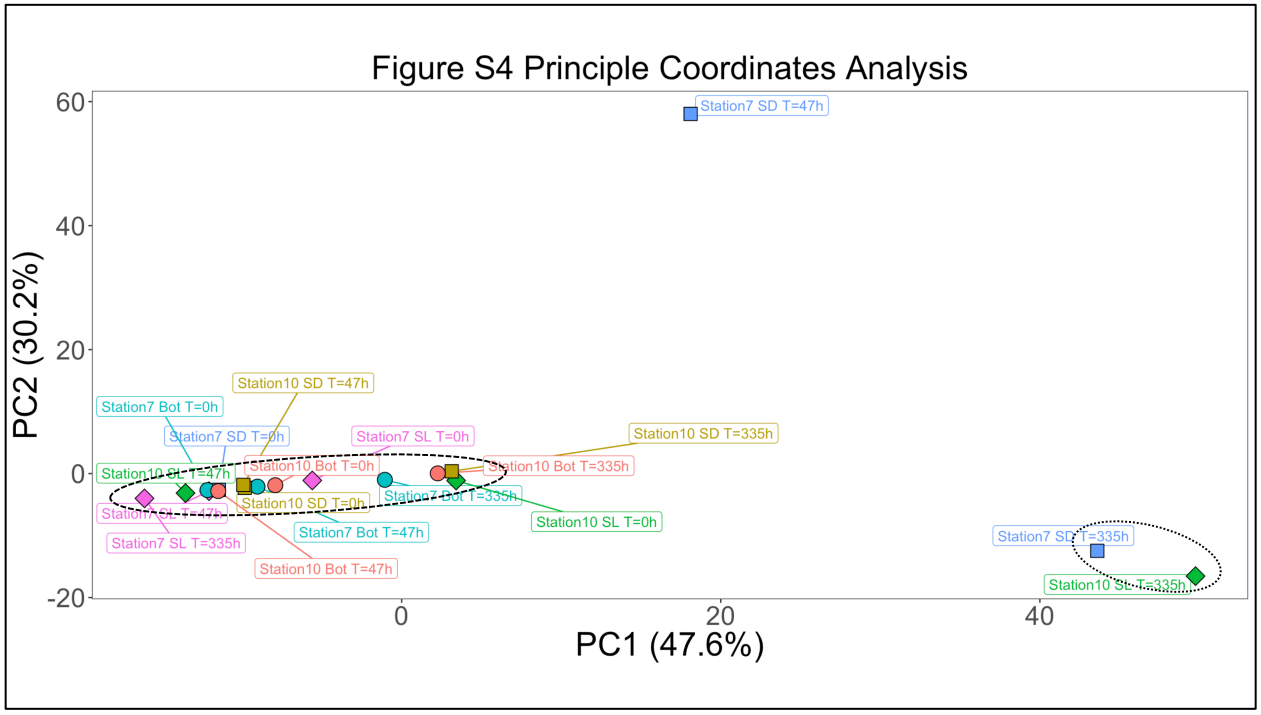

Figure A5. Heat map was constructed using the community data from the 2014 incubation, in which the correlations between *Microcystis* abundance and $^{15}NH_4^+$ (NH_4^+ originated from the spiked ^{15}N-urea) as well as NH_4^+-^{15}N: removed urea-^{15}N ratio are not significant (Pearson correlation; $p = 0.148$ and 0.5266, respectively). Heterotrophic bacteria *Actinobacteria*, *Proteobacteria*, and *Deinococcus-Thermus* were correlated significantly to the NH_4^+-^{15}N: removed urea-^{15}N ratio (Pearson correlation; *Actinobacteria*, $p = 0.03943$; *Deinococcus-Thermus*, $p = 0.02199$), indicating that heterotrophic bacteria are crucial in the urea metabolism in Lake Taihu.

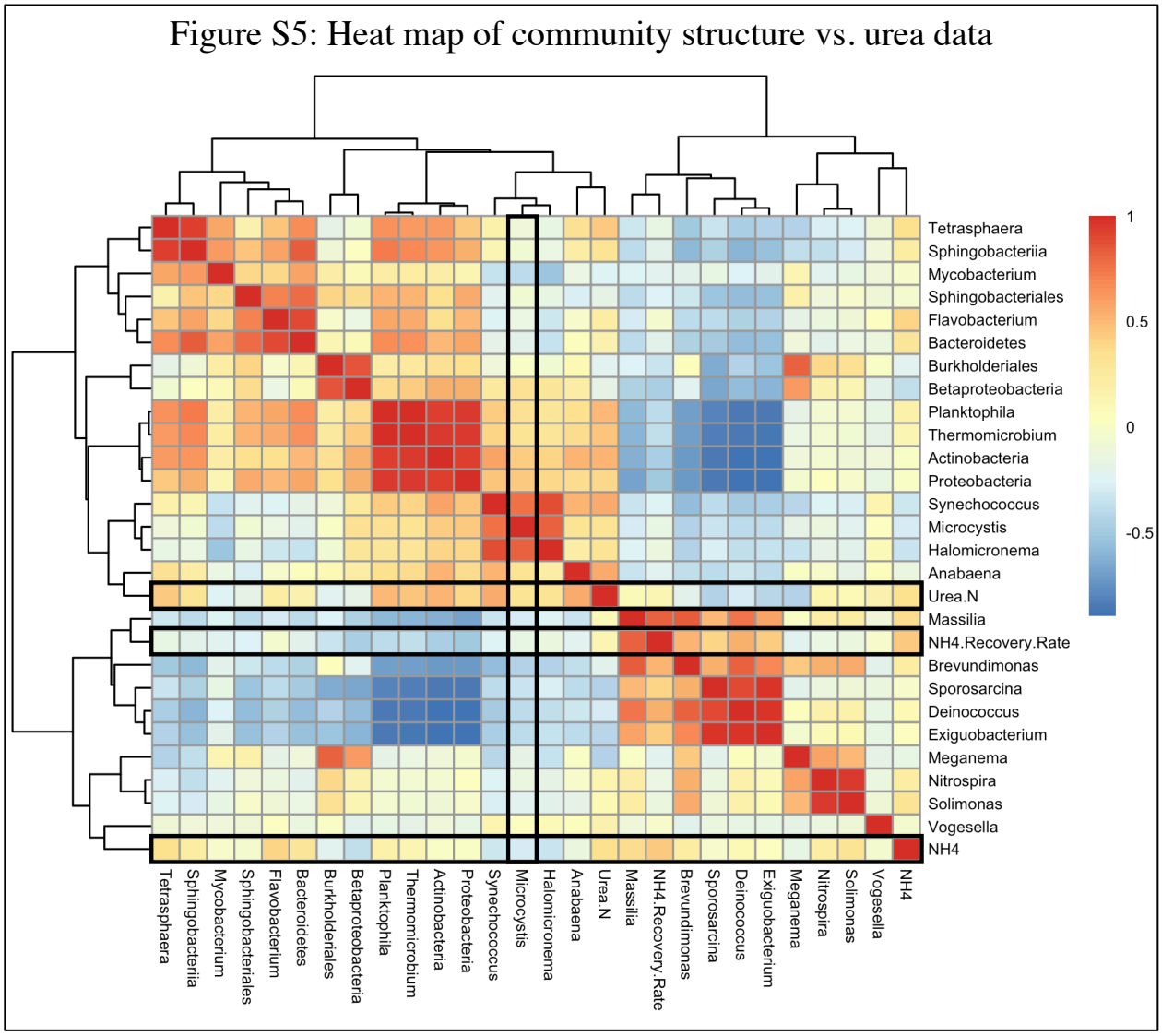

Table A1. Cell abundance in 2015 pure *Microcystis* incubation

Treatments	Cell Abundance ($\times 10^9$ cells L^{-1})	
	T_0 (0h)	T_1 (24h)
Filtered Lake Water + *Microcystis* + $^{15}NH_4^+$ Light	2.87 ± 0.35	3.52 ± 0.02
Filtered Lake Water + *Microcystis* + $^{15}NH_4^+$ Dark	2.61 ± 0.02	3.10 ± 0.16
Filtered Lake Water + *Microcystis* + ^{15}N-Urea Light	3.49 ± 0.18	4.38 ± 0.07
Filtered Lake Water + *Microcystis* + ^{15}N-Urea Dark	3.20 ± 0.62	4.79 ± 0.07

APPENDIX B. USING ^{15}N LABELED PEPTIDE TO TRACE THE FATES OF NITROGEN AFTER DEGRADATION AND THE FORMATION OF DISSOLVED ORGANIC NITROGEN IN COASTAL SEAWATER

Figure B1. THAA concentration in 2016 AVFA incubation experiment. (A) Surface water (2 m) incubation; (B) Bottom water (14 m) incubation.

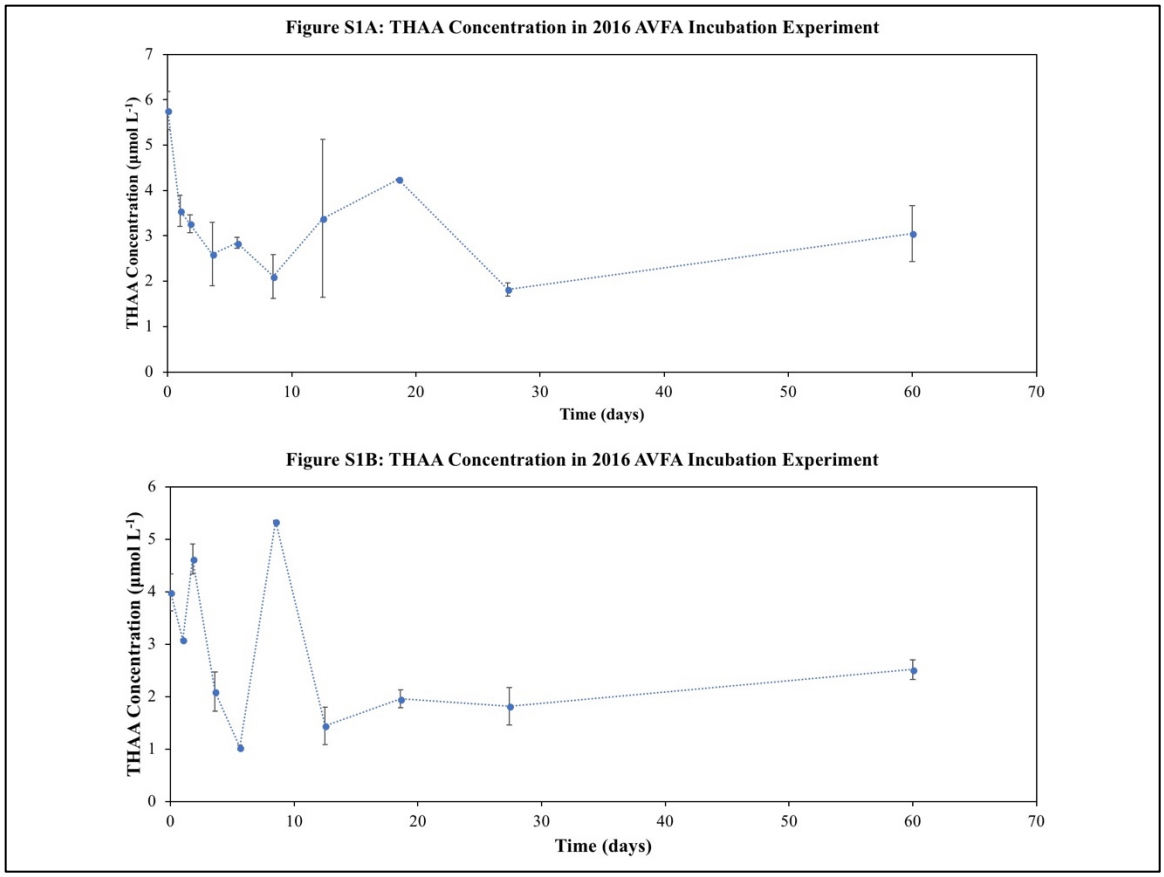

Figure B2. Concentrations of individual amino acids in 2016 AVFA incubation experiment. (A) Total concentrations of Ala + Val + Phe; (B) Concentration of Ala; (C) Concentration of Val; (D) Concentration of Phe.

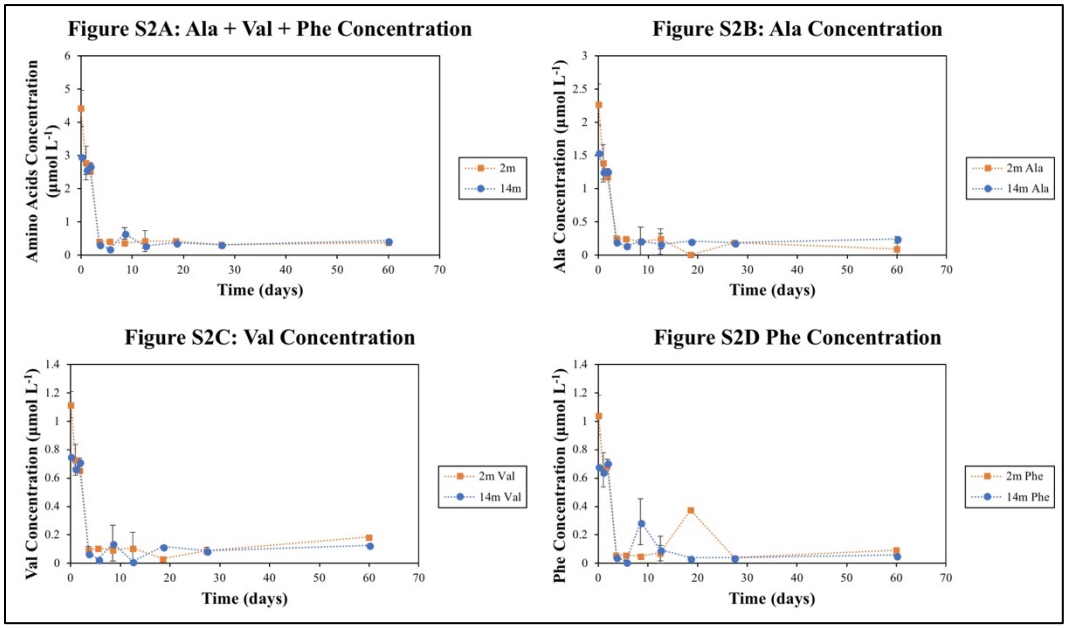

Figure B3. $PO^{15}N$ concentration in 2013 AVFA incubation experiment.

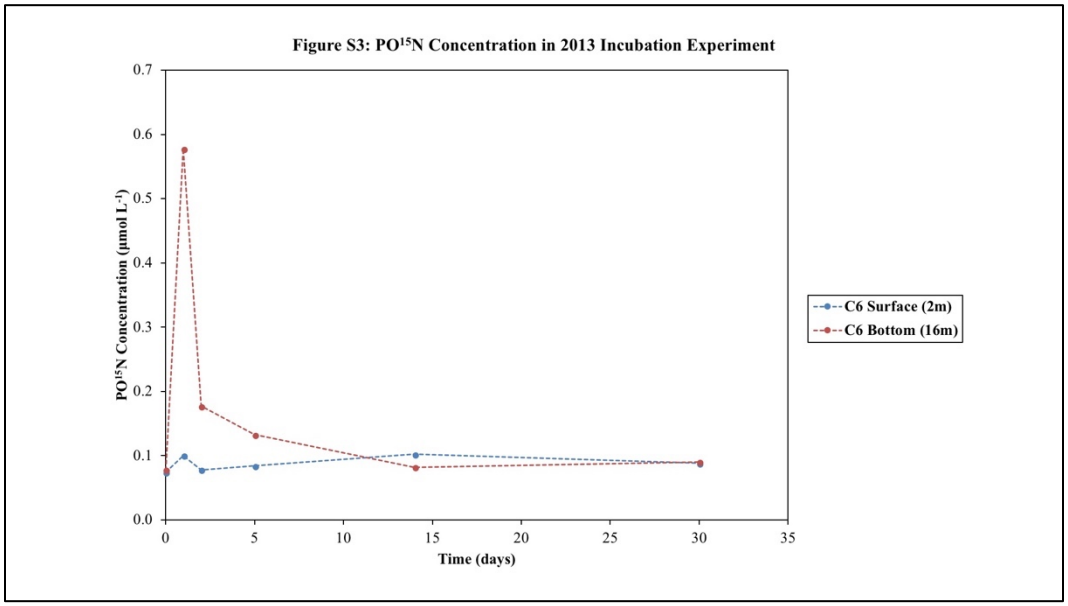

APPENDIX C. MOLECULAR STRUCTURE CHARACTERIZATION OF RIVERINE AND COASTAL DISSOLVED ORGANIC MATTER WITH ION MOBILITY QUADRUPOLE TIME OF FLIGHT LCMS (IM Q-TOF LCMS)

This supporting information includes:

- 2 pages of supporting methods and discussion
    - Instrumentation details
    - Acquisition settings for MS, untargeted MS/MS, and IM-MS
    - Criteria for formula assignment
- 4 tables
    - Elemental composition from different samples in different ESI modes (Table C1)
    - Elemental composition at different retention times in different ESI modes (Table C2)
    - Number of features detected in IM-MS under ESI+ mode (Table C3)
    - Correlations between CCS and elemental composition (Table C4)
- 9 figures
    - Sampling sites (Figure C1)
    - Schematic instrumentation figure (Figure C2)
    - Chromatograms of LC retention time vs. ion intensity under ESI- mode (Figure C3)
    - van Krevelen diagrams of ESI+ and ESI- modes based on LC-MS result (Figure C4)

- van Krevelen diagram based on retention time in ESI+ mode (Figure C5)
- van Krevelen diagram based on retention time in ESI- mode (Figure C6)
- van Krevelen diagrams of ESI+ and ESI- modes based on LC-MS/MS result (Figure C7)
- Two examples from non-targeted LC-MS/MS results (Figure C8)
- van Krevelen diagrams of ESI+ mode based on LC-IM-MS result (Figure C9)

Instrumentation details.

As shown schematically (Figure C2), a drift tube is coupled to a quadrupole time-of-flight mass spectrometer with an orthogonal electrospray ionization (ESI) source (Agilent 6560 IM Q-TOF LCMS). A heated sheath gas nebulizer is incorporated to focus and desolvate ions prior to introduction into the vacuum system.(May et al. 2014) Ions from the ESI are introduced to a single-bore glass capillary tube. Upon exiting the capillary tube, ions are enriched in the high-pressure front funnel and excess gas is removed. The continuous ion beam is converted into a pulsed ion beam by the discrete release function in trapping funnel, prior to ion mobility separation. Ion mobility separation occurs in a 78-cm uniform field drift tube with high purity N_2 as the buffer gas. Ions traverse the drift tube under a weak electric field (10 to 20 $V \cdot cm^{-1}$)(May et al. 2014) to ensure that mobility of ions depends solely on their structures and interactions with the buffer gas. The estimated resolving power of ion mobility exceeds 60.(May et al. 2014) Ions exiting the drift region are refocused by the rear ion funnel into a narrower beam before entering the optics of the mass spectrometer, which incorporates a quadrupole mass filter and collision cell to enable mass-selective ion fragmentation experiments. The TOF MS alone has resolving power greater than 40 000 at *m/z* of 1200,(May et al. 2014) and the whole instrument IM Q-TOF LC/MS can be up to 2 000 000 at *m/z* of 300.

MS data acquisition.

The orthogonal electrospray ionization source (Dual Agilent Jet Stream ESI) was operated with N_2 sheath gas temperature of 350 °C at a flow rate of 12 L min^{-1}. N_2 drying

gas applied at the source entrance was heated to 225 °C, and maintained at a flow rate of 13 L min^{-1} with a nebulizer pressure of 45 psig. The source operated in positive mode with 3500 V VCap voltage, and 0 V nozzle voltage. Q-TOF operated in positive ion polarity in MS mode, with an MS mass range of 70-1200 *m/z*, an acquisition rate of 1 spectrum/s, and an acquisition time of 1000 ms/spectrum. Reference masses of 121.050873 and 922.009798 (Agilent Tuning Mix) were used for mass calibration.

The ion source for ESI- mode was also the Dual AJS ESI. Sheath gas parameters were the same as described in ESI+ mode. Drying gas, however, was heated to 225 °C, with a flow rate of 5 L min^{-1} and nebulizer pressure of 20 psig. The source operated in negative mode with 3500 V VCap voltage, and 2000 V nozzle voltage. QTOF settings of ESI- mode resembled those of ESI+ mode, except that QTOF was operated under negative ion polarity, with reference masses of 112.985587 and 1033.988109 (Agilent Tuning Mix).

Non-targeted MS/MS data acquisition.

Collision Induced Dissociation (CID) data were acquired for both ESI+ and ESI- modes. For ESI+ mode, Q-TOF was set to positive ion polarity and Auto MS/MS mode, with an MS mass range of 100-1200 *m/z*, and an MS/MS mass range of 50-1200 *m/z*. The MS acquisition rate was 4 spectra/s, and acquisition time was 250 ms/spectrum. The MS/MS acquisition rate was 2 spectra/s, and acquisition time was 500 ms/spectrum. Collision energy for ESI+ mode was 30 V. The threshold to trigger MS/MS was at least 2000 counts for the precursor ion. Active Exclusion excluded the ion after 2 spectra. Rather than auto MS/MS, a preferred ID list containing the information of compounds *m/z* and

retention time was created to guide each sample run in MS/MS based on its MS result, and was imported in parameters settings to achieve optimal MS/MS results. Compounds detected in MS/MS mode are not limited to the ones in preferred ID list. Other settings of MS/MS, i.e. LC settings, ion source settings and reference ions, followed those of ESI+ MS. For ESI- mode, the Q-TOF was operated under negative ion polarity and in Auto MS/MS mode. Settings for ESI- MS/MS followed those of ESI+, except for the precursor threshold set at 6000, and the collision energy at 40 V. Other settings of ESI- MS/MS followed those of ESI- MS.

IM-MS data acquisition.

For ESI+ mode, Q-TOF operated under IM-QTOF Acquisition mode. General parameters of IM followed those described in ESI+ MS. Default voltages were the funnel parameters. For ESI- mode, general parameters of IM followed those described for ESI- MS above. Most IM specific funnel parameters were default voltages except for a few modifications: high pressure funnel RF -150 V, trap funnel RF -125 V, trap entrance grid delta -4 V, trap exit grid 1 delta -6 V, trap exit grid 2 delta -12 V, drift tube entrance voltage -1500 V, and rear funnel RF -100 V.

Criteria for formula assignment: isotopic spacing and abundance.

The isotopic spacing and abundance for each assigned formula were considered automatically with the built-in software. In particular, for a singularly charged compound with a *m/z* of M, peaks with *m/z* of M+1.003355 (containing one ^{13}C) and M+2.00671

(containing two ^{13}C) were investigated to check if it is possible for the computed formula to have one and two ^{13}C contained isotopic compounds with the observed abundance. The final score for the generated formula is a combination of 100% of the mass score, 60% of the isotope abundance score, and 50% of the isotope spacing score. Unable to meet the isotopic criteria, i.e., higher abundance than the calculated value or absence of isotopic peak, will penalize the final formula score. Any formula with a score lower than the preset minimum threshold (score=60) was excluded.

Table C1. Elemental composition from different samples in different ESI modes

	ESI+			ESI-		
	H/C	O/C	N/C	H/C	O/C	N/C
Ship Channel	1.5880	0.1882	0.0710	1.3056	0.2903	0.0780
Aransas River	1.4926	0.2652	0.0891	1.2616	0.2778	0.0721
Nueces Dam	1.4533	0.2635	0.0868	1.2628	0.2824	0.0719
Lavaca River 1	1.4907	0.2628	0.0900	1.3175	0.2700	0.0654
Lavaca River 2	1.4826	0.2630	0.0897	1.2002	0.2978	0.0704
Mission River	1.4826	0.2631	0.0906	1.2437	0.2884	0.0696
San Antonio River 1	1.4751	0.2718	0.0902	1.2338	0.2902	0.0692
San Antonio River 2	1.4790	0.2699	0.0905	1.3047	0.2719	0.0706

Table C2. Elemental composition at different retention times in different ESI modes

	ESI+				ESI-		
	H/C	O/C	N/C		H/C	O/C	N/C
F1: 0.0-3.0 min	1.4125	0.2332	0.1582	F1: 0.0-3.0 min	1.5054	0.3259	0.0364
F2: 3.0-9.0 min	1.4160	0.2510	0.0845	F2: 3.0-9.0 min	1.1906	0.2885	0.0773
F3: 9.0-15.0 min	1.4833	0.2888	0.0993	F3: 9.0-15.0 min	1.3096	0.2827	0.0678
F4: 15.0-20.0 min	1.6556	0.1861	0.0623	F4: 15.0-20.0 min	1.4053	0.2528	0.0444
F5: 20.0-21.0 min	1.7632	0.1289	0.0533	F5: 20.0-21.0 min	1.4664	0.2565	0.0323

Table C3. Number of features detected in IM-MS under ESI+ mode

	Number of features detected in IM-MS	Number of compounds assigned with formula	Number of compounds annotated in MS/MS
Ship Channel	266	149	76
Aransas River	230	158	13
Nueces Dam	216	133	16
Lavaca River 1	460	293	20
Lavaca River 2	46	27	4
Mission River	215	133	14
San Antonio River 1	249	152	14
San Antonio River 2	248	167	13

Table C4. Correlations between CCS and elemental composition (Pearson)

	CCS vs. H/C	CCS vs. O/C	CCS vs. N/C
t	2.4133	6.3825	-13.568
df	3420	3420	3420
p	1.59×10^{-2}	1.98×10^{-10}	2.20×10^{-16}
R^2	0.0017	0.0118	0.0511

Figure C1. Sampling sites. Samples from 7 sites in five south Texas rivers (Aransas River, AR: N 28.13°, W 97.43°; Lavaca River 1, LR1: N 28.96°, W 96.68°; Lavaca River 2, LR2: N 28.83°, W 96.58°; Mission River, MR: N 28.29°, W 97.28°; Nueces Dam, DAM: N 27.88°, W 97.63°; San Antonio River 1, SR1: N 28.53°, W 97.04°; San Antonio River 2, SR2: N 28.48°, W 96.86°) were collected in May 2016 using a 2-L Van Dorn sampler. Samples from the Marine Ship Channel (SC: N 27.84°, W 97.05°) connected to the open Gulf, were collected in September 2016.

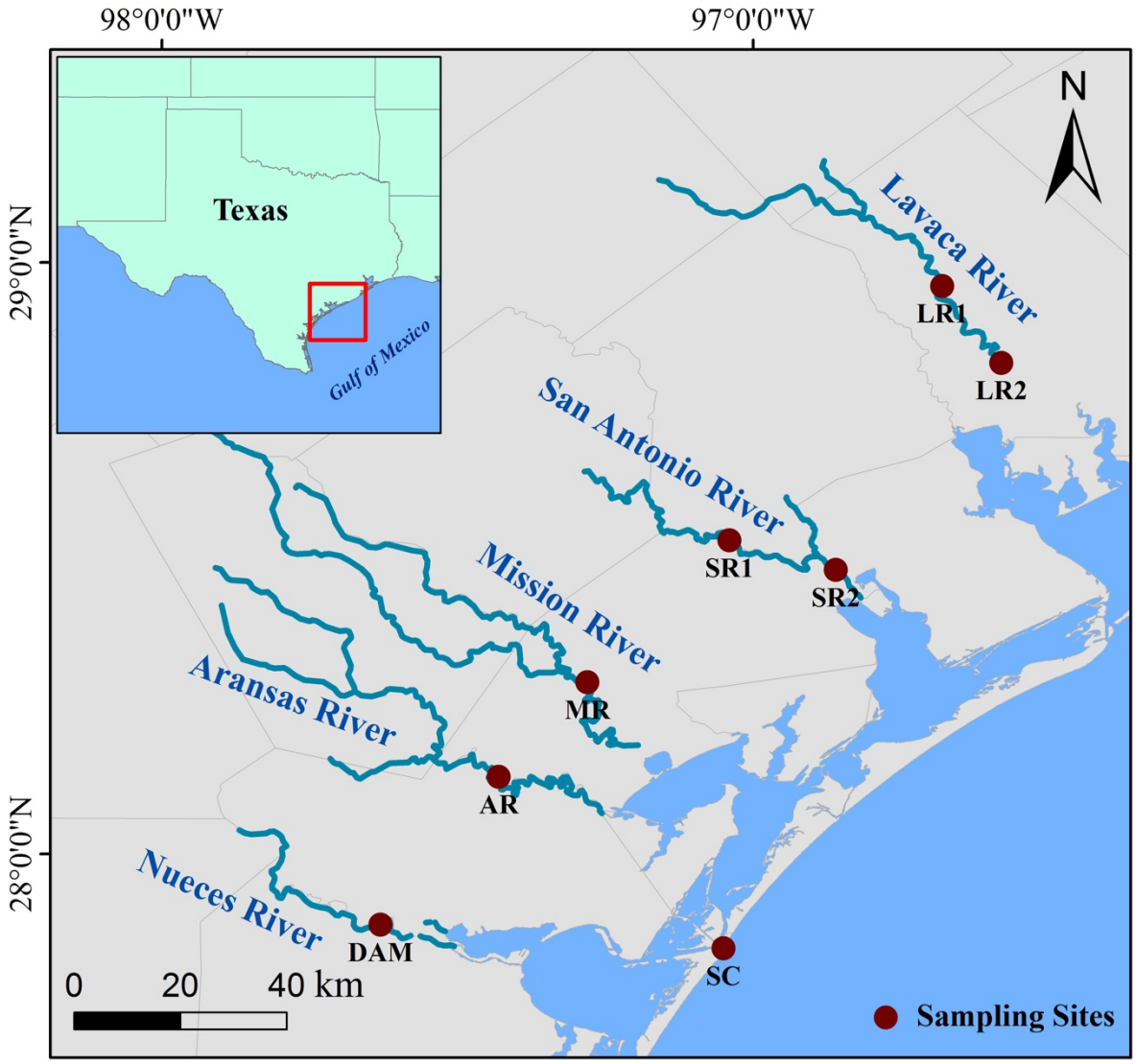

Figure C2. A representative schematic of the IM Q-TOF LC/MS with significant components annotated. In ion mobility drift tube, ions with larger CCS are delayed more easily than smaller ones due to their higher number of collisions with the buffer gas molecules. Separated ions will then go through high resolution Q-TOF MS.

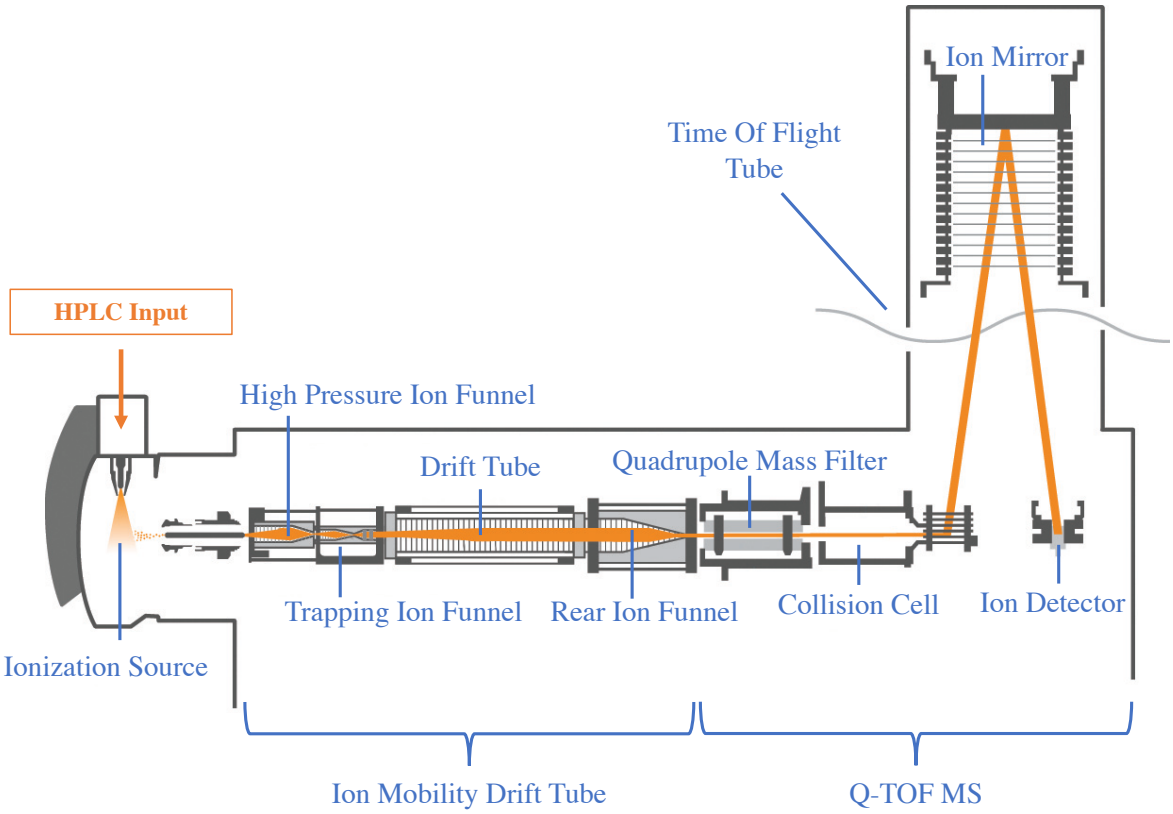

Figure C3. Chromatograms of LC retention time vs. ion intensity under ESI- mode. Different fractions (F1-F5) are determined based on the mobile phase (see the main text) and the distribution of chromatographic peaks. (a) Riverine samples under ESI- mode; (b) Ship Channel under ESI- mode. Note that the ion intensity of the Ship Channel sample is one order of magnitude higher than that of the riverine sample.

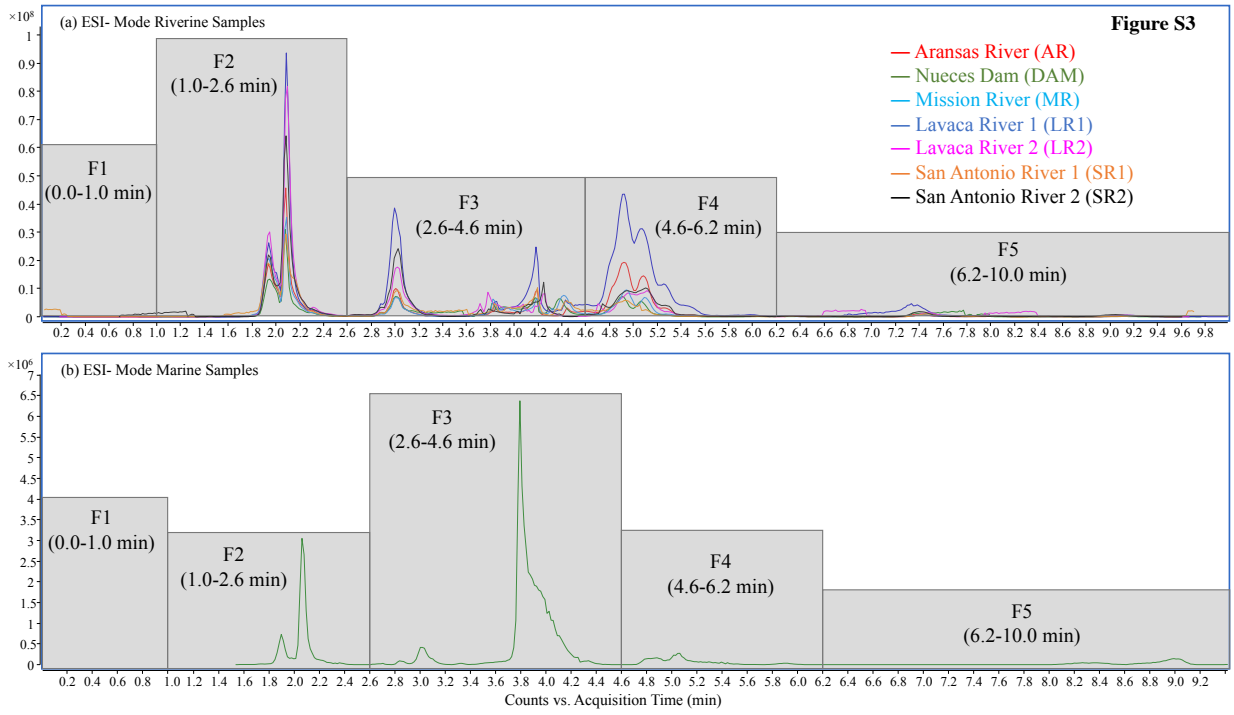

Figure C4. van Krevelen diagram showing all detected molecular formulas by their H/C and O/C atomic ratios (minimum score threshold = 60). (a) ESI+ mode. (b) ESI- mode.

Figure S4

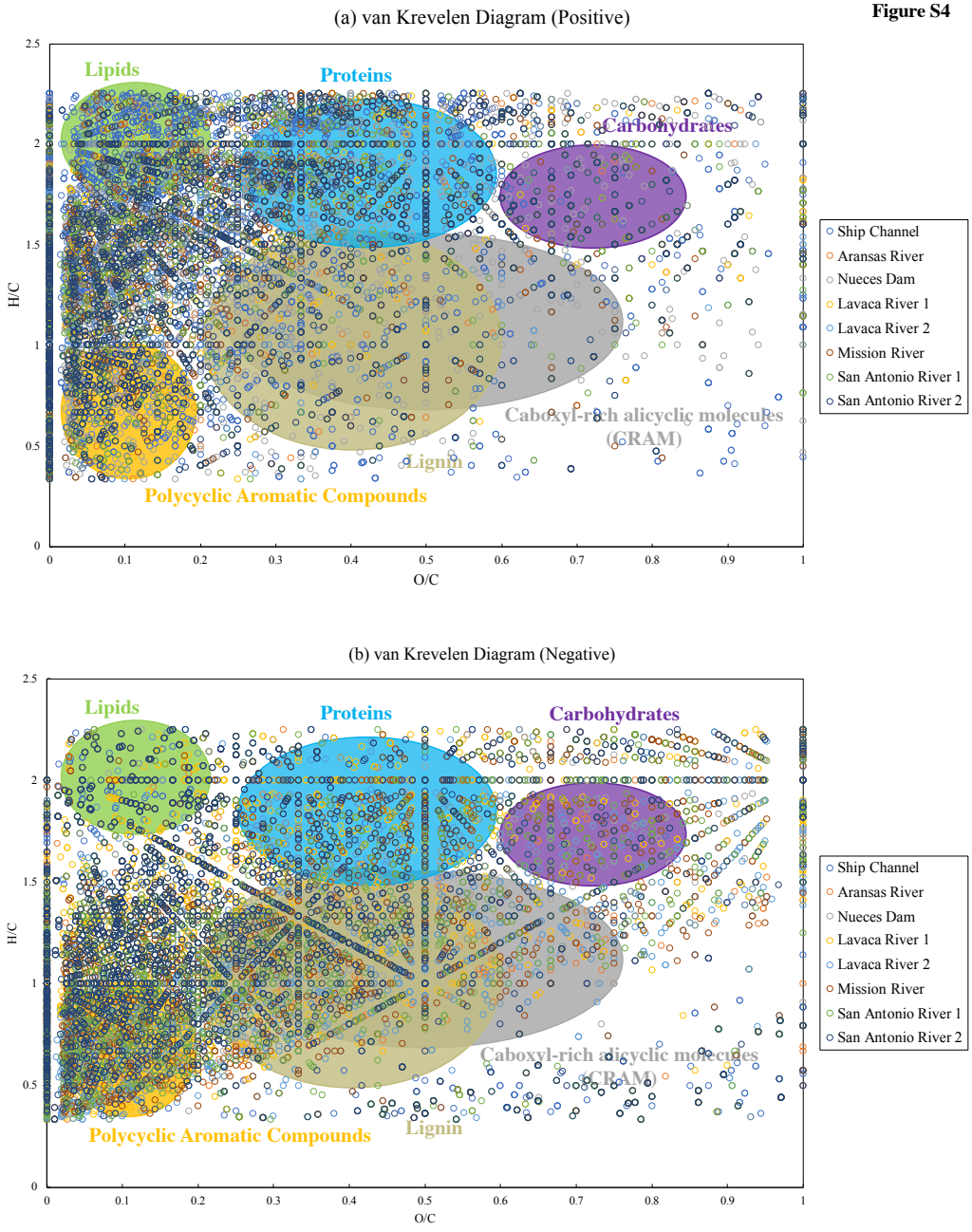

Figure C5. van Krevelen diagram based on retention time in ESI+ mode. Different fractions (F1-F5) are determined based on the mobile phase (see the main text) and the distribution of chromatographic peaks (Figure 5.3). (a) Overlay of the consolidated ions: 0.0-3.0 min (blue), 3.0-9.0 min (orange), 9.0-15.0 min (grey), 15.0-20.0 min (yellow), and 20.0-21.0 min (light blue). (b) Ions from F1. (c) Ions from F2. (d) Ions from F3. (e) Ions from F4. (f) Ions from F5.

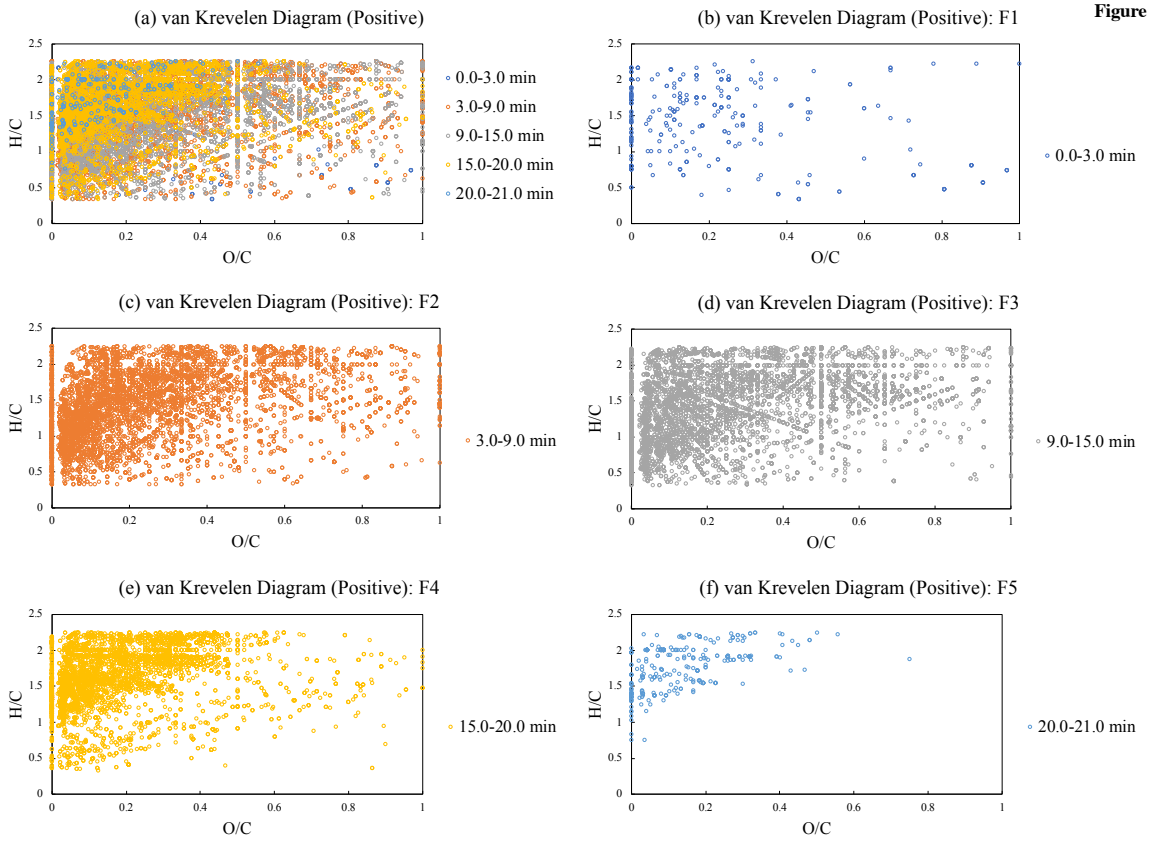

Figure C6. van Krevelen diagram based on retention time in ESI- mode. Different fractions (F1-F5) are determined based on the mobile phase (see the main text) and the distribution of chromatographic peaks (Figure C2). (a) Overlay of the consolidated ions: 0.0-1.0 min (blue), 1.0-2.6 min (orange), 2.6-4.6 min (grey), 4.6-6.2 min (yellow), and 6.2-10.0 min (light blue). (b) Ions from F1. (c) Ions from F2. (d) Ions from F3. (e) Ions from F4. (f) Ions from F5.

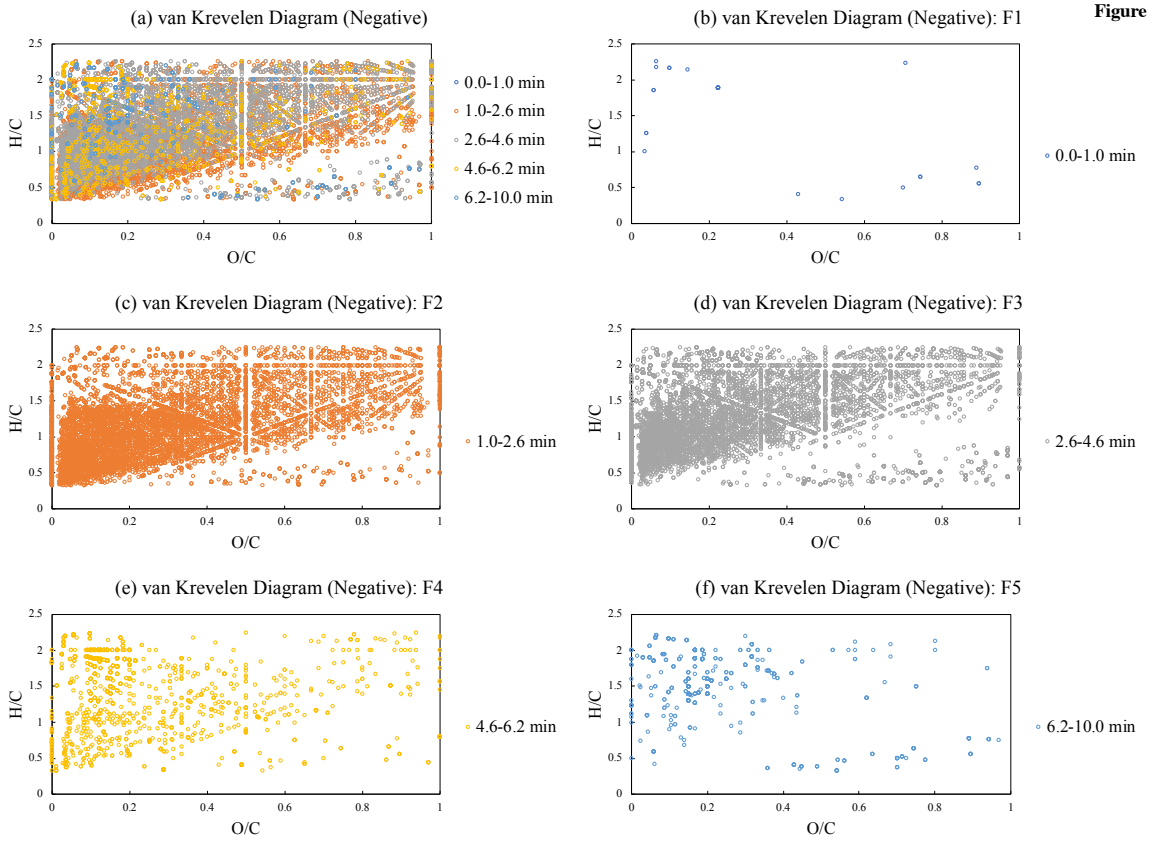

Figure S6

Figure C7. van Krevelen diagram showing the overlay of the consolidated ions from different sampling sites based on MS/MS data: Aransas River (blue), Nueces Dam (orange), Lavaca River 1 (grey), Lavaca River 2 (yellow), Mission River (light blue), San Antonio River 1 (green), San Antonio River 2 (dark blue), and Ship Channel (brown). (a) van Krevelen diagram in ESI+ mode. (b) van Krevelen diagram in ESI- mode.

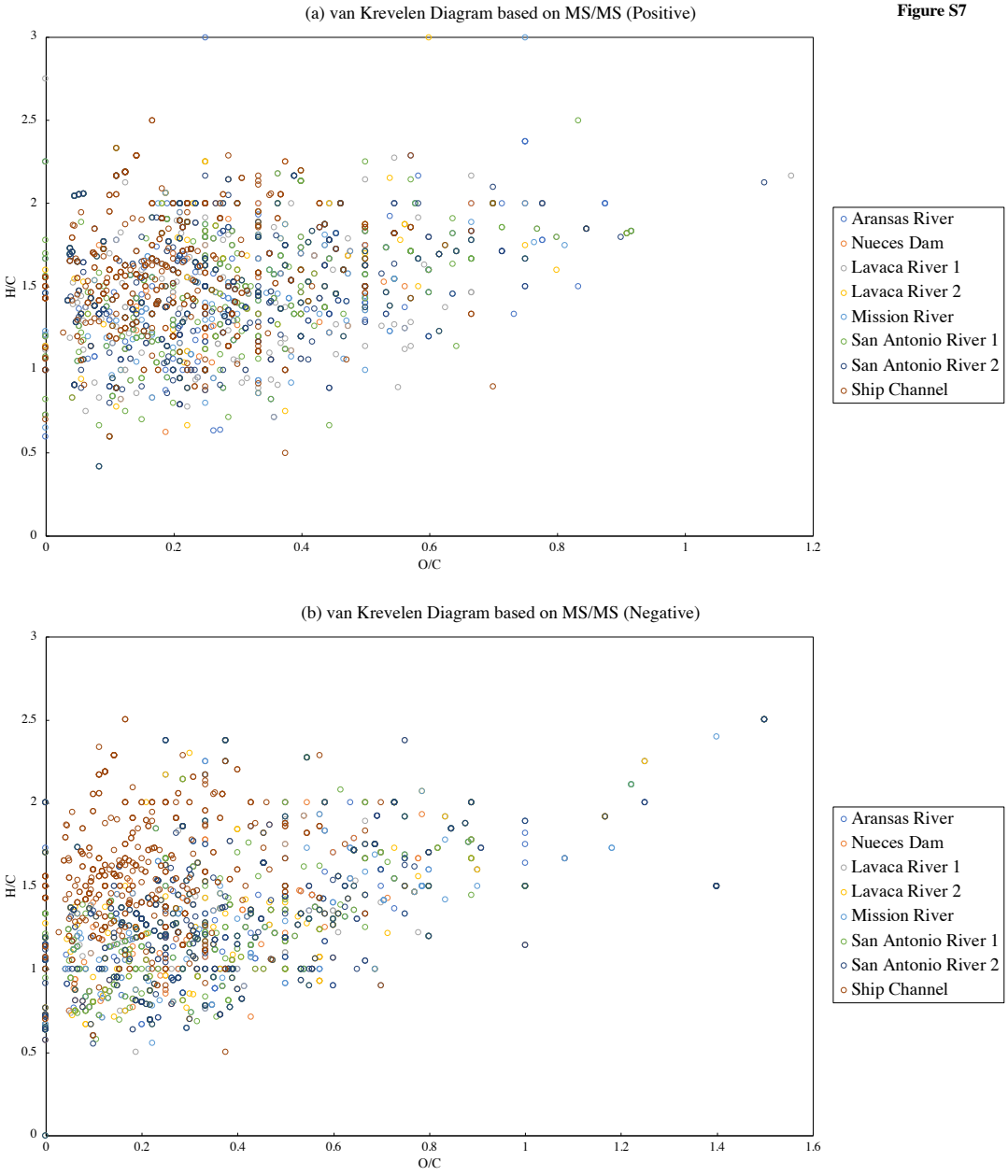

Figure S7

Figure C8. Two examples presented here show the structural information gained from non-targeted MS/MS results. (a) Compound from marine DOM sample at 6.6 min in ESI+ mode with a m/z at 340. Product ions spectrum showed that the most abundant fragment of 340 m/z was at 100.1120 m/z, along with several small fragments below 100 m/z, leading to the aliphatic structure as a reasonable choice. From the fragmentation pattern, we speculated that the compound may be a tri-leucine like compound (with the loss of a neutral H_2O). (b) Compound from AR, DAM, LR1, LR2, SR1, SR2 and marine samples at around 6.0 min in ESI- mode with a m/z at 311. Largest fragment ion after collision occurred at 183.0110 m/z, identified by the software as benzenesulfonic acid. The presence of fragment 79.9572 m/z, which is likely a sulfuric group, supports the speculation of a benzenesulfonic group. Also, the fact that not many fragments occurred between 80 m/z and 170 m/z indicates the presence of a rigid structure that is difficult to break, making a benzene group a likely possibility. The aliphatic structure is confirmed further by the presence of a series of compounds differing from 311 m/z in mass by 14 m/z (data not shown), indicating the presence of alkyl chain like structure. Note that the structure shown here is likely not the exact structure of compound 311 m/z, since many possible structures exist for the alkyl chain. Nonetheless, this approach offers further structural information about the DOM molecules beyond elemental composition (The database in the appendix provides holistic structures of DOM molecules).

Figure S8

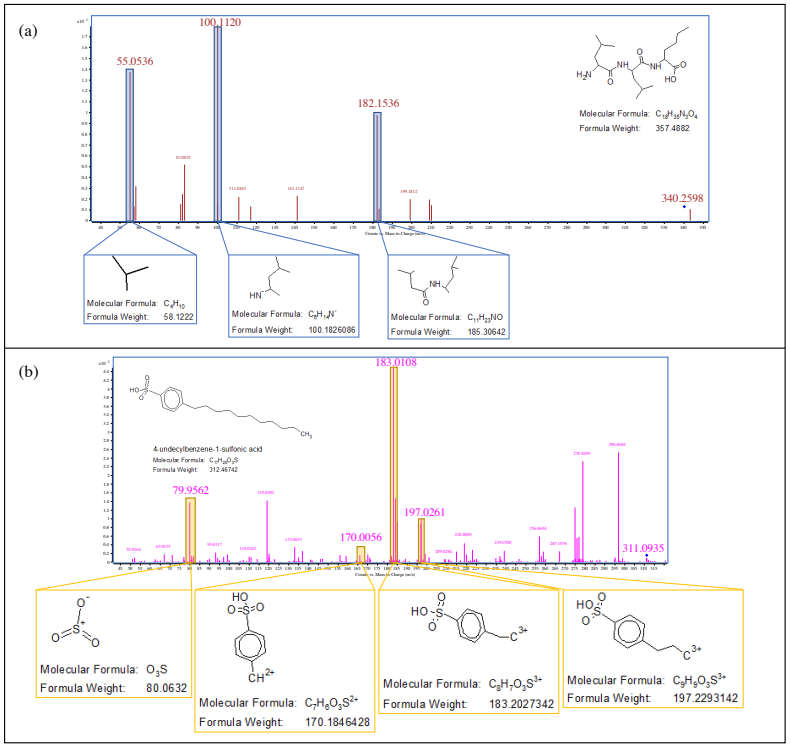

Figure C9. van Krevelen diagram showing the overlay of the consolidated ions from different sampling sites based on IM-MS data: Aransas River (blue), Nueces Dam (orange), Lavaca River 1 (grey), Lavaca River 2 (yellow), Mission River (light blue), San Antonio River 1 (green), San Antonio River 2 (dark blue), and Ship Channel (brown).

Figure S9

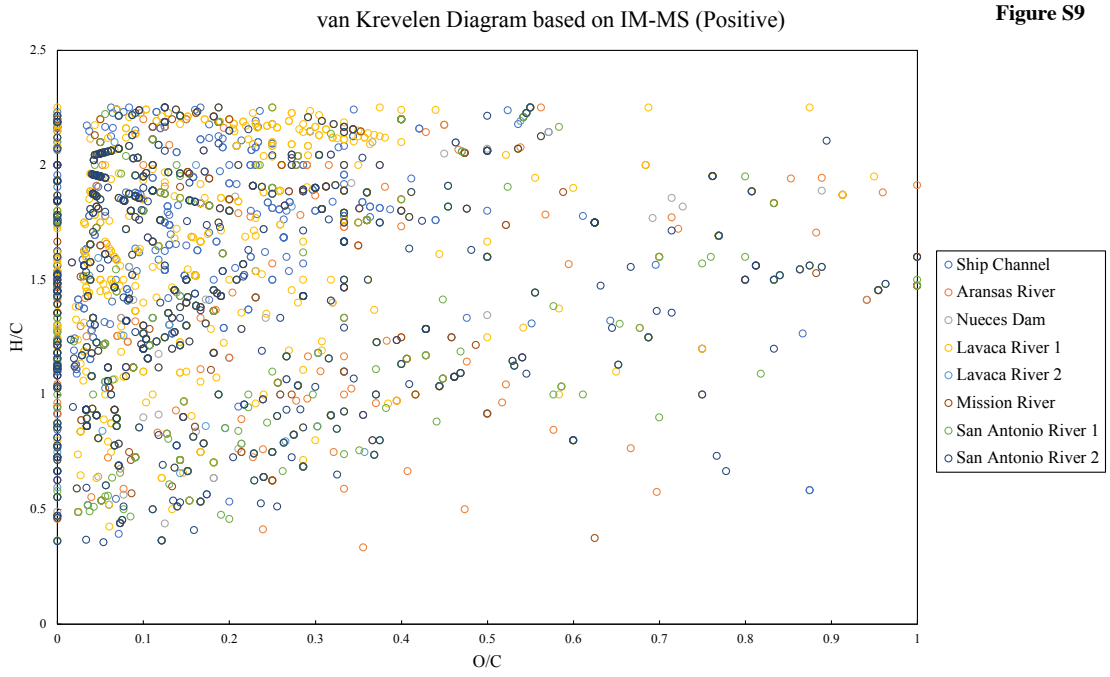

References

Allen, A. E., C. L. Dupont, M. Oborník, and others. 2011. Evolution and metabolic significance of the urea cycle in photosynthetic diatoms. Nature **473**: 203–207.

Alpert, A. J. 1990. Hydrophilic-interaction chromatography for the separation of peptides, nucleic acids and other polar compounds. Journal of Chromatography A **499**: 177–196. doi:10.1016/S0021-9673(00)96972-3

Aluwihare, L. I., and T. Meador. 2008. Chemical composition of marine dissolved Organic Nitrogen, p. 95–140. *In* D.G. Capone, D.A. Bronk, M.R. Mulholland, and E.J. Carpenter [eds.], Nitrogen in the Marine Environment (2nd Edition). Academic Press.

Amano, M., S. Hara, and N. Taga. 1982. Utilization of dissolved amino acids in seawater by marine bacteria. Marine Biology **68**: 31–36. doi:10.1007/BF00393138

Amon, R. M. W., and R. Benner. 1996. Bacterial utilization of different size classes of dissolved organic matter. Limnology and Oceanography **41**: 41–51. doi:10.4319/lo.1996.41.1.0041

Armstrong, F. a. J., and S. Tibbitts. 1968. Photochemical combustion of organic matter in sea water, for nitrogen, phosphorus and carbon determination. Journal of the Marine Biological Association of the United Kingdom **48**: 143–152. doi:10.1017/S0025315400032483

Arnosti, C. 2011. Microbial extracellular enzymes and the marine carbon cycle. Annual review of marine science **3**: 401–425.

Arrieta, J. M., E. Mayol, R. L. Hansman, G. J. Herndl, T. Dittmar, and C. M. Duarte. 2015. Dilution limits dissolved organic carbon utilization in the deep ocean. Science **348**: 331–333. doi:10.1126/science.1258955

Axler, R. P., and J. E. Reuter. 1987. A simple method for estimating the ^{15}N content of dissolved organic matter ($DO^{15}N$) in N-cycling studies. Can. J. Fish. Aquat. Sci. **44**: 130–133. doi:10.1139/f87-016

Baer, S. E., R. E. Sipler, Q. N. Roberts, P. L. Yager, M. E. Frischer, and D. A. Bronk. 2017. Seasonal nitrogen uptake and regeneration in the western coastal Arctic. Limnology and Oceanography **62**: 2463–2479. doi:10.1002/lno.10580

Baker, E. S., B. H. Clowers, F. Li, K. Tang, A. V. Tolmachev, D. C. Prior, M. E. Belov, and R. D. Smith. 2007. Ion mobility spectrometry–mass spectrometry performance using electrodynamic ion funnels and elevated drift gas pressures. Journal of the American Society for Mass Spectrometry **18**: 1176–1187. doi:10.1016/j.jasms.2007.03.031

Beckers, G., A. K. Bendt, R. Krämer, and A. Burkovski. 2004. Molecular identification of the urea uptake system and transcriptional analysis of urea transporter- and urease-encoding genes in *Corynebacterium glutamicum*. J. Bacteriol. **186**: 7645–7652. doi:10.1128/JB.186.22.7645-7652.2004

Bedard-Haughn, A., J. W. van Groenigen, and C. van Kessel. 2003. Tracing ^{15}N through landscapes: potential uses and precautions. Journal of Hydrology **272**: 175–190. doi:10.1016/S0022-1694(02)00263-9

Belisle, B. 2014. Urea as a nitrogen source for *Microcystis aeruginosa*. Masters Theses.

Belisle, B. S., M. M. Steffen, H. L. Pound, S. B. Watson, J. M. DeBruyn, R. A. Bourbonniere, G. L. Boyer, and S. W. Wilhelm. 2016. Urea in Lake Erie: organic nutrient sources as potentially important drivers of phytoplankton biomass. Journal of Great Lakes Research **42**: 599–607. doi:10.1016/j.jglr.2016.03.002

Benner, R. 2002. Chemical Composition and Reactivity, p. 59–90. *In* D.A. Hansell and C.A. Carlson [eds.], Biogeochemistry of marine dissolved organic matter (First Edition). Academic Press.

Bergbauer, M., and S. Y. Newell. 1992. Contribution to lignocellulose degradation and DOC formation from a salt marsh macrophyte by the ascomycete *Phaeosphaeria spartinicola*. FEMS Microbiology Letters **86**: 341–347. doi:10.1016/0378-1097(92)90798-S

Berman, T., and D. A. Bronk. 2003. Dissolved organic nitrogen: a dynamic participant in aquatic ecosystems. Aquat Microb Ecol **31**: 279–305. doi:10.3354/ame031279

Berman, T., and S. Chava. 1999. Algal growth on organic compounds as nitrogen sources. J. Plankton Res. **21**: 1423–1437. doi:10.1093/plankt/21.8.1423

Blackburn, T. H. 1979. Method for measuring rates of NH_4^+ turnover in anoxic marine sediments, using a ^{15}N-NH_4^+ dilution technique. Appl Environ Microbiol **37**: 760–765.

Bogard, M. J., D. B. Donald, K. Finlay, and P. R. Leavitt. 2012. Distribution and regulation of urea in lakes of central North America. Freshwater Biology **57**: 1277–1292. doi:10.1111/j.1365-2427.2012.02775.x

Bouillon, S., A. Yambélé, R. G. M. Spencer, D. P. Gillikin, P. J. Hernes, J. Six, R. Merckx, and A. V. Borges. 2012. Organic matter sources, fluxes and greenhouse gas exchange in the Oubangui River (Congo River basin). Biogeosciences; Katlenburg-Lindau **9**: 2045.

Bronk, D. A. 2002. Dynamics of DON, p. 153–247. *In* D.A. Hansell and C.A. Carlson [eds.], Biogeochemistry of marine dissolved organic matter (First Edition). Academic Press.

Bronk, D. A., P. M. Glibert, T. C. Malone, S. Banahan, and E. Sahlsten. 1998. Inorganic and organic nitrogen cycling in Chesapeake Bay: autotrophic versus heterotrophic processes and relationships to carbon flux. Aquat Microb Ecol **15**: 177–189. doi:10.3354/ame015177

Bronk, D. A., M. W. Lomas, P. M. Glibert, K. J. Schukert, and M. P. Sanderson. 2000. Total dissolved nitrogen analysis: comparisons between the persulfate, UV and high temperature oxidation methods. Marine Chemistry **69**: 163–178. doi:10.1016/S0304-4203(99)00103-6

Bronk, D. A., J. H. See, P. Bradley, and L. Killberg. 2007. DON as a source of bioavailable nitrogen for phytoplankton. Biogeosciences **4**: 283–296. doi:10.5194/bg-4-283-2007

Brophy, J. E., and D. J. Carlson. 1989. Production of biologically refractory dissolved organic carbon by natural seawater microbial populations. Deep Sea Research Part A. Oceanographic Research Papers **36**: 497–507. doi:10.1016/0198-0149(89)90002-2

Buszewski, B., and S. Noga. 2012. Hydrophilic interaction liquid chromatography (HILIC)—a powerful separation technique. Anal Bioanal Chem **402**: 231–247. doi:10.1007/s00216-011-5308-5

Cao, X., M. R. Mulholland, J. R. Helms, P. W. Bernhardt, P. Duan, J. Mao, and K. Schmidt-Rohr. 2017. A major step in opening the black box of high-molecular-weight dissolved organic nitrogen by isotopic labeling of *Synechococcus* and multibond two-dimensional NMR. Anal. Chem. **89**: 11990–11998. doi:10.1021/acs.analchem.7b02335

Caperon, J., D. Schell, J. Hirota, and E. Laws. 1979. Ammonium excretion rates in Kaneohe Bay, Hawaii, measured by a ^{15}N isotope dilution technique. Mar. Biol. **54**: 33–40. doi:10.1007/BF00387049

Carini, S. A., M. J. McCarthy, and W. S. Gardner. 2010. An isotope dilution method to measure nitrification rates in the northern Gulf of Mexico and other eutrophic waters. Continental Shelf Research **30**: 1795–1801. doi:10.1016/j.csr.2010.08.001

Carlson, C. A. 2002. Production and removal process, p. 91–151. *In* Biogeochemistry of Marine Dissolved Organic Matter (First Edition). Academic Press.

Chaffin, J. D., and T. B. Bridgeman. 2014. Organic and inorganic nitrogen utilization by nitrogen-stressed cyanobacteria during bloom conditions. J. Appl. Phycol. **26**: 299–309. doi:10.1007/s10811-013-0118-0

Chen, Y., C. Fan, K. Teubner, and M. Dokulil. 2003a. Changes of nutrients and phytoplankton chlorophyll-a in a large shallow lake, Taihu, China: an 8-year

investigation. Hydrobiologia **506–509**: 273–279. doi:10.1023/B:HYDR.0000008604.09751.01

Chen, Y., B. Qin, K. Teubner, and M. T. Dokulil. 2003b. Long-term dynamics of phytoplankton assemblages: *Microcystis*-domination in Lake Taihu, a large shallow lake in China. J. Plankton Res. **25**: 445–453. doi:10.1093/plankt/25.4.445

Chiou, C. T., R. L. Malcolm, T. I. Brinton, and D. E. Kile. 1986. Water solubility enhancement of some organic pollutants and pesticides by dissolved humic and fulvic acids. Environmental science & technology **20**: 502–508.

Chipot, C., R. Jaffe, B. Maigret, D. A. Pearlman, and P. A. Kollman. 1996. Benzene Dimer: A good model for π–π interactions in proteins? A comparison between the benzene and the toluene dimers in the gas phase and in an aqueous solution. J. Am. Chem. Soc. **118**: 11217–11224. doi:10.1021/ja961379l

Cimbleris, A. C. P., and O. Cáceres. 1991. Kinetics of urea uptake by Melosira italica (Ehr.) Kütz at different luminosity conditions. Hydrobiologia **220**: 211–216. doi:10.1007/BF00006577

Collier, J. L., K. M. Baker, and S. L. Bell. 2009. Diversity of urea-degrading microorganisms in open-ocean and estuarine planktonic communities. Environmental microbiology **11**: 3118–3131.

Constant, K. M., W. F. Sheldrick, and B. Mundial. 1992. World nitrogen survey, World Bank.

D'Andrilli, J., W. T. Cooper, C. M. Foreman, and A. G. Marshall. 2015. An ultrahigh-resolution mass spectrometry index to estimate natural organic matter lability. Rapid Commun. Mass Spectrom. **29**: 2385–2401. doi:10.1002/rcm.7400

Davis, T. W., G. S. Bullerjahn, T. Tuttle, R. M. McKay, and S. B. Watson. 2015. Effects of increasing nitrogen and phosphorus concentrations on phytoplankton community growth and toxicity during *Planktothrix* blooms in Sandusky Bay, Lake Erie. Environ. Sci. Technol. **49**: 7197–7207. doi:10.1021/acs.est.5b00799

De Paolis, F., and J. Kukkonen. 1997. Binding of organic pollutants to humic and fulvic acids: influence of pH and the structure of humic material. Chemosphere **34**: 1693–1704. doi:10.1016/S0045-6535(97)00026-X

Dittmar, T. 2015. Reasons behind the long-term stability of dissolved organic matter, p. 369–388. *In* C.A. Carlson [ed.], Biogeochemistry of Marine Dissolved Organic Matter (Second Edition). Academic Press.

Dittmar, T., and G. Kattner. 2003. Recalcitrant dissolved organic matter in the ocean: major contribution of small amphiphilics. Marine Chemistry **82**: 115–123. doi:10.1016/S0304-4203(03)00068-9

Dittmar, T., B. Koch, N. Hertkorn, and G. Kattner. 2008. A simple and efficient method for the solid-phase extraction of dissolved organic matter (SPE-DOM) from seawater. Limnol. Oceanogr. Methods **6**: 230–235.

Dittmar, T., and J. Paeng. 2009. A heat-induced molecular signature in marine dissolved organic matter. Nature Geosci **2**: 175–179. doi:10.1038/ngeo440

Dittmar, T., and A. Stubbins. 2014. Dissolved organic matter in aquatic systems. Treatise on Geochemistry (Second Edition). Elsevier 125–156.

Dodds, J. N., J. C. May, and J. A. McLean. 2017a. Investigation of the complete suite of the leucine and isoleucine isomers: toward prediction of ion mobility separation capabilities. Anal. Chem. **89**: 952–959. doi:10.1021/acs.analchem.6b04171

Dodds, J. N., J. C. May, and J. A. McLean. 2017b. Correlating resolving power, resolution, and collision cross section: unifying cross-platform assessment of separation efficiency in ion mobility spectrometry. Anal. Chem. **89**: 12176–12184. doi:10.1021/acs.analchem.7b02827

Dwivedi, P., B. Bendiak, B. H. Clowers, and H. H. Hill Jr. 2007. Rapid resolution of carbohydrate isomers by electrospray ionization ambient pressure Ion Mobility Spectrometry-Time-of-Flight Mass Spectrometry (ESI-APIMS-TOFMS). Journal of the American Society for Mass Spectrometry **18**: 1163–1175. doi:10.1016/j.jasms.2007.04.007

Emerson, S., and J. Hedges. 2008. Chemical oceanography and the marine carbon cycle, Cambridge University Press.

Fenn, L. S., M. Kliman, A. Mahsut, S. R. Zhao, and J. A. McLean. 2009. Characterizing ion mobility-mass spectrometry conformation space for the analysis of complex biological samples. Anal Bioanal Chem **394**: 235–244. doi:10.1007/s00216-009-2666-3

Fuhrman, J. 1987. Close coupling between release and uptake of dissolved free amino acids in seawater studied by an isotope dilution approach. Marine Ecology-progress Series - MAR ECOL-PROGR SER **37**: 45–52. doi:10.3354/meps037045

Fuhrman, J. 1992. Bacterioplankton roles in cycling of organic matter: the microbial food web, p. 361–383. *In* P.G. Falkowski, A.D. Woodhead, and K. Vivirito [eds.], Primary Productivity and Biogeochemical Cycles in the Sea. Springer US.

Fukuda, R., H. Ogawa, T. Nagata, and I. Koike. 1998. Direct determination of carbon and nitrogen contents of natural bacterial assemblages in marine environments. Appl. Environ. Microbiol. **64**: 3352–3358.

Gardner, W. S., H. A. Bootsma, C. Evans, and P. A. S. John. 1995. Improved chromatographic analysis of ^{15}N:^{14}N ratios in ammonium or nitrate for isotope addition experiments. Marine Chemistry **48**: 271–282. doi:10.1016/0304-4203(94)00060-Q

Gardner, W. S., J. B. Cotner, and L. R. Herche. 1993. Chromatographic measurement of nitrogen mineralization rates in marine coastal waters with ^{15}N. Marine Ecology Progress Series **93**: 65–73.

Gardner, W. S., L. R. Herche, P. A. St. John, and S. P. Seitzinger. 1991. High-performance liquid chromatographic determination of nitrogen-15 to nitrogen-14 plus nitrogen-15 ammonium ion ratios in sea water for isotope dilution experiments. Anal. Chem. **63**: 1838–1843. doi:10.1021/ac00017a031

Gardner, W. S., S. E. Newell, M. J. McCarthy, and others. 2017. Community biological ammonium demand: a conceptual model for cyanobacteria blooms in eutrophic lakes. Environ. Sci. Technol. **51**: 7785–7793. doi:10.1021/acs.est.6b06296

Gardner, W. S., and J. A. Stephens. 1978. Stability and composition of terrestrially derived dissolved organic nitrogen in continental shelf surface waters. Marine Chemistry **6**: 335–342. doi:10.1016/0304-4203(78)90014-2

Gardner, W. S., and H. A. Vanderploeg. 1982. Microsample-filtering device for liquid chromatography or flow injection analysis. Analytical Chemistry **54**: 2129–2130.

Gasol, J. M., and P. A. del Giorgio. 2000. Using flow cytometry for counting natural planktonic bacteria and understanding the structure of planktonic bacterial communities. Scientia Marina **64**: 197–224.

Gaspar, A., E. V. Kunenkov, R. Lock, M. Desor, I. Perminova, and P. Schmitt-Kopplin. 2009. Combined utilization of ion mobility and ultra-high-resolution mass spectrometry to identify multiply charged constituents in natural organic matter. Rapid Commun. Mass Spectrom. **23**: 683–688. doi:10.1002/rcm.3924

Gika, H. G., G. A. Theodoridis, R. S. Plumb, and I. D. Wilson. 2014. Current practice of liquid chromatography–mass spectrometry in metabolomics and metabonomics. Journal of Pharmaceutical and Biomedical Analysis **87**: 12–25. doi:10.1016/j.jpba.2013.06.032

Glibert, P. M., J. Harrison, C. Heil, and S. Seitzinger. 2006. Escalating worldwide use of urea – a global change contributing to coastal eutrophication. Biogeochemistry **77**: 441–463. doi:10.1007/s10533-005-3070-5

Glibert, P. M., R. Maranger, D. J. Sobota, and L. Bouwman. 2014. The Haber Bosch–harmful algal bloom (HB–HAB) link. Environ. Res. Lett. **9**: 105001. doi:10.1088/1748-9326/9/10/105001

Glibert, P. M., F. P. Wilkerson, R. C. Dugdale, and others. 2016. Pluses and minuses of ammonium and nitrate uptake and assimilation by phytoplankton and implications for productivity and community composition, with emphasis on nitrogen-enriched conditions. Limnol. Oceanogr. **61**: 165–197. doi:10.1002/lno.10203

Gobler, C. J., J. M. Burkholder, T. W. Davis, M. J. Harke, T. Johengen, C. A. Stow, and D. B. Van de Waal. 2016. The dual role of nitrogen supply in controlling the growth and toxicity of cyanobacterial blooms. Harmful Algae **54**: 87–97. doi:10.1016/j.hal.2016.01.010

Goecks, J., A. Nekrutenko, and J. Taylor. 2010. Galaxy: a comprehensive approach for supporting accessible, reproducible, and transparent computational research in the life sciences. Genome Biology **11**: R86. doi:10.1186/gb-2010-11-8-r86

González López, C. V., M. del C. C. García, F. G. A. Fernández, C. S. Bustos, Y. Chisti, and J. M. F. Sevilla. 2010. Protein measurements of microalgal and cyanobacterial biomass. Bioresource Technology **101**: 7587–7591. doi:10.1016/j.biortech.2010.04.077

Gruber, D. F., J.-P. Simjouw, S. P. Seitzinger, and G. L. Taghon. 2006. Dynamics and characterization of refractory dissolved organic matter produced by a pure bacterial culture in an experimental predator-prey system. Appl. Environ. Microbiol. **72**: 4184–4191. doi:10.1128/AEM.02882-05

Guo, Y., S. Srinivasan, and S. Gaiki. 2007. Investigating the effect of chromatographic conditions on retention of organic acids in hydrophilic interaction chromatography Using a Design of Experiment. Chroma **66**: 223–229. doi:10.1365/s10337-007-0264-0

Häder, D.-P., H. D. Kumar, R. C. Smith, and R. C. Worrest. 2007. Effects of solar UV radiation on aquatic ecosystems and interactions with climate change. Photochem. Photobiol. Sci. **6**: 267–285. doi:10.1039/B700020K

Hagedorn, F., and P. Schleppi. 2000. Determination of total dissolved nitrogen by persulfate oxidation. Journal of Plant Nutrition and Soil Science **163**: 81–82. doi:10.1002/(SICI)1522-2624(200002)163:1<81::AID-JPLN81>3.0.CO;2-1

Hampel, J. J., M. J. McCarthy, W. S. Gardner, L. Zhang, H. Xu, G. Zhu, and S. E. Newell. 2018. Nitrification and ammonium dynamics in Taihu Lake, China: seasonal competition for ammonium between nitrifiers and cyanobacteria. Biogeosciences **15**: 733–748. doi:10.5194/bg-15-733-2018

Hansell, D. A., and J. J. Goering. 1989. A method for estimating uptake and production rates for urea in seawater using [^{14}C] urea and [^{15}N] urea. Can. J. Fish. Aquat. Sci. **46**: 198–202. doi:10.1139/f89-027

Hanus, M., M. Kabeláč, J. Rejnek, F. Ryjáček, and P. Hobza. 2004. Correlated ab Initio study of nucleic acid bases and their tautomers in the gas phase, in a microhydrated environment, and in aqueous solution. Part 3. Adenine. J. Phys. Chem. B **108**: 2087–2097. doi:10.1021/jp036090m

Hao, Z., B. Xiao, and N. Weng. 2008. Impact of column temperature and mobile phase components on selectivity of hydrophilic interaction chromatography (HILIC). J. Sep. Science **31**: 1449–1464. doi:10.1002/jssc.200700624

Hasegawa, T., I. Koike, and H. Mukai. 2000. Dissolved organic nitrogen dynamics in coastal waters and the effect of copepods. Journal of Experimental Marine Biology and Ecology **244**: 219–238. doi:10.1016/S0022-0981(99)00145-8

Hawkes, J. A., T. Dittmar, C. Patriarca, L. J. Tranvik, and J. Bergquist. 2016. Evaluation of the Orbitrap mass spectrometer for the molecular fingerprinting analysis of natural dissolved organic matter (DOM). Analytical Chemistry **88**: 7698–7704.

Hawkes, J. A., C. Patriarca, P. J. R. Sjöberg, L. J. Tranvik, and J. Bergquist. 2018. Extreme isomeric complexity of dissolved organic matter found across aquatic environments. Limnol. Oceanogr. n/a-n/a. doi:10.1002/lol2.10064

Heissenberger, A., and G. J. Herndl. 1994. Formation of high molecular weight material by free-living marine bacteria. Marine Ecology Progress Series **111**: 129–135.

Heissenberger, A., G. G. Leppard, and G. J. Herndl. 1996. Relationship between the intracellular integrity and the morphology of the capsular envelope in attached and free-living marine bacteria. Appl. Environ. Microbiol. **62**: 4521–4528.

Hertkorn, N., R. Benner, M. Frommberger, P. Schmitt-Kopplin, M. Witt, K. Kaiser, A. Kettrup, and J. I. Hedges. 2006. Characterization of a major refractory component of marine dissolved organic matter. Geochimica et Cosmochimica Acta **70**: 2990–3010. doi:10.1016/j.gca.2006.03.021

Hertkorn, N., M. Frommberger, M. Witt, B. P. Koch, P. Schmitt-Kopplin, and E. M. Perdue. 2008. Natural organic matter and the event horizon of mass spectrometry. Anal. Chem. **80**: 8908–8919. doi:10.1021/ac800464g

Hertkorn, N., M. Harir, B. P. Koch, B. Michalke, and P. Schmitt-Kopplin. 2013. High-field NMR spectroscopy and FTICR mass spectrometry: powerful discovery tools for the molecular level characterization of marine dissolved organic matter. Biogeosciences **10**: 1583–1624.

Hertkorn, N., A. Permin, I. Perminova, D. Kovalevskii, M. Yudov, V. Petrosyan, and A. Kettrup. 2002. Comparative analysis of partial structures of a peat humic and fulvic acid using one- and two-dimensional nuclear magnetic resonance spectroscopy. Journal of Environmental Quality; Madison **31**: 375–87.

Hertkorn, N., C. Ruecker, M. Meringer, R. Gugisch, M. Frommberger, E. M. Perdue, M. Witt, and P. Schmitt-Kopplin. 2007. High-precision frequency measurements: indispensable tools at the core of the molecular-level analysis of complex systems. Anal Bioanal Chem **389**: 1311–1327. doi:10.1007/s00216-007-1577-4

Hines, K. M., J. C. May, J. A. McLean, and L. Xu. 2016. Evaluation of collision cross section calibrants for structural analysis of lipids by traveling wave ion mobility-mass spectrometry. Anal. Chem. **88**: 7329–7336. doi:10.1021/acs.analchem.6b01728

Hockaday, W. C., A. M. Grannas, S. Kim, and P. G. Hatcher. 2007. The transformation and mobility of charcoal in a fire-impacted watershed. Geochimica et Cosmochimica Acta **71**: 3432–3445. doi:10.1016/j.gca.2007.02.023

Hoppe, H.-G. 1983. Significance of exoenzymatic activities in the ecology of brackish water: measurements by means of methylumbelliferyl-substrates. Marine Ecology Progress Series **11**: 299–308.

Hoppe, H.-G., S.-J. Kim, and K. Gocke. 1988. Microbial decomposition in aquatic environments: combined process of extracellular enzyme activity and substrate uptake. Appl. Environ. Microbiol. **54**: 784–790.

Huang, W., Y. Bi, and Z. Hu. 2014. Effects of fertilizer-urea on growth, photosynthetic activity and microcystins production of *Microcystis aeruginosa* isolated from Dianchi Lake. Bull Environ Contam Toxicol **92**: 514–519. doi:10.1007/s00128-014-1217-6

Isobe, K., Y. Suwa, J. Ikutani, and others. 2011. Analytical techniques for quantifying $^{15}N/^{14}N$ of nitrate, nitrite, total dissolved nitrogen and ammonium in environmental samples using a gas chromatograph equipped with a quadrupole mass spectrometer. Microbes Environ. **26**: 46–53. doi:10.1264/jsme2.ME10159

Jannasch, H. W. 1967. Growth of marine bacteria at limiting concentrations of organic carbon in seawater. Limnology and Oceanography **12**: 264–271. doi:10.4319/lo.1967.12.2.0264

Jiang, H., and B. Qiu. 2005. Photosynthetic adaptation of a bloom-forming cyanobacterium *Microcystis Aeruginosa* (cyanophyceae) to prolonged UV-B exposure. Journal of Phycology **41**: 983–992. doi:10.1111/j.1529-8817.2005.00126.x

Jørgensen, N., N. Kroer, R. Coffin, X. Yang, and C. Lee. 1993. Dissolved free amino-acids, combined amino-acids, and DNA as sources of carbon and nitrogen to marine bacteria. Mar. Ecol.-Prog. Ser. **98**: 135–148. doi:10.3354/meps098135

Kalle, K. 1966. The problem of the Gelbstoff in the sea. Oceanogr. Mar. Biol. Ann. Rev. **4**: 91–104.

Kirchman, D. L., and R. Mitchell. 2008. Microbial ecology of the oceans, John Wiley & Sons, Incorporated.

Knowles, R., and T. H. Blackburn, eds. 1993. Nitrogen isotope techniques, Academic Press.

Kudela, R. M., J. Q. Lane, and W. P. Cochlan. 2008. The potential role of anthropogenically derived nitrogen in the growth of harmful algae in California, USA. Harmful algae **8**: 103–110.

Kujawinski, E. B. 2011. The impact of microbial metabolism on marine dissolved organic matter. Annual review of marine science **3**: 567–599.

Kujawinski, E. B., and M. D. Behn. 2006. Automated analysis of electrospray ionization Fourier Transform Ion Cyclotron Resonance Mass Spectra of natural organic matter. Anal. Chem. **78**: 4363–4373. doi:10.1021/ac0600306

Kuznetsova, M., and C. Lee. 2002. Dissolved free and combined amino acids in nearshore seawater, sea surface microlayers and foams: Influence of extracellular hydrolysis. Aquat. Sci. **64**: 252–268. doi:10.1007/s00027-002-8070-0

Langille, M. G., J. Zaneveld, J. G. Caporaso, and others. 2013. Predictive functional profiling of microbial communities using 16S rRNA marker gene sequences. Nature biotechnology **31**: 814–821.

Lanucara, F., S. W. Holman, C. J. Gray, and C. E. Eyers. 2014. The power of ion mobility-mass spectrometry for structural characterization and the study of conformational dynamics. Nature Chemistry **6**: nchem.1889. doi:10.1038/nchem.1889

Lee, C., S. G. Wakeham, and J. I. Hedges. 2000. Composition and flux of particulate amino acids and chloropigments in equatorial Pacific seawater and sediments. Deep Sea Research Part I: Oceanographic Research Papers **47**: 1535–1568. doi:10.1016/S0967-0637(99)00116-8

Lee, S., and J. A. Fuhrman. 1987. Relationships between biovolume and biomass of naturally derived marine bacterioplankton. Appl. Environ. Microbiol. **53**: 1298–1303.

Leenheer, J. A., and J.-P. Croué. 2003. Characterizing aquatic dissolved organic matter. Environ. Sci. Technol. **37**: 18A-26A. doi:10.1021/es032333c

Leinweber, P., J. Kruse, C. Baum, and others. 2013. Advances in understanding organic nitrogen chemistry in soils using state-of-the-art analytical techniques, p. 83–151. *In* D.L. Sparks [ed.], Advances in Agronomy. Academic Press.

Letscher, R. T., D. A. Hansell, C. A. Carlson, R. Lumpkin, and A. N. Knapp. 2013. Dissolved organic nitrogen in the global surface ocean: distribution and fate. Global Biogeochem. Cycles **27**: 141–153. doi:10.1029/2012GB004449

Lewis, E. J. 1973. The protein, peptide and free amino acid composition in species of Champia from Saurashtra Coast, India. Botanica Marina **16**: 145–147. doi:10.1515/botm.1973.16.3.145

L'Helguen, S., G. Slawyk, and P. Le Corre. 2005. Seasonal patterns of urea regeneration by size-fractionated microheterotrophs in well-mixed temperate coastal waters. J Plankton Res **27**: 263–270. doi:10.1093/plankt/fbh174

Li, N., L. Zhang, F. Li, Y. Wang, Y. Zhu, H. Kang, S. Wang, and S. Qin. 2011. Metagenome of microorganisms associated with the toxic Cyanobacteria *Microcystis aeruginosa* analyzed using the 454 sequencing platform. Chin. J. Ocean. Limnol. **29**: 505–513. doi:10.1007/s00343-011-0056-0

Liesenfeld, D. B., N. Habermann, R. W. Owen, A. Scalbert, and C. M. Ulrich. 2013. Review of mass spectrometry–based metabolomics in cancer research. Cancer Epidemiol Biomarkers Prev **22**: 2182–2201. doi:10.1158/1055-9965.EPI-13-0584

Lin, X., M. J. McCarthy, S. A. Carini, and W. S. Gardner. 2011. Net, actual, and potential sediment–water interface NH_4^+ fluxes in the northern Gulf of Mexico (NGOMEX): evidence for NH_4^+ limitation of microbial dynamics. Continental Shelf Research **31**: 120–128. doi:10.1016/j.csr.2010.11.012

Liu, J., H. P. Bacosa, and Z. Liu. 2017a. Potential environmental factors affecting oil-degrading bacterial populations in deep and surface waters of the northern Gulf of Mexico. Front. Microbiol. **7**. doi:10.3389/fmicb.2016.02131

Liu, S., and Z. Liu. 2015a. Comparing extracellular enzymatic hydrolysis between plain peptides and their corresponding analogs in the northern Gulf of Mexico

Mississippi River plume. Marine Chemistry **177**: 398–407. doi:10.1016/j.marchem.2015.06.021

Liu, S., and Z. Liu. 2015b. Comparing extracellular enzymatic hydrolysis between plain peptides and their corresponding analogs in the northern Gulf of Mexico Mississippi River plume. Marine Chemistry **177**, **Part 2**: 398–407. doi:10.1016/j.marchem.2015.06.021

Liu, S., and Z. Liu. 2018. Free extracellular enzymes dominate initial peptide hydrolysis in coastal seawater. Marine Chemistry **199**: 37–43. doi:10.1016/j.marchem.2018.01.005

Liu, S., A. Riesen, and Z. Liu. 2015. Differentiating the role of different-sized microorganisms in peptide decomposition during incubations using size-fractioned coastal seawater. Journal of Experimental Marine Biology and Ecology **472**: 97–106. doi:10.1016/j.jembe.2015.07.004

Liu, S., B. Wawrik, and Z. Liu. 2017b. Different bacterial communities involved in peptide decomposition between normoxic and hypoxic coastal waters. Front. Microbiol. **8**. doi:10.3389/fmicb.2017.00353

Liu, Z., M. E. Kobiela, G. A. McKee, T. Tang, C. Lee, M. R. Mulholland, and P. G. Hatcher. 2010. The effect of chemical structure on the hydrolysis of tetrapeptides along a river-to-ocean transect: AVFA and SWGA. Marine Chemistry **119**: 108–120. doi:10.1016/j.marchem.2010.01.005

Liu, Z., and S. Liu. 2015c. High phosphate concentrations accelerate bacterial peptide decomposition in hypoxic bottom waters of the northern Gulf of Mexico. Environ. Sci. Technol. doi:10.1021/acs.est.5b03039

Liu, Z., and S. Liu. 2016. High phosphate concentrations accelerate bacterial peptide decomposition in hypoxic bottom waters of the Northern Gulf of Mexico. Environ. Sci. Technol. **50**: 676–684. doi:10.1021/acs.est.5b03039

Liu, Z., S. Liu, J. Liu, and W. S. Gardner. 2013. Differences in peptide decomposition rates and pathways between hypoxic and oxic coastal environments. Marine Chemistry **157**: 67–77. doi:10.1016/j.marchem.2013.08.003

Liu, Z., R. L. Sleighter, J. Zhong, and P. G. Hatcher. 2011. The chemical changes of DOM from black waters to coastal marine waters by HPLC combined with ultrahigh resolution mass spectrometry. Estuarine, Coastal and Shelf Science **92**: 205–216. doi:10.1016/j.ecss.2010.12.030

Lomas, M. W., T. M. Trice, P. M. Glibert, D. A. Bronk, and J. J. McCarthy. 2002. Temporal and spatial dynamics of urea uptake and regeneration rates and concentrations in Chesapeake Bay. Estuaries **25**: 469–482. doi:10.1007/BF02695988

Lønborg, C., X. A. Álvarez-Salgado, K. Davidson, and A. E. J. Miller. 2009. Production of bioavailable and refractory dissolved organic matter by coastal heterotrophic microbial populations. Estuarine, Coastal and Shelf Science **82**: 682–688. doi:10.1016/j.ecss.2009.02.026

Marie, D., F. Partensky, S. Jacquet, and D. Vaulot. 1997. Enumeration and cell cycle analysis of natural populations of marine picoplankton by flow cytometry using the nucleic acid stain SYBR Green I. Appl. Environ. Microbiol. **63**: 186–193.

Mason, E. A., and H. W. Schamp. 1958. Mobility of gaseous lons in weak electric fields. Annals of Physics **4**: 233–270. doi:10.1016/0003-4916(58)90049-6

May, J. C., C. R. Goodwin, N. M. Lareau, and others. 2014. Conformational ordering of biomolecules in the gas phase: nitrogen collision cross sections measured on a prototype high resolution drift tube ion mobility-mass spectrometer. Anal. Chem. **86**: 2107–2116. doi:10.1021/ac4038448

May, J. C., and J. A. McLean. 2015. Ion mobility-mass spectrometry: time-dispersive instrumentation. Anal. Chem. **87**: 1422–1436. doi:10.1021/ac504720m

McCarthy, J. J. 1970. A urease method for urea in seawater. Limnology and Oceanography **15**: 309–313.

McCarthy, M. J., R. T. James, Y. Chen, T. L. East, and W. S. Gardner. 2009. Nutrient ratios and phytoplankton community structure in the large, shallow, eutrophic, subtropical Lakes Okeechobee (Florida, USA) and Taihu (China). Limnology **10**: 215–227. doi:10.1007/s10201-009-0277-5

McCarthy, M. J., P. J. Lavrentyev, L. Yang, L. Zhang, Y. Chen, B. Qin, and W. S. Gardner. 2007. Nitrogen dynamics and microbial food web structure during a summer cyanobacterial bloom in a subtropical, shallow, well-mixed, eutrophic lake (Lake Taihu, China). Hydrobiologia **581**: 195–207. doi:10.1007/s10750-006-0496-2

McCarthy, M. J., S. E. Newell, S. A. Carini, and W. S. Gardner. 2015. Denitrification dominates sediment nitrogen removal and is enhanced by bottom-water hypoxia in the Northern Gulf of Mexico. Estuaries and Coasts **38**: 2279–2294. doi:10.1007/s12237-015-9964-0

McDaniel, E. W. 1964. Collision phenomena in ionized gases. New York: Wiley, 1964.

McDaniel, E. W., and E. A. Mason. 1973. The mobility and diffusion of ions in gases,.

McPhail, K. L., J. Correa, R. G. Linington, J. González, E. Ortega-Barría, T. L. Capson, and W. H. Gerwick. 2007. Antimalarial linear lipopeptides from a Panamanian strain of the marine cyanobacterium Lyngbya majuscula. Journal of natural products **70**: 984–988.

Mercado, J. M., T. Ramírez, D. Cortésand, and E. Liger. 2010. Isotopic composition of particulate organic nitrogen and its relationship to nitrate assimilation in the Mediterranean Sea. Scientia Marina **74**: 745–753. doi:10.3989/scimar.2010.74n4745

Mopper, K., A. Stubbins, J. D. Ritchie, H. M. Bialk, and P. G. Hatcher. 2007. Advanced instrumental approaches for characterization of marine dissolved organic matter: extraction techniques, mass spectrometry, and nuclear magnetic resonance spectroscopy. Chem. Rev. **107**: 419–442. doi:10.1021/cr050359b

Moran, M. A., and R. E. Hodson. 1989. Formation and bacterial utilization of dissolved organic carbon derived from detrital lignocellulose. Limnology and Oceanography **34**: 1034–1047.

Mulholland, M. R., and M. W. Lomas. 2008. Nitrogen uptake and assimilation. Nitrogen in the marine environment 303–384.

Nydahl, F. 1978. On the peroxodisulphate oxidation of total nitrogen in waters to nitrate. Water Research **12**: 1123–1130. doi:10.1016/0043-1354(78)90060-X

Ogawa, H., Y. Amagai, I. Koike, K. Kaiser, and R. Benner. 2001. Production of refractory dissolved organic matter by bacteria. Science **292**: 917–920. doi:10.1126/science.1057627

Ohno, T., R. L. Sleighter, and P. G. Hatcher. 2016. Comparative study of organic matter chemical characterization using negative and positive mode electrospray ionization ultrahigh-resolution mass spectrometry. Anal Bioanal Chem **408**: 2497–2504. doi:10.1007/s00216-016-9346-x

Oliver, R. L., D. P. Hamilton, J. D. Brookes, and G. G. Ganf. 2012. Physiology, blooms and prediction of planktonic cyanobacteria, p. 155–194. *In* B.A. Whitton [ed.], Ecology of Cyanobacteria II. Springer Netherlands.

Otten, T. G., H. Xu, B. Qin, G. Zhu, and H. W. Paerl. 2012. Spatiotemporal patterns and ecophysiology of toxigenic *Microcystis* blooms in Lake Taihu, China: implications for water quality management. Environ. Sci. Technol. **46**: 3480–3488. doi:10.1021/es2041288

Paerl, H. W., N. S. Hall, and E. S. Calandrino. 2011. Controlling harmful cyanobacterial blooms in a world experiencing anthropogenic and climatic-induced change. Science of The Total Environment **409**: 1739–1745. doi:10.1016/j.scitotenv.2011.02.001

Paerl, H. W., H. Xu, N. S. Hall, and others. 2014. Controlling cyanobacterial blooms in hypertrophic Lake Taihu, China: will nitrogen reductions cause replacement of non-N_2 fixing by N_2 fixing taxa? PLoS ONE **9**: e113123. doi:10.1371/journal.pone.0113123

Pantoja, S., and C. Lee. 1999. Peptide decomposition by extracellular hydrolysis in coastal seawater and salt marsh sediment. Marine Chemistry **63**: 273–291. doi:10.1016/S0304-4203(98)00067-X

Pantoja, S., C. Lee, and J. F. Marecek. 1997. Hydrolysis of peptides in seawater and sediment. Marine Chemistry **57**: 25–40. doi:10.1016/S0304-4203(97)00003-0

Pantoja, S., C. Lee, J. F. Marecek, and B. P. Palenik. 1993. Synthesis and use of fluorescent molecular probes for measuring cell-surface enzymatic oxidation of amino acids and amines in seawater. Analytical Biochemistry **211**: 210–218. doi:10.1006/abio.1993.1259

Parsons, T. R., Y. Maita, and C. M. Lalli. 1984. Determination of urea, p. 17–22. *In* A Manual of Chemical & Biological Methods for Seawater Analysis. Pergamon.

Petras, D., I. Koester, R. Da Silva, and others. 2017. High-resolution liquid chromatography tandem mass spectrometry enables large scale molecular characterization of dissolved organic matter. Front. Mar. Sci. **4**: 405. doi:10.3389/fmars.2017.00405

Purchase, B. S. 1974. The influence of phosphate deficiency on nitrification. Plant Soil **41**: 541–547. doi:10.1007/BF02185815

Qin, B., P. Xu, Q. Wu, L. Luo, and Y. Zhang. 2007. Environmental issues of Lake Taihu, China, p. 3–14. *In* B. Qin, Z. Liu, and K. Havens [eds.], Eutrophication of Shallow Lakes with Special Reference to Lake Taihu, China. Springer Netherlands.

Qin, B., G. Zhu, G. Gao, Y. Zhang, W. Li, H. W. Paerl, and W. W. Carmichael. 2009. A Drinking water crisis in Lake Taihu, China: linkage to climatic variability and lake management. Environmental Management **45**: 105–112. doi:10.1007/s00267-009-9393-6

Rabalais, N. N., R. E. Turner, and W. J. Wiseman. 2001. Hypoxia in the Gulf of Mexico. Journal of Environment Quality **30**: 320. doi:10.2134/jeq2001.302320x

Rabalais, N. N., R. E. Turner, and W. J. Wiseman. 2002. Gulf of Mexico hypoxia, A.K.A. "The Dead Zone." Annual Review of Ecology and Systematics **33**: 235–263. doi:10.1146/annurev.ecolsys.33.010802.150513

Rathgeb, A., T. Causon, R. Krachler, and S. Hann. 2017. From the peat bog to the estuarine mixing zone: Common features and variances in riverine dissolved organic matter determined by non-targeted analysis. Marine Chemistry **194**: 158–167. doi:10.1016/j.marchem.2017.06.012

Rees, T. a. V., and P. J. Syrett. 1979. The uptake of urea by the diatom, *Phaeodactylum*. New Phytologist **82**: 169–178. doi:10.1111/j.1469-8137.1979.tb07572.x

Repeta, D. J. 2015. Chemical characterization and cycling of dissolved organic matter, p. 21–63. *In* D.A.H.A. Carlson [ed.], Biogeochemistry of Marine Dissolved Organic Matter (Second Edition). Academic Press.

Reyna, N. E., A. Hardison, and Z. Liu. 2017. Influence of major storm events on the quantity and composition of particulate organic matter and the phytoplankton community in a subtropical estuary, Texas. Frontiers in Marine Science **4**: 43.

Reynolds, C. S., and A. E. Walsby. 1975. Water-Blooms. Biological Reviews **50**: 437–481. doi:10.1111/j.1469-185X.1975.tb01060.x

Ridgwell, A., and S. Arndt. 2015. Why dissolved organics matter: DOC in ancient oceans and past climate change, p. 1–20. *In* D.A.H.A. Carlson [ed.], Biogeochemistry of Marine Dissolved Organic Matter (Second Edition). Academic Press.

Rubert, J., M. Zachariasova, and J. Hajslova. 2015. Advances in high-resolution mass spectrometry based on metabolomics studies for food – a review. Food Additives & Contaminants: Part A **32**: 1685–1708. doi:10.1080/19440049.2015.1084539

Saiya-Cork, K. R., R. L. Sinsabaugh, and D. R. Zak. 2002. The effects of long term nitrogen deposition on extracellular enzyme activity in an Acer saccharum forest soil. Soil Biology and Biochemistry **34**: 1309–1315. doi:10.1016/S0038-0717(02)00074-3

Saxton, M. A., R. J. Arnold, R. A. Bourbonniere, R. M. McKay, and S. W. Wilhelm. 2012. Plasticity of total and intracellular phosphorus quotas in *Microcystis aeruginosa* cultures and Lake Erie algal assemblages. Front. Microbiol. **3**. doi:10.3389/fmicb.2012.00003

Schindler, D. W. 1977. Evolution of phosphorus limitation in lakes. Science **195**: 260–262.

Schloss, P. D., S. L. Westcott, T. Ryabin, and others. 2009. Introducing mothur: Open-Source, Platform-Independent, Community-Supported Software for Describing and Comparing Microbial Communities. Appl. Environ. Microbiol. **75**: 7537–7541. doi:10.1128/AEM.01541-09

Šejnohová, L., and B. Maršálek. 2012. *Microcystis*. 195–228. doi:10.1007/978-94-007-3855-3_7

Sharp, J. H. 1973. Size classes of organic carbon in seawater. Limnology and Oceanography **18**: 441–447. doi:10.4319/lo.1973.18.3.0441

Siewe, R. M., B. Weil, A. Burkovski, L. Eggeling, R. Krämer, and T. Jahns. 1998. Urea uptake and urease activity in *Corynebacterium glutamicum*. Arch Microbiol **169**: 411–416. doi:10.1007/s002030050591

Sigman, D. M., and K. L. Casciotti. 2001. Nitrogen isotopes in the ocean, p. 1884–1894. *In* Encyclopedia of Ocean Sciences. Elsevier.

Sigman, D. M., K. L. Casciotti, M. Andreani, C. Barford, M. Galanter, and J. K. Böhlke. 2001. A bacterial method for the nitrogen isotopic analysis of nitrate in seawater and freshwater. Anal. Chem. **73**: 4145–4153. doi:10.1021/ac010088e

Sipler, R. E., and D. A. Bronk. 2015. Dynamics of dissolved organic nitrogen, p. 127–232. *In* D.A.H.A. Carlson [ed.], Biogeochemistry of Marine Dissolved Organic Matter (Second Edition). Academic Press.

Skujiņš, J., and R. G. Burns. 1976. Extracellular enzymes in soil. CRC Critical Reviews in Microbiology **4**: 383–421. doi:10.3109/10408417609102304

Slawyk, G., and P. Raimbault. 1995. Simple procedure for simultaneous recovery of dissolved inorganic and organic nitrogen in ^{15}N-tracer experiments and improving the isotopic mass balance. Marine Ecology Progress Series **124**: 289–299.

Smith, C. A., G. O. Maille, E. J. Want, and others. 2005. METLIN: A metabolite mass spectral database. Therapeutic Drug Monitoring **27**: 747–751.

Solomon, C. M. 2006. Regulation of estuarine phytoplankton and bacterial urea uptake and urease activity by environmental factors.

Solomon, C. M., J. L. Collier, G. M. Berg, and P. M. Glibert. 2010a. Role of urea in microbial metabolism in aquatic systems: a biochemical and molecular review. Aquatic Microbial Ecology **59**: 67–88.

Sommaruga, R., Y. Chen, and Z. Liu. 2009. Multiple strategies of bloom-forming *Microcystis* to minimize damage by solar ultraviolet radiation in surface waters. Microb Ecol **57**: 667–674. doi:10.1007/s00248-008-9425-4

Srebalus Barnes, C. A., A. E. Hilderbrand, S. J. Valentine, and D. E. Clemmer. 2002. Resolving isomeric peptide mixtures: a combined HPLC/ion mobility-TOFMS analysis of a 4000-component combinatorial library. Anal. Chem. **74**: 26–36. doi:10.1021/ac0108562

Steffen, M. M., Z. Li, T. C. Effler, L. J. Hauser, G. L. Boyer, and S. W. Wilhelm. 2012. Comparative metagenomics of toxic freshwater cyanobacteria bloom Communities on Two Continents. PLOS ONE **7**: e44002. doi:10.1371/journal.pone.0044002

Sterner, R. W. 2008. On the phosphorus limitation paradigm for lakes. International Review of Hydrobiology **93**: 433–445. doi:10.1002/iroh.200811068

Stubbins, A., R. G. M. Spencer, H. Chen, and others. 2010. Illuminated darkness: Molecular signatures of Congo River dissolved organic matter and its photochemical alteration as revealed by ultrahigh precision mass spectrometry. Limnol. Oceanogr. **55**: 1467–1477. doi:10.4319/lo.2010.55.4.1467

Taihu Basin Authority. 2016. The health status report of Taihu Lake 2016. Ministry of Water Resources of the People's Republic of China.

Takamura, N., T. Iwakuma, and M. Yasuno. 1987. Uptake of ^{13}C and ^{15}N (ammonium, nitrate and urea) by *Microcystis* in Lake Kasumigaura. J. Plankton Res. **9**: 151–165. doi:10.1093/plankt/9.1.151

Tang, K., J. S. Page, and R. D. Smith. 2004. Charge competition and the linear dynamic range of detection in electrospray ionization mass spectrometry1. Journal of the American Society for Mass Spectrometry **15**: 1416–1423. doi:10.1016/j.jasms.2004.04.034

Tao, L., J. R. McLean, J. A. McLean, and D. H. Russell. 2007. A collision cross-section database of singly-charged peptide Ions. Journal of the American Society for Mass Spectrometry **18**: 1232–1238. doi:10.1016/j.jasms.2007.04.003

Tobias, D. J., and C. L. Brooks. 1992. Conformational equilibrium in the alanine dipeptide in the gas phase and aqueous solution: a comparison of theoretical results. J. Phys. Chem. **96**: 3864–3870. doi:10.1021/j100188a054

Tolar, B. B., G. M. King, and J. T. Hollibaugh. 2013. An analysis of thaumarchaeota populations from the northern gulf of Mexico. Front Microbiol **4**: 72. doi:10.3389/fmicb.2013.00072

Toshihiro, M., Y. Tanaka, and I. Koike. 2005. Determining ^{15}N enrichment of dissolved organic nitrogen in environmental waters by gas chromatography/negative-ion chemical ionization mass spectrometry. Limnology and Oceanography: Methods **3**: 164–173. doi:10.4319/lom.2005.3.164

Tranvik, L. J. 1993. Microbial transformation of labile dissolved organic matter into humic-like matter in seawater. FEMS Microbiology Ecology **12**: 177–183. doi:10.1111/j.1574-6941.1993.tb00030.x

Tripathi, A., J. Puddick, M. R. Prinsep, M. Rottmann, and L. T. Tan. 2010. Lagunamides A and B: cytotoxic and antimalarial cyclodepsipeptides from the marine *Cyanobacterium Lyngbya majuscula*. J. Nat. Prod. **73**: 1810–1814. doi:10.1021/np100442x

Valderrama, J. C. 1981. The simultaneous analysis of total nitrogen and total phosphorus in natural waters. Marine Chemistry **10**: 109–122. doi:10.1016/0304-4203(81)90027-X

Varela, M. M., A. Bode, E. Fernández, N. Gónzalez, V. Kitidis, M. Varela, and E. M. S. Woodward. 2005. Nitrogen uptake and dissolved organic nitrogen release in planktonic communities characterized by phytoplankton size–structure in the Central Atlantic Ocean. Deep Sea Research Part I: Oceanographic Research Papers **52**: 1637–1661. doi:10.1016/j.dsr.2005.03.005

Viant, M. R., and U. Sommer. 2013. Mass spectrometry based environmental metabolomics: a primer and review. Metabolomics **9**: 144–158. doi:10.1007/s11306-012-0412-x

Wang, J., Q. Zhao, Y. Pang, and K. Hu. 2017. Research on nutrient pollution load in Lake Taihu, China. Environ Sci Pollut Res **24**: 17829–17838. doi:10.1007/s11356-017-9384-8

Weiss, M. S., U. Abele, J. Weckesser, W. u Welte, E. Schiltz, and G. E. Schulz. 1991. Molecular architecture and electrostatic properties of a bacterial porin. Science(Washington) **254**: 1627–1630.

Wilhelm, S. W., S. E. Farnsley, G. R. LeCleir, and others. 2011. The relationships between nutrients, cyanobacterial toxins and the microbial community in Taihu (Lake Tai), China. Harmful Algae **10**: 207–215. doi:10.1016/j.hal.2010.10.001

Worsfold, P. J., P. Monbet, A. D. Tappin, M. F. Fitzsimons, D. A. Stiles, and I. D. McKelvie. 2008. Characterisation and quantification of organic phosphorus and organic nitrogen components in aquatic systems: A Review. Analytica Chimica Acta **624**: 37–58. doi:10.1016/j.aca.2008.06.016

Xu, H., H. W. Paerl, B. Qin, G. Zhu, N. S. Hall, and Y. Wu. 2015. Determining critical nutrient thresholds needed to control harmful cyanobacterial blooms in eutrophic Lake Taihu, China. Environ. Sci. Technol. **49**: 1051–1059. doi:10.1021/es503744q

Xu, J., P. M. Glibert, H. Liu, K. Yin, X. Yuan, M. Chen, and P. J. Harrison. 2012. Nitrogen sources and rates of phytoplankton uptake in different regions of Hong

Kong waters in summer. Estuaries and Coasts **35**: 559–571. doi:10.1007/s12237-011-9456-9

Yang, J., H. Gao, P. M. Glibert, Y. Wang, and M. Tong. 2017. Rates of nitrogen uptake by cyanobacterially-dominated assemblages in Lake Taihu, China, during late summer. Harmful Algae **65**: 71–84. doi:10.1016/j.hal.2017.04.001

Yin, G., L. Hou, M. Liu, Z. Liu, and W. S. Gardner. 2014. A novel membrane inlet mass spectrometer method to measure $^{15}NH_4^+$ for isotope-enrichment experiments in aquatic ecosystems. Environ. Sci. Technol. **48**: 9555–9562. doi:10.1021/es501261s

Yoshida, T. 2004. Peptide separation by hydrophilic-interaction chromatography: a review. Journal of Biochemical and Biophysical Methods **60**: 265–280. doi:10.1016/j.jbbm.2004.01.006

Zark, M., J. Christoffers, and T. Dittmar. 2017. Molecular properties of deep-sea dissolved organic matter are predictable by the central limit theorem: Evidence from tandem FT-ICR-MS. Marine Chemistry **191**: 9–15. doi:10.1016/j.marchem.2017.02.005

Zhu, M., B. Bendiak, B. Clowers, and H. H. Hill. 2009. Ion mobility-mass spectrometry analysis of isomeric carbohydrate precursor ions. Anal Bioanal Chem **394**: 1853–1867. doi:10.1007/s00216-009-2865-y